NASA Contractor Report 3859

Flight Tests of the Digital Integrated Automatic Landing System (DIALS)

Nesim Halyo

CONTRACT NAS1-16158
DECEMBER 1984

NASA

NASA Contractor Report 3859

Flight Tests of the Digital Integrated Automatic Landing System (DIALS)

Nesim Halyo
Information & Control Systems, Incorporated
Hampton, Virginia

Prepared for
Langley Research Center
under Contract NAS1-16158

National Aeronautics
and Space Administration

**Scientific and Technical
Information Branch**

1984

FOREWORD

The work described in this report was performed by Information & Control Systems, Incorporated (ICS) under Contract NAS1-16158. The work was sponsored by the National Aeronautics and Space Administration, Langley Research Center, Flight Control Systems Division, Applied Controls Branch. Mr. R. M. Hueschen served as the NASA Technical Representative monitoring this contract.

TABLE OF CONTENTS

	page
FOREWORD	iii
LIST OF FIGURES	vi
LIST OF TABLES	viii
LIST OF SYMBOLS	ix
I. INTRODUCTION	1
II. CONTROL LAW FORMULATION	7
A. LONGITUDINAL DESIGN MODEL	8
B. LATERAL DESIGN MODEL	14
C. STOCHASTIC SAMPLED-DATA FORMULATION	21
D. STATE AND WIND ESTIMATION	29
III. IMPLEMENTATION OF THE DIGITAL CONTROL LAW	33
A. SCALING AND ROUND-OFF ERROR ANALYSIS	33
B. CONTROL IMPLEMENTATION FORM	37
C. MISCELLANEOUS IMPLEMENTATION ISSUES	39
1. STABILIZER TRIM	40
2. SAMPLING RATE	40
3. USE OF "EASY-ON" SMOOTHING	41
4. BAROMETRIC SINK RATE	42
5. ENGINE PRESSURE RATIO VERSUS THRUST	42
IV. FLIGHT TEST RESULTS	44
A. LOCALIZER CAPTURE	45
B. GLIDESLOPE CAPTURE	47
C. LOCALIZER AND GLIDESLOPE TRACK	51
D. A WIND SHEAR ENCOUNTER	54

TABLE OF CONTENTS (CONCLUDED)

page

E. CRAB AND DECRAB 55

F. FLARE 57

G. FILTER PERFORMANCE 62

V. CONCLUSIONS AND RECOMMENDATIONS 65

REFERENCES 111

LIST OF FIGURES

page

FIGURE 1. DIALS FLIGHT PATH GEOMETRY 68

FIGURE 2. DEFINITION OF COORDINATE AXES, ANGLES AND FORCES . 69

FIGURE 3. DIALS FUNCTIONAL BLOCK DIAGRAM 70

FIGURE 4. BLOCK DIAGRAM OF FEEDBACK LOOP 70

FIGURE 5(a). LATERAL FLIGHT PATH VARIABLES (FLIGHT NO. 1) . . . 71

FIGURE 5(b). LATERAL FLIGHT PATH VARIABLES (FLIGHT NO. 1) . . . 72

FIGURE 5(c). LATERAL FLIGHT PATH VARIABLES (FLIGHT NO. 1) . . . 73

FIGURE 6. LATERAL CONTROL VARIABLES (FLIGHT NO. 1) 74

FIGURE 7(a). LATERAL FLIGHT PATH VARIABLES (FLIGHT NO. 2) . . . 75

FIGURE 7(b). LATERAL FLIGHT PATH VARIABLES (FLIGHT NO. 2) . . . 76

FIGURE 7(c). LATERAL FLIGHT PATH VARIABLES (FLIGHT NO. 2) . . . 77

FIGURE 8. LATERAL CONTROL VARIABLES (FLIGHT NO. 2) 78

FIGURE 9(a). LATERAL FLIGHT PATH VARIABLES (FLIGHT NO. 3) . . . 79

FIGURE 9(b). LATERAL FLIGHT PATH VARIABLES (FLIGHT NO. 3) . . . 80

FIGURE 9(c). LATERAL FLIGHT PATH VARIABLES (FLIGHT NO. 3) . . . 81

FIGURE 10. LATERAL CONTROL VARIABLES (FLIGHT NO. 3) 82

FIGURE 11(a). LONGITUDINAL FLIGHT PATH VARIABLES (FLIGHT NO. 1). 83

FIGURE 11(b). LONGITUDINAL FLIGHT PATH VARIABLES (FLIGHT NO. 1). 84

FIGURE 11(c). LONGITUDINAL FLIGHT PATH VARIABLES (FLIGHT NO. 1). 85

FIGURE 12(a). LONGITUDINAL CONTROL VARIABLES (FLIGHT NO. 1). . . 86

FIGURE 12(b). LONGITUDINAL CONTROL VARIABLES (FLIGHT NO. 1). . . 87

FIGURE 13(a). LONGITUDINAL FLIGHT PATH VARIABLES (FLIGHT NO. 2). 88

FIGURE 13(b). LONGITUDINAL FLIGHT PATH VARIABLES (FLIGHT NO. 2). 89

FIGURE 13(c). LONGITUDINAL FLIGHT PATH VARIABLES (FLIGHT NO. 2). 90

LIST OF FIGURES (CONCLUDED)

page

FIGURE 14(a). LONGITUDINAL CONTROL VARIABLES (FLIGHT NO. 2). . . 91

FIGURE 14(b). LONGITUDINAL CONTROL VARIABLES (FLIGHT NO. 2). . . 92

FIGURE 15(a). LONGITUDINAL FLIGHT PATH VARIABLES (FLIGHT NO. 3). 93

FIGURE 15(b). LONGITUDINAL FLIGHT PATH VARIABLES (FLIGHT NO. 3). 94

FIGURE 15(c). LONGITUDINAL FLIGHT PATH VARIABLES (FLIGHT NO. 3). 95

FIGURE 16(a). LONGITUDINAL CONTROL VARIABLES (FLIGHT NO. 3). . . 96

FIGURE 16(b). LONGITUDINAL CONTROL VARIABLES (FLIGHT NO. 3). . . 97

FIGURE 17(a). POSITION INNOVATIONS (FLIGHT NO. 2). 98

FIGURE 17(b). ATTITUDE INNOVATIONS (FLIGHT NO. 2). 99

FIGURE 17(c). ACCELEROMETER INNOVATIONS (FLIGHT NO. 2) 100

FIGURE 17(d). AIRSPEED AND SINK RATE INNOVATIONS (FLIGHT NO. 2). 101

LIST OF TABLES

page

TABLE 1. SENSOR ERROR MODEL PARAMETERS. 102

TABLE 2. RANGE/RESOLUTION/UNITS FOR PRIMARY INPUTS. 103

TABLE 3. RANGE/UNITS FOR MEASUREMENT VECTORS. 104

TABLE 4. RANGE/UNITS AND ACCURACY FOR ESTIMATED AND PREDICTED STATE VECTORS. 105

TABLE 5. RANGE/UNITS AND ACCURACY FOR WIND STATES AND BIASES. . 106

TABLE 6. RANGE/UNITS FOR RESIDUALS OR INNOVATIONS 107

TABLE 7. RANGE/UNITS AND ACCURACY FOR COMMAND VARIABLES 108

TABLE 8. LOCALIZER OVERSHOOT STATISTICS 109

TABLE 9. GLIDESLOPE OVERSHOOT STATISTICS. 109

TABLE 10. AUTOMATIC TOUCHDOWN STANDARD DEVIATIONS. 109

TABLE 11. AUTOMATIC TOUCHDOWN STATISTICS 110

LIST OF SYMBOLS

VARIABLE	DESCRIPTION
A	System matrix
a_{ij}	Element of A in i^{th} row and j^{th} column
a_{x_s}	Acceleration along x_s
a_{y_s}	Acceleration along y_s
a_{z_s}	Acceleration along z_s
B	Control effectiveness matrix
b	Aircraft wing span
C	Measurement matrix
C_{D_o}	Coefficient drag at nominal flight condition
$C_{Du}, C_{D\delta e}, C_{D\delta s}$	Drag stability and control derivatives
C_{Lo}	Lift coefficient at nominal flight condition
$C_{Lq}, C_{Lu}, C_{L\alpha}$	Lift stability and control derivatives
C_{Mo}	Pitching moment coefficient at nominal flight condition
$C_{Mq}, C_{Mu}, C_{M\alpha}, C_{M\delta e}, C_{M\delta s}, C_{M\delta T}, C_{MT\alpha}$	Pitching moment stability and control derivatives
C_{spa}	Spoiler aileron interconnect coefficient
$C_{T_{xo}}$	Thrust coefficient along x_s at nominal flight condition
$C_{T_x u}, C_{T_x \delta T}$	Thrust stability and control derivatives
c	Mean aerodynamic chord
$c_{\ell i}$	Glideslope capture criterion coefficient
D	Wind effect matrix
DELVF	Normalized perturbed airspeed command
DELVFR	Airspeed command rate

LIST OF SYMBOLS (CONTINUED)

VARIABLE	DESCRIPTION
d	Distrubance vector
$d_{\ell i}$	Glideslope capture criterion coefficient
e	State error vector
F	Kalman filter gain
G_u	Transfer function for longitudinal turbulence
G_{ij}	Intermediate optimal gain
G_q	Transfer function for pitch rate turbulence
G_α	Transfer function for vertical turbulence
GEZ	Easy-on gain
g	Gravitational acceleration
$H_{(.)}$	Optimal control gain matrix
H_{1k}	Error feedback control gain matrix
H_{2k}	Feedforward control gain matrix
h_{ij}	Element (i,j) wind effect matrix
h_{GSC}	Glideslope capture altitude
I	Identity matrix
I_{xx}, I_{yy}, I_{zz}	Aircraft moments of inertia about stability axes
J_c	Objective or cost function for continuous system
K	Feedback gain
k	Integer index
L	Scale of turbulence
L_{ES}	Matrix tranformation from the stability to the Earth-fixed axes
L_{SE}	Matrix tranformation from the Earth-fixed axes to the stability axes

VARIABLES	DESCRIPTION
$\bar{L}_{ij}$	Filtered estimate of $L_{ES}(i,j)$
M	Cross-weight matrix
m	Aircraft mass
N	Cross-weight matrix
P_{ik}	Discrete optimal control Riccati equation solution
p	Roll rate about x_s
Q	Quadratic weight matrix for state vector
q	Pitch rate
$\bar{q}_o$	Nominal dynamic pressure
R	Quadratic weight matrix for control vector
r	Yaw rate about z_s
S	Effective wing area
s	Independent variable in Laplace transform
T_o	Nominal sampling period
t	Independent variable denoting time
t_f	Final time in cost function
U_o	Nominal airspeed along x_s
u	Perturbation in inertial speed along x_s
v	Perturbation in inertial speed along y_x
W	Wind state vector
w	Inertial speed along z_s
x_ℓ	Longitudinal state vector
x_e, x_b, x_s	Position coordinates along Earth-fixed, body and stability x-axes, respectively

VARIABLES	DESCRIPTION
y	Distance of aircraft c.g. from runway centerline
y_k	Measurement vector
y_e, y_b, y_s	Position coordinates along Earth-fixed, body and stability y-axes, respectively
z	Desired (or commanded) trajectory (state) vector
z_ℓ	Longitudinal desired trajectory (state) vector
z_e, z_b, z_s	Position coordinates along Earth-fixed, body and stability z-axes, respectively

VARIABLE (GREEK)	DESCRIPTION
α	Angle of attack
β	Sideslip angle
Γ	Control effectiveness matrix (discrete model)
γ_o	Nominal and desired glideslope angle
δe	Elevator position
δs	Perturbation of stabilizer position
δsp	Perturbation of spoiler position
δT	Perturbation of thrust
δth	Perturbation of throttle position
ε	Round-off error vector
ζ_z	Desired (or commanded) trajectory forcing function
η	Second order effects vector
θ	Perturbation of pitch angle
λ	Closed-loop eigenvalue

VARIABLE (GREEK	DESCRIPTION
ν	Innovations vector
ξ	Wind model white noise forcing function
π	3.141...
ρ	Closed-loop implementation eigenvalue
σ	Variance
τ	Dummy variable, time
ϕ	Roll angle, discrete state transition matrix
ψ	Perturbation of yaw angle
ω	Gaussian white noise process

SUBSCRIPTS	DESCRIPTION
b	Body axis
d	Disturbance
E	Elevation angle
e	Earth-fixed axes
f	Flare
g	Gust
k	Sample number
q	Pitch rate
r	Yaw rate
s	Steady state
sh	Wind shear

LIST OF SYMBOLS (CONCLUDED)

SUBSCRIPTS	DESCRIPTION
sp	Spoiler
u	Speed along x_s
v	Speed along y_s
w	Component due to wind velocity
x	Component along x_e
y	Component along y_e
z	Component along z_e
ℓ	Longitudinal

ACRONYM	DESCRIPTION
ATOPS	Advanced Transport Operating Systems
CAS	Calibrated Airspeed
DIALS	Digital Integrated Automatic Landing System
EPR	Engine Pressure Ratio
EASILY	Experimental Avionics System Integration Laboratory
GPIP	Glide Path Intercept Point
LRC	Langley Research Center
LQG	Linear-Quadratic-Gaussian
MLS	Microwave Landing System
TSRV	Transport Systems Research Vehicle

I. INTRODUCTION

The design, development and flight tests of the Digital Integrated Automatic Landing System (DIALS) described in this report were performed within the context of the Advanced Transport Operating Systems (ATOPS) program conducted by the Langley Research Center of the National Aeronautics and Space Administration. ATOPS is a research and development program aimed at developing capabilities for increased terminal area capacity, safe and accurate flight in adverse weather conditions including shear winds, noise reduction, the avoidance of wake vortices and reduced fuel consumption. Advances in digital flight computers and modern control theory, coupled with accurate guidance information such as that provided by the Microwave Landing System can be effectively used to achieve some of these goals. The work described in this report has evolved within the ATOPS program framework [1], [2].

The design of the Digital Integrated Automatic Landing System (DIALS) was completed in 1980. The automatic landing system was implemented on the Transport System Research Vehicle (TSRV), a Boeing 737-100. DIALS was flight tested with successful test results by NASA's Langley Research Center at the NASA Wallops Flight Center, demonstrating the application of modern control theory to a complex aircraft control design problem. The DIALS flight tests were completed in December 1981.

Exceptionally few automatic control systems designed with modern optimal control techniques have been successfully flight tested. In fact, the author is aware of no such flight tests on jet aircraft prior to, or since, the DIALS flight tests. DIALS is also the first digital automatic landing system designed with a modern control structure and methodology which has been successfully flight tested, to the author's knowledge. Thus, DIALS represents a milestone in the actual demonstration that linear modern control theory,

when appropriately interpreted and applied, can result in working designs for the most complex systems and tasks. This link between theory and practice is one of the basic underlying objectives of the work performed. This report describes the design of the Digital Integrated Automatic Landing System, and presents an analysis of the flight test results.

During the DIALS flight tests, ten "hands-off" automatic landings were performed on the TSRV aircraft. These automatic landings were performed under diverse wind conditions, including a wind shear case. The final approach flights included the modes of localizer capture, steep glideslope capture, localizer and glideslope track, crab/decrab, and flare to touchdown. On three of the approaches, a conventional 3° glideslope was selected. On the remaining seven automatic landings, steep approaches with a 4.5° glideslope were made. Also, several approaches capturing and tracking 5° glideslopes were made without continuing till touchdown.

DIALS uses the Microwave Landing System (MLS) which is a guidance system providing high accuracy position information in the form of azimuth, elevation, and range measurements. As the Microwave Landing System is less sensitive to weather conditions than conventional systems, automatic landing systems using the MLS can be used to reduce the congestion in terminal areas due to adverse weather conditions. Furthermore, the volumetric coverage provided by the MLS enables the use of curved flight paths and steep glideslopes in the final approach and landing phase of the flight. The MLS guidance system consists of a DME providing range information, an azimuth antenna, generally colocated with the DME antenna, providing the aircraft's azimuth angle relative to the runway centerline up to ±60°, and an elevation antenna located at the glidepath intercept point but offset to the side of the runway providing the aircraft's elevation angle up to 20°. An onboard MLS receiver provides high accuracy

position information that can be used for steep approaches and curved flight paths in the terminal area.

The control system uses MLS position information, as well as onboard sensor measurements but does not require inertial platforms. The system was developed using modern digital control methodologies [3] - [7]. The phases of the final approach and landing considered are localizer and glideslope capture and track, crab/decrab, and flare. The system captures, tracks, and flares from a steep glideslope selected by the pilot prior to engaging the capture mode. Thus, the control system modes designed are:

1) Localizer capture
2) Steep glideslope capture
3) Localizer track
4) Steep glideslope track
5) Decrab
6) Flare

Two features of this sytem are: (1) the simultaneous capture of the localizer and glideslope and (2) the selectable steep glideslope (2.5° - 5.5° for the B-737).

Typically, the aircraft is positioned, manually or automatically, below the selected glideslope so as to intercept the localizer at a selected airspeed, as shown in Figure 1. When the localizer or glideslope capture criteria are satisfied, the corresponding capture mode is engaged; so that depending on the initial aircraft position and attitude, the localizer and glideslope can be captured simultaneously or sequentially. As the aircraft reaches the localizer or glideslope, the corresponding track (or hold) modes are engaged. When a cross-wind component is present, the control system crabs the aircraft into the wind, followed by the decrab maneuver when the decrab altitude is reached.

A flare path which depends on the glideslope selected for a given approach is generated on-line, and the aircraft is controlled about this path until touchdown.

The main considerations in the development of DIALS include:

- low overshoots of the localizer and steep glideslope under adverse wind conditions
- quick settling on the trajectory
- overall smoothness of the flight during the final approach
- accurate tracking in adverse weather conditions including gusts and wind shear.

The ability to follow various steep glideslopes (selectable until glideslope capture) provides a flexibility which can increase the efficiency of terminal area operations, reduce the noise perceived on the ground, and can be used for vortex avoidance when following a large aircraft, while reducing fuel consumption during a steep final approach. Capturing the glideslope and localizer simultaneously and with quick settling times allows close-in captures, while low overshoots of the localizer under adverse wind conditions enhance the independence of close parallel runway operations. Finally, the low degradation of the MLS information accuracy in adverse weather conditions enhances performance capabilities under low visibility conditions.

The overall objective in the development of DIALS has been the direct-digital-design, using modern control methods, of an automatic landing system which controls the aircraft for glideslope angles ranging between 2.5° - 5.5°, nominal airspeeds between 115 - 135 knots, aircraft weights between 70,000 - 90,000 lb, c.g., locations between .2 - .3 under adverse wind conditions and low visibility. As the control objectives during different phases of the

final approach vary, the most important desirable characteristics of the control law in the various portions of the flight are different. For example, while low overshoot characteristics are important during capture, vertical path accuracy becomes more significant in flare. A more detailed description of the desirable characteristics in the various control modes is given in Section IV. To achieve these varying objectives, it appears that some changes in the control law, from one phase of the flight to the next, are necessary. From a strict optimal control point of view, it would be necessary to change all the control gains for each phase of flight and aircraft condition. To avoid many changes, the following approach was adopted:

1) obtain an optimal control law for a nominal condition as a starting point,
2) using realistic nonlinear simulations, modify and update this law to account for the various nonlinearities in the actuator servomechanisms, hydraulic systems, engine dynamics and the aerodynamic response, as well as to enhance desirable characteristics which may not adequately be reflected in a quadratic cost function,
3) identify a small number of modifications which can be made at each phase of flight to achieve the differing objectives of each mode.

The employment of modern digital design techniques is well-suited to the discrete nature of the MLS position information and the use of digital flight computers. From the point of view of using lower sampling rates, it is also preferable to the alternate approach of designing an analog system whose response is then approximated by a digital system, as the latter approach usually

results in rather high sampling rates. The control law was developed using optimal stochastic digital control methods.

Section II summarizes the design of the control law. Section III describes the implementation of DIALS on the TSRV flight computer. Section IV describes the modes of the automatic landing system and presents the flight test results.

II. CONTROL LAW FORMULATION

The design of the Digital Integrated Automatic Landing System (DIALS) is based on modern optimal control design techniques. The design uses a sampled-data formulation of the Linear-Quadratic-Gaussian (LQG) [8] problem coupled with optimal disturbance accommodation [7]. The basic structure of the control system contains a fixed gain (steady-state) Kalman filter which estimates the aircraft states as well as the wind velocities, a desired flight path generator which produces the flight path and attitude commands as well as the offsets or errors from the commanded trajectory during the various phases of the final approach and landing, and the control command unit containing the control gains, mode switching, limiters, etc.

The approach is to develop a linear design model for the plant consisting of the aircraft dynamics, wind conditions, actuator dynamics, and the control law structure desired. Using the design model, a digital control law to track the desired trajectory is obtained by applying optimal stochastic sampled-date techniques. The control law obtained is tested in a detailed nonlinear simulation of the aircraft and its subsystems. Finally, the control law is flight tested in automatic landings to test the design method, with the performance measure of the design method being the capability of the aircraft to perform the various functions accurately and completely.

During most of the final approach and landing phases of flight, the aircraft maintains a level wings attitude with small deviations of bank angle. Thus, the flight condition corresponding to the tracking of the desired glideslope and the localizer was selected as the reference condition about which the perturbation equations were obtained. In this condition, the longitudinal and lateral perturbation equations are decoupled; i.e., small changes in the lateral variables affect the longitudinal variables only as second order effects;

conversely, the effect of the longitudinal variables on the lateral motion is also of second order. Thus, the control and modeling of the longitudinal and lateral dynamics are considered separately.

Three sets of coordinate axes are used: the Earth-fixed axes, the body axes, and the stability axes. The Earth-fixed coordinate frame (x_e, y_e, z_e) has its origin fixed at the glidepath intercept point (GPIP) on the runway. The x_e axis is along the runway centerline, the direction in which the aircraft lands being chosen positive along the x_e. The z_e axis is the local vertical, positive downwards; y_e is perpendicular to both x_e and z_e, with its positive end directed so as to make the coordinate frame right-handed. The Earth is assumed to be stationary with respect to inertial space; so that the Earth-fixed axes form an inertial frame.

The body axes (x_b, y_b, z_b) and the stability axes (x_s, y_s, z_s) are fixed to the body of the aircraft; i.e., they are body-fixed axes. The origin of both axes is fixed at the aircraft center of mass. The x_b axis is along the fuselage reference line of the aircraft, positive towards the nose, the y_b axis is positive towards the tip of the right wing, the z_b axis is perpendicular to both x_b and y_b and is positive downwards (when the aircraft pitch angle is zero). The stability axes (x_s, y_s, z_s) are obtained from the body axes by a rotation of α_o, the steady-state angle of attack, about the y_b axis. The three sets of coordinate frames are shown in Figure 2.

A. LONGITUDINAL DESIGN MODEL

The general equations of motion for rigid aircraft can be linearized about a steady flight condition as described in [9], [10]. The nominal flight condition used here corresponds to flight among the selected glideslope and localizer, at a constant airspeed with the flaps at 40 degrees and the gear down in the landing

configuration. The longitudinal perturbation equations for describing the aircraft's motion in the vertical plane can be expressed in the stability axes as:

$$m\dot{u} = - mg \cos\gamma_o \theta + \bar{q}_o S\left\{(-C_{D\underline{u}'} + 2C_{D_o} + C_{T_x\underline{u}} + 2C_{T_{xo}}) \underline{u}' + (C_{Lo} - C_{D\underline{\alpha}}) \underline{\alpha} - C_{D\delta e} \delta e - C_{D\delta s} \delta s + C_{T_x\delta T} \delta T\right\} \quad (1)$$

$$m(\dot{w} - U_o q) = - mg \sin\gamma_o \theta + \bar{q}_o S \left\{ - (C_{L\underline{u}'} + 2C_{Lo}) \underline{u}' - (C_{L\underline{\alpha}} + C_{Do}) \underline{\alpha} - C_{L\dot{\underline{\alpha}}} \dot{\underline{\alpha}} - C_{L\underline{q}} \underline{q} \right\} \quad (2)$$

$$I_{yy} \dot{q} = \bar{q}_o Sc \left\{ (C_{M\underline{u}'} + 2C_{Mo}) \underline{u}' + (C_{M\underline{\alpha}} + C_{MT\underline{\alpha}}) \underline{\alpha} + C_{M\dot{\underline{\alpha}}} \dot{\underline{\alpha}} + C_{M\underline{q}} \underline{q} + C_{M\delta e} \delta e + C_{M\delta s} \delta s + C_{M\delta T} \delta T \right\}. \quad (3)$$

$$\underline{u}' = \frac{u + u_w}{U_o} \quad (4)$$

$$\underline{\alpha} = \alpha + \alpha_w , \quad (5)$$

$$\underline{q} = q + q_w , \quad (6)$$

where U_o is the reference inertial speed in the x_s direction, γ_o the desired glideslope angle, m the aircraft mass, θ the perturbation in pitch angle, q the pitch rate, u the perturbation in inertial speed along the x_s direction, w the inertial speed along the z_s direction; u_w, α_w, and q_w are the components due to wind, $\bar{q}_o$ is the steady-state value of the dynamic pressure at the selected airspeed, S is the effective wing area, δe, δs, and δT are the perturbations of elevator, stabilizer and thrust, respectively.

Equations (1) - (3) describe the linear and angular velocities of the aircraft in the vertical plane. The position of the aircraft can be obtained by

integrating the inertial velocity components over time. Thus,

$$\dot{x}'_e = \frac{\dot{x}_e}{U_o} = L_{ES}\ (1,1)(1 + u') + L_{ES}\ (1,2)\beta + L_{ES}\ (1,3)\alpha \quad , \tag{7}$$

$$\dot{z}'_e = \frac{\dot{z}_e}{U_o} = L_{ES}\ (3,1)(1 + u') + L_{ES}\ (3,2)\beta + L_{ES}\ (3,3)\alpha \quad , \tag{8}$$

where $L_{ES}\ (i,j)$ is the element in i^{th} row and j^{th} column of the matrix, L_{ES}, which represents the transformation from the stability axes to the Earth-fixed axes. Note that α and β are inertial quantities and correspond to normalized velocity components in the stability axes; under no wind conditions these would be the same as the aerodynamic angle of attack and sideslip. The position equations can be rewritten in the following form

$$\dot{x}'_e = -\sin\gamma_o\ \theta + \cos\gamma_o\ u' + \sin\gamma_o\ \alpha + \eta_x \quad , \tag{9}$$

$$\dot{z}'_e = -\cos\gamma_o\ \theta - \sin\gamma_o\ u' + \cos\gamma_o\ \alpha + \eta_z \quad , \tag{10}$$

where

$$\eta_x = L_{ES}\ (1,1)(1 + u') - \cos\gamma_o\ u' + \sin\gamma_o\ \theta + L_{ES}\ (1,2)\beta + (L_{ES}\ (1,3) - \sin\gamma_o)\alpha \quad , \tag{11}$$

$$\eta_z = L_{ES}\ (3,1)(1 + u') + \sin\gamma_o\ u' + \cos\gamma_o\ \theta + L_{ES}\ (3,2)\beta + (L_{ES}\ (3,3) - \cos\gamma_o)\alpha \quad , \tag{12}$$

In this form, the differential equations are linear with a forcing function that contains the nonlinear part, which are second order terms with respect to the steady flight conditions considered. With this approach it is possible to use linear theory in the development of the filter and control law without neglecting the nonlinear terms completely. To obtain the second order

terms for the remaining variables, consider the equations

$$\dot{\theta} = \cos\phi\ q - \sin\phi\ r \quad , \tag{13}$$

$$a_{x_s} = \dot{u} + qw - rv \quad , \tag{14}$$

$$a_{z_s} = \dot{w} - q(U_o + u) + pv \tag{15}$$

Rearranging these equations, we obtain

$$\dot{\theta} = q + \eta_\theta \quad , \tag{16}$$

$$\dot{u}' = \frac{a_{x_s}}{U_o} + \eta_{u'} \quad , \tag{17}$$

$$\dot{\alpha} = \frac{\dot{w}}{U_o} = \frac{a_{z_s}}{U_o} + q + \eta_\alpha \ , \tag{18}$$

where

$$\eta_\theta = (\cos\phi - 1)\ q - \sin\phi\ r \quad , \tag{19}$$

$$\eta_{u'} = -\ q\ \alpha + r\ \beta \quad , \tag{20}$$

$$\eta_\alpha = q\ u' - p\ \beta \tag{21}$$

It should be noted that the perturbation equations (1) - (3) neglect the second order terms represented by η_θ, $\eta_{u'}$, and η_α. The second order terms introduce some coupling between the longitudinal and lateral equations.

A simple first order model is used to represent the engine dynamics which are relatively slow due to spool-up time. The engine dynamics tend to behave with a 1 sec time constant when reducing thrust, while a 2 sec time constant behavior seems to dominate when increasing thrust, except when a rate limit is active to avoid enging overheating. The design model uses the 2 sec time constant to avoid lags in the actual operation of the control law.

$$\dot{\delta T} = .5\ \delta T + .298\ \delta th \quad , \tag{22}$$

where δT is the thrust perturbation in units of 1000 lb per unit δT, and δth is the throttle perturbation in throttle degrees.

A control structure of rate command is used for the throttle and stabilizer to obtain relatively slow control commands. For this purpose, the design model is augmented by the equations,

$$\dot{\delta th} = u_2 \quad , \tag{23}$$

$$\dot{\delta s} = u_3 \quad , \tag{24}$$

where δs is the stabilizer perturbation in radians. As the elevator actuator system is fast, with an approximate time constant of 1/16 sec, the elevator dynamics are neglected in the design model.

To complete the model of the longitudinal equations of motion, it is necessary to model the wind velocities which affect the motion of the aircraft. The longitudinal wind model contains the components of steady wind velocities, turbulence and shear winds in the longitudinal axes. The turbulence model uses the Dryden spectra for the various components varying with altitude. The turbulence model has three components: u_g' in the x_b direction, α_g in the z_b direction, and q_g which models the effect of turbulence on the pitch rate of the aircraft. The u_g' component is independent of α_g and q_g; however, α_g and q_g are correlated. The Dryden spectra can be factored using spectral factorization methods to obtain a linear system driven by white noise which generates an output having the desired spectral characteristics [9], [6], [11]. Thus, the following transfer functions (i.e., the ratio of the Laplace transforms of the gust generating system output to its input) are obtained to generate u_g', α_g and q_g.

$$G_u(s) = \frac{1}{1 + \frac{L_u}{U_o} s} \tag{25}$$

$$G_\alpha(s) = \frac{1 + 3\frac{L_w}{U_o}s}{1 + 2\frac{L_w}{U_o}s + \left(\frac{L_w}{U_o}\right)^2 s^2} \quad , \tag{26}$$

$$G_q(s) = \frac{q_g(s)}{\alpha_g(s)} = \frac{s}{1 + \frac{4b}{\pi U_o}s} \tag{27}$$

where α_g is the input to the system $G_q(s)$ which generates q_g with the specified spectrum and cross-spectral density, and L_a, L_w are the scales of turbulence.

The steady and shear wind in the longitudinal directions is modeled by

$$\dot{u}'_s = u'_{sh} \quad , \qquad \dot{u}'_{sh} = \xi_{\ell 3} \quad , \tag{28}$$

$$\alpha_s = \xi_4 \quad . \tag{29}$$

Thus, to simulate a specified shear profile for $\dot{u}'_s$, with appropriate initial conditions, e.g., to obtain a linear profile u'_s changing at a rate of u'_{sho}, the initial condition for u'_{sh} is set to u'_{sho} and $\xi_{\ell 3}$ is set equal to zero; alternately, an impluse in $\xi_{\ell 3}$ will also achieve the same profile. The aircraft's longitudinal equations of motion, the position equations, the actuator equations and the wind model above can be combined and after some manipulation can be expressed in state variable form.

$$\dot{x}_\ell = A_\ell x_\ell + B_\ell u_\ell + D_\ell w_\ell + \eta_\ell \quad , \tag{30}$$

$$\dot{w}_\ell = A_{w\ell} W_\ell + B_{w\ell} \xi_\ell \quad , \tag{31}$$

$$w_\ell = C_{w\ell} W_\ell \quad , \tag{32}$$

$$x_\ell^T = (\theta \quad u' \quad \alpha \quad q \quad x'_e \quad z'_e \quad \delta T \quad \delta th \quad \delta s) \quad , \tag{33}$$

$$u_\ell^T = (\delta e \quad \dot{\delta s} \quad \dot{\delta th}) \ , \tag{34}$$

$$w_\ell^T = (u'_w \quad \alpha_w \quad q_w) \quad , \tag{35}$$

$$\eta_\ell^T = (\eta_\theta \quad \eta_{u'} \quad \eta_\alpha \quad 0 \quad \eta_x \quad \eta_z \quad 0 \quad 0 \quad 0) \quad , \tag{36}$$

where A_ℓ, B_ℓ, and D_ℓ are matrices of appropriate size corresponding to the coefficients in the original equations. Expressions for the elements of these matrices can be obtained in terms of the stability derivatives of the aircraft. Equations (30) - (36) form the design model for the longitudinal control law.

B. LATERAL DESIGN MODEL

The design model for the lateral control law is obtained using the same approach as the longitudinal (vertical) model. The general equations of motion are linearized about a flight condition corresponding to level wings, a constant airspeed equal to the desired airspeed, a flight path angle equal to the selected glideslope angle, with flaps and gear down in the landing configuration. The lateral perturbation equations can then be expressed as

$$\dot{\phi} = \sec\theta_o \ (\cos\gamma_o \ p + \sin\gamma_o \ r) \tag{37}$$

$$\dot{\psi} = \sec\theta_o \ (\sin\alpha_o \ p + \cos\alpha_o \ r) \tag{38}$$

$$\begin{aligned} \dot{\beta} = {} & a_{31} \ \phi + a_{33} \ \beta + a_{34} \ p + a_{35} \ r + b_{31} \ \delta A + b_{32} \ \delta R \\ & + b_{33} \ \delta sp + h_{31} \ \beta_w + h_{32} \ p_w + h_{33} \ r_w \end{aligned} \tag{39}$$

$$\begin{aligned} \dot{p} = {} & a_{43} \ \beta + a_{44} \ p + a_{45} \ r + b_{41} \ \delta A + b_{42} \ \delta R + b_{43} \ \delta sp \\ & + h_{41} \ \beta_w + h_{42} \ p_w + h_{43} \ r_w \end{aligned} \tag{40}$$

$$\dot{r} = a_{53}\,\beta + a_{54}\,p + a_{55}\,r + b_{51}\,\delta A + b_{52}\,\delta R + b_{53}\,\delta sp$$

$$+ h_{51}\,\beta_w + h_{52}\,p_w + h_{53}\,r_w \qquad (41)$$

where β, p and r are the sideslip angle, roll rate, and yaw rate, respectively, β_w, p_w and r_w are the sideslip angle, the roll rate, and yaw rate due to wind velocities only, δA, δR and δsp are the perturbations of the ailerons, rudder, and spoilers, respectively. The coefficients a_{ij} in the above equations depend on the aircraft stability derivatives.

The position of the aircraft relative to runway centerline is expressed by the perpendicular distance of the aircraft center of mass to the runway centerline. This distance, normalized by the aircraft's steady-state airspeed, U_o, will be used as a state variable in addition to the equations already obtained. Then, the lateral distance y (in feet) of the aircraft can be expressed by

$$\dot{y} = U_o\left[L_{ES}(2,1)(1 + u') + L_{ES}(2,2)\beta + L_{ES}(2,3)\alpha\right], \qquad (42)$$

where u' is the normalized inertial perturbation in the speed along the x_s direction and α is the perturbation in the inertial angle of attack, and

$$L_{ES}(2,1) = \cos\alpha_o \cos(\theta_o + \theta) \sin\psi + \cos\phi \sin\alpha_o \sin(\theta_o + \theta) \sin\psi$$

$$- \sin\alpha_o \sin\phi \cos\psi \qquad (43)$$

$$L_{ES}(2,2) = \sin\phi \sin(\theta_o + \theta) \sin\psi + \cos\phi \cos\psi \qquad (44)$$

$$L_{ES}(2,3) = -\sin\alpha_o \cos(\theta_o + \theta) \sin\psi + \cos\alpha_o \cos\phi \sin(\theta_o + \theta) \sin\psi$$

$$- \cos\alpha_o \sin\phi \cos\psi \quad . \qquad (45)$$

Rearranging the terms in equation (42)

$$\dot{y}' = \beta + \cos(\alpha_o - \theta_o)\,\psi - \sin\alpha_o\,\phi + \eta_y \quad , \qquad (46)$$

where η_y and y' are given by

$$\eta_y = (L_{ES}(2,2) - 1)\beta + L_{ES}(2,1)(1 + u') - \cos(\alpha_o - \theta_o)\psi + L_{ES}(2,3)\alpha + \sin\alpha_o\ \phi \quad , \tag{47}$$

$$y' = y/U_o \quad . \tag{48}$$

Note that equation (46) contains no approximation when α in (47) is interpreted as the normalized inertial velocity component in the z_s direction, but is simply a rearranged form of (42) with the nonlinear terms grouped into a single term. To obtain the second order terms for the remaining variables, note that

$$\dot{\phi} = \sec\theta_o\ (\cos\gamma_o\ p + \sin\gamma_o\ r) + \eta_\phi \quad , \tag{49}$$

$$\dot{\psi} = \sec\theta_o\ (\sin\alpha_o\ p + \cos\alpha_o\ r) + \eta_\psi \quad , \tag{50}$$

$$\dot{\beta} = \frac{a_{y_s}}{U_o} - r + \eta_\beta \quad , \tag{51}$$

where

$$\eta_\phi = (\cos\phi\ \tan(\theta_o + \theta) - \tan\theta_o)(\cos\alpha_o\ r + \sin\alpha_o\ p) \quad , \tag{52}$$

$$\eta_\phi = (\cos\phi\ \sec(\theta_o + \theta) - \sec\theta_o)(\cos\alpha_o\ r + \sin\alpha_o\ p) \quad , \tag{53}$$

$$\eta_\beta = p\alpha - ru \quad , \tag{54}$$

when q is assumed to be small.

The servo systems, hydraulic and mechanical actuator systems on this aircraft have clearly noticeable nonlinear effects. These effects include usual nonlinearities such as hysteresis, rate and position limits, as well as d.c. gain variations as a function of actuator position, dynamic pressure, etc.,

and nonlinear spoiler feedforward and feedback systems. These nonlinear effects were not included in the "control design model" described here. However, these nonlinearities were included in the simulation model, and design changes were made to accommodate these nonlinear effects during the control development using the nonlinear simulation and later during the flight tests.

The controls which affect the lateral motion of the aircraft are the aileron, rudder and spoiler surface settings as can be seen from equations (37) - (41), where the spoiler action is used mainly to aid the effect of the ailerons during turns. Thus, the spoiler setting is programmed according to the aileron setting. This is approximated and modeled here as

$$\delta s_p = C_{spa}\, \delta A \quad , \qquad C_{spa} = 1.73 \quad . \tag{55}$$

A rate command structure is used for the rudder control; hence, the rudder position is considered a state variable which is obtained by integrating the rudder rate command,

$$\dot{\delta R} = u_2 \quad , \tag{56}$$

where u_2 is considered to be the rudder rate control.

If the relation between the spoiler and aileron given in (55) is substituted in (39), (40), and (41), then the spoiler terms are eliminated from the equations. Now, forming a state vector x such that

$$x^T = (\phi \quad \psi \quad \beta \quad p \quad r \quad y' \quad \delta R) \tag{57}$$

and a control vector u such that

$$u^T = (\delta A \quad \dot{\delta R}) \quad , \tag{58}$$

equations (37) - (41), (46), (55), and (56) can be combined into a state variable

model of the lateral motion of the aicraft of the form

$$\dot{x} = Ax + Bu + Dw + \bar{\eta} \quad , \tag{59}$$

where $w^T = (\beta_w \quad p_w \quad r_w)$ and $\bar{\eta}^T = (\eta_\phi \quad \eta_\psi \quad \eta_\beta \quad 0 \quad 0 \quad \eta_y \quad 0)$.

The lateral motion of the aircraft is described by the state variable model given in equation (59); this model describes the response of the aircraft when a control is applied or when the wind velocities such as gusts or steady winds are nonzero. The effects of the wind velocities are introduced through the vector w. The components of this vector are β_w or the wind velocity along the y_s direction normalized by the airspeed of the aircraft, p_w or the rotation of the air around the aircraft about the x_s axis, and r_w or the rotation of the air around the aircraft about the z_s axis, respectively. The roll rate p_w and yaw rate r_w components of the wind vector w consist only of the effects of wind gusts, thus having an average value of zero; i.e., these components do not have a steady state effect but introduce turbulence effects into the equations. On the other hand, the β_w or the normalized lateral wind velocity contains terms for both wind gusts and steady winds; thus, it is modeled as

$$\beta_w = \beta_g + \beta_s \quad , \tag{60}$$

where β_g is the gust or turbulence term, and β_s is the steady wind term. The gust terms are of a random nature and can be modeled using the well-known Dryden spectrum. The transfer functions (i.e., the ratio of the Laplace transforms of the gust generating system output to its input) for the gust model can be expressed by

$$G_\beta(s) = -\sigma_v \left[\frac{L_v}{\pi U_o^3}\right]^{\frac{1}{2}} \frac{1 + \frac{3 L_v s}{U_o}}{\left(1 + \frac{L_v s}{U_o}\right)^2} \quad , \tag{61}$$

$$G_p(s) = \sigma_w \left[\frac{1}{L_w U_o}\right]^{\frac{1}{2}} \frac{\left[8\left(\frac{\pi L_w}{4b}\right)^{\frac{1}{3}}\right]^{\frac{1}{2}}}{1 + \frac{4b\ s}{\pi U_o}} \quad , \tag{62}$$

$$G_r(s) = \frac{r_w(s)}{\beta_g(s)} = \frac{-s}{1 + \frac{3b\ s}{\pi U_o}} \tag{63}$$

It should be noted that even though p_w is statistically independent of β_w and r_w, the latter two are not independent of each other. As shown in equation (63), the lateral gust, β_g, must be input to the system represented by the transfer function, $G_r(s)$, to obtain r_w. Since r_w is obtained from β_g, the two variables are highly correlated.

Consider the case of a steady wind. In the Earth-fixed coordinate system, the wind velocity has a component in the direction of runway centerline W_x, and a component perpendicular to the runway centerline say W_5; it is assumed that there is no steady wind in the vertical direction although gusts may be present. Hence, if L_{SE} is the transformation matrix from Earth-fixed to stability coordinates, then the steady component, β_s, of the normalized lateral wind velocity is given by

$$\beta_s = L_{SE}(2,2)\ W_5 + L_{SE}(2,1)\ W_x \quad , \tag{64}$$

$$L_{SE}(2,1) = \sin(\theta_o + \theta)\ \sin\phi\ \cos\psi - \cos\phi\ \sin\psi \quad , \tag{65}$$

$$L_{SE}(2,2) = \sin(\theta_o + \theta)\ \sin\phi\ \sin\psi + \cos\phi\ \cos\psi \quad . \tag{66}$$

To include wind shear into the model, the steady lateral wind velocity can be described as

$$\dot{W}_5 = W_6 + \omega_3 \quad , \tag{67}$$

$$\dot{W}_6 = \omega_4 \quad , \tag{68}$$

where ω_3 and ω_4 are Gaussian white noise processes independent of each other and of β_g, p_w and r_w. Now, the transfer function for the gusts described in (61), (62), and (63) can be combined into a state variable model of fourth order. Adding (67) and (68) to this model, we obtain a sixth-order model of the form

$$\dot{W} - A_w W + B_w \omega \ , \tag{69}$$

where β_w can be expressed as

$$\beta_w = \beta_g + \beta_s = W_1 + W_5 + \xi_1 \tag{70}$$

$$\xi_1 = (L_{SE}(2,2) - 1)W_5 + L_{SE}(2,1)W_x \quad . \tag{71}$$

Defining the remaining elements of the vector ξ to be zero, w can be written as

$$w = C_w W + \xi \tag{72}$$

This expression can now be substituted into (59) to obtain

$$\dot{x} = Ax + Bu + DC_w W + \eta \tag{73}$$

$$\eta = D\xi + \bar{\eta} \tag{74}$$

The design model for the lateral dynamics, including the aircraft aerodynamics, the actuators and wind conditions, is given by (73) and (74).

C. STOCHASTIC SAMPLED-DATA FORMULATION

As the aim of the study is to design and flight test a digital automatic landing system obtained by modern control techniques, this section formulates an optimal control problem using the design models obtained in the previous sections. The solution to this optimal control problem is used as an initial design in the development of DIALS. Although some modifications to the design were made to account for nonlinearities and other unmodeled effects, the basic structure of the optimal control law was left unchanged.

The optimal control problem is formulated as a stochastic sampled-data quadratic regulator with random disturbances [3] - [8] . The longitudinal and lateral control laws are treated separately, but using the same basic approach. Both the longitudinal and lateral plant models can be expressed in the form

$$\dot{x} = Ax + Bu + DC_w W + \eta \quad , \tag{75}$$

$$\dot{W} = A_w W + B_w \omega \ . \tag{76}$$

The trajectory of the aircraft during a final approach and landing includes the localizer and glideslope capture and tracking phases with the capability to crab and decrab, followed by the flare maneuver. Thus, the model of the desired trajectory must be general enough to accommodate the various phases of flight involved. It is further desirable to obtain a constant gain control law for the various phases of the final approach and landing, to the extent possible. To accommodate these characteristics, the desired trajectory is modeled in the form

$$\dot{z} = A_z z + \zeta_z \quad , \tag{77}$$

$$\dot{\zeta}_z = \xi_z \tag{78}$$

where ξ_z is assumed to be a white noise process. The desired trajectory z(t), is thus modeled as a random process whose statistical properties are determined by (77), (78). The assumption of a random trajectory is a conceptually appealing one, as it stresses the fact that the trajectory may be altered at any time; the future values of the trajectory are thus not certain, but can be predicted using the model of the trajectory. In general, for an arbitrary deterministic trajectory, the optimal control depends on future values of the trajectory [12], except when the trajectory can be expressed as the output of a homogeneous dynamic system.

The error in the actual trajectory, x(t), can now be defined as

$$e(t) = x(t) - z(t) \tag{79}$$

The models of the aircraft dynamics (75), (76) and the desired trajectory (77), (78) can be combined, and expressed in terms of the trajectory error, e(t), in the form

$$\dot{e} = Ae + Bu + DC_w W + (A - A_z)z - \zeta_z + \eta \quad , \tag{80}$$

$$\dot{W} = A_w W + B_w \omega \quad , \tag{81}$$

$$\dot{z} = A_z z + \zeta_z \quad , \tag{82}$$

$$\dot{\zeta}_z = \xi_z \quad , \tag{83}$$

$$\dot{\eta} = \xi_\eta \quad , \tag{84}$$

where ω, ξ_z and ξ_η are assumed to be Gaussian white noise processes.

Rearranging the terms in (80) - (84),

$$\dot{e} = Ae + Bu + \bar{D}d \quad , \tag{85}$$

$$\dot{d} = A_d\, d + \xi \quad , \tag{86}$$

where

$$d^T = (W^T\ z^T\ \zeta_z^T\ \eta^T) \tag{87}$$

and ξ is a white noise vector. In (85), (86), the disturbance form of the problem is apparent, where the disturbance, d, is uncontrollable by u, and is the output of a marginally stable system.

As the basic objective of the control law is to track the desired trajectory, a cost function which reduces the error vector, e, is suitable. Considerations of the closed-loop system damping make it desirable to also include cross-coupling terms. As a quadratic objective function accommodates these characteristics, results in a linear feedback law and is computationally feasible, the objective function is selected as

$$J_c = \frac{1}{2t_f} \int_o^{t_f} E\left\{e^T(t)\ Q\ e(t) + 2\ e^T(t)\ M\ u(t) + u^T(t)\ R\ u(t)\right\} dt \tag{88}$$

To obtain a discrete control law for digital implementation, the usual constraint of a constant control between sampling instants is placed

$$u(t) = u_k \quad , \quad kT_o \le t < (k+1)T_o \quad . \tag{89}$$

With the assumption of (89), the system equations in (85) and (86) and the cost function in (88) can be expressed in terms of the state variables at the sampling instants [8].

$$e_{k+1} = \phi e_k + \Gamma u_k + \Gamma_d\, d_k + \xi_{1k} \quad , \tag{90}$$

$$d_{k+1} = \phi_d \, d_k + \xi_{2k} \tag{91}$$

where e_k and d_k represent the samples $e(kT_o)$ and $d(kT_o)$, and ξ_{1k}, ξ_{2k} are white noise sequences. Similarly, the cost function (88) can be discretized in the form

$$J = \frac{1}{2(N+1)} E\left\{ \sum_{k=0}^{N} \left[e_k^T \hat{Q} \, e_k + u_k^T \hat{R} \, u_k + 2 \, e_k^T \hat{N} \, d_k + 2 \, e_k^T \hat{M} \, u_k + 2 \, d_k^T \hat{S} \, u_k \right] \right\} . \tag{92}$$

It is important to note that the discrete cost J and the continuous cost J_c differ by a constant independent of the control sequence used. Thus, to find the control sequence which minimizes the continuous cost J_c, it suffices to obtain the control which minimizes J. The control which minimizes the cost J subject to the constraints of (90) and (91), is given by [7],

$$u_k = - H_{1k} \, \bar{e}_k - H_{2k} \, \bar{d}_k \quad , \tag{93}$$

where $\bar{e}_k$ and $\bar{d}_k$ are the least mean-square estimates of e_k and d_k, respectively, given past and current measurements, and the gains H_{1k} and H_{2k} are given by

$$H_{1k} = \hat{R}_k^{-1} \, G_{1k} \quad , \qquad H_{2k} = \hat{R}_k^{-1} \, G_{2k} \quad , \tag{94}$$

$$G_{1k} = \Gamma^T \, P_{1k} \, \phi + \hat{M} \quad , \quad G_{2k} = \Gamma^T \, D_k + \hat{S} \quad , \tag{95}$$

$$D_k = P_{1k} \, \Gamma_d + P_{2k} \, \phi_d , \quad \hat{R}_k = \hat{R} + \Gamma^T \, P_{1k} \, \Gamma \, , \tag{96}$$

while P_{1k} and P_{2k} are given by the nonlinear difference equations:

$$P_{1k-1} = \phi^T \, P_{1k} \, \phi - G_{1k}^T \, \hat{R}_k^{-1} \, G_{1k} + \hat{Q} \quad , \quad P_{1N} = \hat{Q} \quad , \tag{97}$$

$$P_{2k-1} = \left[\phi - \Gamma \, \hat{R}_k^{-1} \, G_{1k} \right]^T D_k + \hat{N} \quad , \quad P_{2N} = \hat{N} \quad , \tag{98}$$

Thus, over a finite optimization interval t_f of N sampling intervals, the optimal control law is specified by (93) - (98). It should be noted that the gain H_{1k} and the cost matrix P_{1k} are the optimal solutions to the LQG problem without any disturbance; i.e., $d_k = 0$. As the optimization interval N increases, it is well-known that $H_{1k} \to H_1$; and $P_{1k} \to P_1$, under loose conditions [13], where the closed-loop system matrix $\phi - \Gamma H$, is stable. If the disturbance matrix ϕ_d satisfies $\rho(\phi_d) \leq 1$, it can be shown that $P_{2k} \to P_2$ as the optimization interval N increases without bounds, and the cost, J, converges to a finite value. It should be noted that, due to the random plant noise added at every sample, the averaging of the cost over the optimization interval is necessary to maintain a finite stochastic cost in any (stochastic) LQG problem. The gains H_1 and H_2 can then be obtained by solving (94) - (98). Using these steady-state gains and expanding the components of d_k, the control law in (93) can be rewritten as

$$u_k = -H_e \bar{e}_k - H_w \bar{W}_k - H_z z_k - H_\zeta \zeta_{zk} - H_\eta \bar{\eta}_k \quad , \tag{99}$$

It is seen that the control law feeds back the estimates of the error in the trajectory to stabilize the error dynamics with the same gain that would be obtained from the no wind, no path following case. However, the control law uses additive terms depending on the desired trajectory, z_k and ζ_{zk}, for tracking purposes, and uses the second order nonlinear term η_k as well. Finally, the wind estimate $\bar{W}_k$ is used directly in the control law to prevent offsets due to wind conditions. The estimates of the trajectory error and wind velocities are obtained using steady-state Kalman filters driven by the onboard sensors and the MLS signal.

The phases of the final approach and landing considered are the localizer and glideslope capture and track, crab/decrab and flare to touchdown. The range of flight conditions considered is 2.5° - 5.5° for glideslope angle, 115 - 135

knots for airspeed, 70,000 - 90,000 lb for aircraft weight, .2 - .3 for c.g. location, and crosswinds below 15 knots.

The main considerations in the development of DIALS include the overall smoothness of the flight during the final approach, low overshoots of the localizer and glideslope, quick settling on the trajectory and accurate tracking in adverse weather conditions including gusts and shear winds. However, the relative importance of these desirable characteristics varies with the phase of the final approach considered. For example, low overshoot characteristics under differing wind conditions are particularly important during the localizer and glideslope capture maneuvers whereas the actual capture path is of secondary importance; however, during the flare maneuver, the vertical path error is more significant, and, in particular, the touchdown pitch attitude must be sufficiently positive to avoid landing on the nose gear. Similarly, when tracking the localizer and glideslope, it is important to avoid any offsets and have low sensitivity to wind gusts. A more detailed description of the desirable characteristics in the various control modes is given in Section IV. To achieve these varying objectives, it appears that some changes in the control law, from one phase of the flight to the next, are necessary.

Some of the differing objectives for each phase of the final approach can be accommodated by different values of the weighting matrices (Q, R) in the cost function. However, in an optimal control design, this would necessitate changing all of the gains of the control law at the initiation of each mode, along with possible transient problems due to switching gains. To avoid possible complexity, the approach taken was to obtain a basic design considering the total trajectory, and then vary a small number of gains using easy-on's and to modify the structure by switching integrators in or out appropriately, at the initiation of each mode. Thus, the basic design model does not contain

any integrators; however, when the objective requires it, integrators are switched in or out. For example, at the initiation of the localizer (or glide-slope) track mode, the integral of the lateral (or vertical) offset is introduced to obtain a type 1 system without steady offsets. Thus, the basic design is obtained as a stable closed-loop system to which modifications are switched in or out at each mode according to the main objectives of that mode. The specific modifications made at each phase are detailed in Section IV.

Nonlinearities in the system and unmodeled effects in the aerodynamic characteristics, actuator systems, sensors and electronics were simulated in as much detail as available to obtain a realistic computer simulation of the overall system. As these nonlinearities are not included in the design model, the optimal control law obtained does not directly accommodate their effects. Although the robustness of the control law will indirectly accommodate some of the nonlinearities and unmodeled dynamics, the remaining effects on the performance were then reduced or eliminated by minor modifications to the control law, using the simulation.

Thus, the approach to the overall design of the digital automatic landing system (before flight tests) was:

1) obtain an optimal control law for a nominal condition as a starting point,

2) using realistic nonlinear simulations, modify and update this law to account for the various nonlinearities in the actuator servomechanisms, hydraulic systems, engine dynamics and the aerodynamic response, as well as to enhance desirable characteristics which may not adequately be reflected in a quadratic cost function,

3) identify a small number of modifications which can be made at each phase of flight to achieve the differing objectives of each mode.

It should also be noted that the cost function (88) penalizes the error in the actual trajectory relative to the desired trajectory; however, it also penalizes the total control u. As noted in [7], such a cost function does not necessarily provide sufficient trim unless the cost matrices are appropriately selected or the control cost is modified to penalize the deviation from a preselected trim [14]. For example, consider the action of the elevator and stabilizer. On the TSRV B-737 research aircraft, the effects of the elevator and stabilizer on the motion of the aircraft are the same, except that the effectiveness of the larger stabilizer surface is twice that of the elevator. It is desirable to make trimming changes using the stabilizer, and maintain the elevator near its equilibrium position (referenced at 0) to avoid high moments on the elevator hinge over sustained periods of time. Of course, the fast motion (due to the actuators) of the elevator is used to stabilize the dynamic modes of the aircraft. Since the trim values required on different glideslopes, or wind conditions, or c.g. locations, etc. vary with the particular condition encountered, it is desirable to have the stabilizer position move to trim the aircraft, while the elevator is maintained at low hinge moment values except in transients. Thus, it is desirable not to penalize stabilizer position, but to penalize elevator position to obtain the desired trimming action. Since, it is also desirable (and necessary) to have slow stabilizer motion, high stabilizer rate should be appropriately penalized to obtain smoother transitions. Thus, appropriate selection of the cost matrices with rate command structure can provide appropriate trimming with optimal control formulation described in the previous section. Similarly, throttle position is not penalized, while a nonzero penalty on throttle rate provides smoother and slower autothrottle action. In general, control activity can be placed at desirable levels by penalizing the control rate.

To obtain a 3-D control law, the variable corresponding to distance along runway centerline ($x_{\ell 5}$) was eliminated from the equations of motion for the design model. However, the filter development model included (and estimated) this variable.

D. STATE AND WIND ESTIMATION

The sampled-data formulation of the design problem requires estimates of all the state variables in its implementation. As the states corresponding to the desired trajectory are known, these variables are not estimated. However, the aircraft motion variables and, in particular, the wind velocity variables including steady winds, shear winds and gusts are required for quick control adjustments to changing wind conditions in the full-state feedback formulation*.

The MLS position information and the on-board sensor signals are fed to the longitudinal and lateral DIALS filters shown in Figures 3 and 4. The filtered estimates are then used to compute the control surface commands as well as to define the desired path. The form of filter used is a discrete Kalman filter with constant gains. The steady-state Kalman filter gains were obtained as a starting point, then some gains were modified to obtain better performance using a nonlinear simulation of the aircraft. The use of constant gains for the Kalman filters reduces the considerable computation requirements imposed by the error covariance updates. The use of discrete filters along with digital controls is well suited to the discrete nature of MLS guidance system. The goals of the filter development include the accurate estimation of the aircraft's position, velocity, attitude and wind velocities using on-board sensors usually available on commercial aircraft, but without using costly inertial platforms,

---

*The author's recent development of a fast, reliable and convergent algorithm for the stochastic output (limited state) feedback problem has made the use of optimal dynamic compensation along with complementary filters practical, and more desirable in high order problems [15].

and angle of attack or sideslip sensors which are not currently available on many aircraft.

The aircraft's position is obtained using the MLS guidance system, which provides volumetric coverage in the terminal area. The aircraft receives range, azimuth and elevation information at discrete intervals from which it can obtain its position with high accuracy even under adverse weather conditions. The ground azimuth antenna is located at the runway centerline with coverage up to ±60°. The DME antenna which provides the range of the aircraft is generally co-located with the azimuth antenna. If the DME is located to the side of the runway, a simple transformation can be used to obtain the aircraft's position. The elevation antenna is located at the glidepath intercept point (GPIP), but is offset to the side of the runway; it provides the aircraft's elevation angle up to 20°. Thus, the aircraft has accurate position information in the volume of space within the limits mentioned above.

Consider a right-handed coordinate frame with its origin at the phase center of the azimuth antenna, the x-axis along runway centerline and positive towards the runway, and the z-axis positive vertically upwards. If the position of the aircraft in this coordinate system (the MLS coordinate frame) is (x_o, y_o, z_o), then the MLS signals have the values given by the formulas below.

$$R = \sqrt{x_o^2 + y_o^2 + z_o^2} \tag{100}$$

$$Az = \sin^{-1} \frac{-y_o}{R} \tag{101}$$

$$El = \tan^{-1} \frac{z_o}{\sqrt{(x_o - x_E)^2 + (y_o - y_E)^2}} \tag{102}$$

where x_E and y_E are the x and y coordinates of the elevation antenna phase center in the MLS coordinate frame.

The onboard sensors used are three body-mounted acceleromaters, attitude gyros for the pitch, roll and yaw angles, attitude rate gyros, baromatric altitude and sink rate, airspeed and radar altitude. The filter does not require expensive inertial platforms for sensor measurements. All of the onboard sensors are usually available on commercial aircraft except for the body accelerometers. However, the acceleromaters are relatively inexpensive instruments and in many of the newer aircraft, a normal accelerometer already exists for pitch axis control. It should be noted that the radar altitude measurement is used in place of the MLS elevation signal only after the aircraft crosses the runway threshold since the aircraft flies out of the MLS elevation coverage during the flare maneuver.

To provide accurate estimates of the wind velocity components in the longitudinal, lateral and vertical directions, the filters were formulated using the aerodynamic properties of the aircraft. In addition, estimates of the bias errors in the three body-mounted accelerometers, barometric altitude and sink rate and attitude sensors are also obtained by the filters. The lateral filter uses the roll and yaw attitude, yaw rate and roll rate, the processed MLS y_o measurement, and the lateral accelerometer. The remaining measurements are used for the longitudinal filter. Discrete longitudinal and lateral Kalman filters were formulated with steady-state gains, with some cross-coupling using second order terms and wind estimates. The measurement bias terms were not included in the Kalman filter formulation and the steady-state gain computations, but the required gain matrices were obtained using simple approximations. The basic form of the filters can be expressed by

$$\nu_k = y_k - C_x \hat{x}_k - C_w \hat{W}_k - C_b \hat{b}_k \quad , \tag{103}$$

$$\hat{x}_{k+1} = \phi \bar{x}_k + \Gamma u_k + \Gamma_w W_k + \psi \bar{\eta}_k \quad , \tag{104}$$

$$\hat{W}_{k+1} = \phi_w \bar{W}_k \quad , \tag{105}$$

$$\bar{x}_k = \hat{x}_k + F_x \nu_k \quad , \tag{106}$$

$$\bar{W}_k = \hat{W}_k + F_w \nu_k \quad , \tag{107}$$

$$\hat{b}_{k+1} = \hat{b}_k + F_b \nu_k \quad , \tag{108}$$

where $\hat{x}_k$, $\hat{W}_k$, $\hat{b}_k$ are predicted values and $\bar{x}_k$, $\bar{W}_k$, $\bar{\eta}_k$ are filtered values.

It should be noted that whereas the control gains are based on the longitudinal and lateral sampled-data formulation of the previous section (i.e., (90) and (91)), the design of the Kalman filters do not use the same models in obtaining the filter gains. As most of the variables in d_k are known trajectory parameters and η_k is a (nonlinear) function of x_k, only attitude, attitude rate, position, inertial velocity and wind velocity need to be estimated or simply be filtered for noise. Thus, in the above equations, the control position variables in the vector x_k are not included in the estimation, and $\bar{\eta}_k$ is computed using $\bar{x}_k$.

The position equations used in the filter implementation have a strong dependence on the glideslope angle, γ_o, selected for the particular approach from the continuous equations (9), (10). While the filter gains F_x, F_w and F_b are kept constant, the elements of the ϕ matrix corresponding to the position variables are modified to account for different glideslope angles. Since the glideslope angle has to be entered into the flight computers prior to glideslope capture, the computation of these elements can be done in real-time.

Table 1 shows the sensor error statistics used in a nonlinear simulation of the sensor outputs. The filter designs were tested in simulation prior to the DIALS flight tests. During the simulation, some gains were modified to obtain better performance of the overall control law.

III. IMPLEMENTATION OF THE DIGITAL CONTROL LAW

The digital integrated automatic landing systems (DIALS) is designed for flight testing on the Transport Systems Research Vehicle (TSRV), a Boeing 737-100. The research aircraft is equipped with various onboard sensors, four General Electric 703 digital computers*, as well as monitoring, testing, and recording facilities. The digital control law is implemented on the GE 703 flight computers.

The flight computers are 16 bit, fractional machines with fixed-point arithmetic. The constraint of fixed-point arithmetic with 16 bit words makes the software implementation of a complex digital control law considerably more complicated than a floating-point arithmetic machine. To insure the accuracy of the control command computations, it is necessary to meticulously keep track of every variable in the computer memory for range and resolution. Since most variables in the software are intermediate variables, not explicitly treated in the design of the control law, this task results in considerable effort.

A. SCALING AND ROUND-OFF ERROR ANALYSIS

By considering the physical meaning of the variables involved, and the expected flight profile, safe upper and lower limits for each variable can be assigned. These limits determine the scaling necessary for each variable. As long as the resolution with 16 bits does not violate the accuracy requirements for that variable, a single precision representation may be possible. Otherwise, a double precision representation is necessary for that variable. As the flight computers use two's complement arithmetic an overflow can have devastating effects, and must be guarded against with great caution. From the point of view

*The GE 703 computers are currently being replaced by Norden 1170 computers.

of overflow, only the position variables require double precision representation in the implementation of DIALS.

The accuracy of the control law computations also depends on round-off errors introduced in the multiply-add operations required. The computations required to obtain the control commands are described by (99), the filter computations by (103) - (108). Equation (99) results in the commanded control variables, and is obtained by a finite number of multiply-add operations whose accuracy is easy to analyze. However, the filter computations are recursive, so that errors introduced in previous computations are processed through the filter every iteration, and may produce much larger errors. If the errors introduced due to round-off exceed the accuracy desired, it is necessary to use double precision arithmetic to reduce these errors.

An analysis of the accumulation of the round-off errors can be made in the following manner. The filter equations in (103) - (108) can be expressed in the form

$$\nu_k = y_k - C_o \hat{X}_k \quad , \tag{109}$$

$$X_k = \hat{X}_k + F_o \nu_k \quad , \tag{110}$$

$$\hat{X}_{k+1} = \phi_o X_k + \Gamma_o U_k \quad , \tag{111}$$

where $\hat{X}_k$ and X_k correspond to predicted and filtered variables, respectively, and are stored in the same locations in computer memory. Each of the variables in the vectors X_k, U_k, ν_k and y_k are scaled by the diagonal matrices S_x, S_u, S_ν and S_y, respectively.

Let the superscript " ~ " denote the actual representation of a vector in the computer. Then the operations actually performed can be expressed in the form

$$\tilde{\nu}_k = \left(S_\nu^{-1}\ I\ S_y\right)\tilde{y}_k - \left(S_\nu^{-1}\ C_o\ S_x\right)\tilde{\hat{X}}_k + \varepsilon_{\nu k} \quad , \tag{112}$$

$$\tilde{X}_k = \tilde{\hat{X}}_k + \left(S_x^{-1}\ F_o\ S_\nu\right)\tilde{\nu}_k + \varepsilon_{xk} \quad , \tag{113}$$

$$\tilde{\hat{X}}_{k+1} = \left(S_x^{-1}\ \phi_o S_x\right)\tilde{X}_k + \left(S_x^{-1}\ \Gamma_o\ S_u\right)\tilde{U}_k + \varepsilon_{\hat{x}k} \quad , \tag{114}$$

where $\varepsilon_{\nu k}$, ε_{xk} and $\varepsilon_{\hat{x}k}$ are the round-off errors introduced in performing the operations implied by (112), (113), and (114), respectively. These errors depend on the order in which the multiply-add operations are performed, the number of bits retained in a product when the add operation is performed, and the actual number of operations which produce round-off error. In general, these errors are nonlinear funtions of the variables which are complicated to treat analytically. However, under some assumptions [16],[17], the statistical nature of the error can be modeled as a sequence of uncorrelated random vectors with uniform distribution. When a large number of operations are involved the probability distribution function resembles the Gaussian distribution [17].

Denoting the scaled coefficient matrices in (112) - (114) by the subscript "1", these equations can be combined to obtain

$$\tilde{\hat{X}}_{k+1} = \left[\phi_1 - \phi_1\ F_1\ C_1\right]\tilde{\hat{X}}_k + \left(\phi_1\ F_1\ I_1\right)\tilde{y}_k + \Gamma_1\ \tilde{U}_k + \bar{\varepsilon}_k \quad , \tag{115}$$

$$\bar{\varepsilon}_k = \varepsilon_{\hat{x}k} + \phi_1\ \varepsilon_{xk} + \phi_1\ F_1\ \varepsilon_{\nu k} \quad . \tag{116}$$

The representation $\tilde{\hat{X}}_k$ corresponds to $S_x\ \tilde{\hat{X}}_k$ in engineering units, thus, let

$$\hat{E}_k = \hat{X}_k - S_x\ \tilde{\hat{X}}_k \quad ; \tag{117}$$

then

$$\hat{E}_{k+1} = \left[\phi_o - \phi_o\ F_o\ C_o\right]\hat{E}_k + \varepsilon_k \quad , \tag{118}$$

$$\varepsilon_k = \phi_o\ F_o\ S_y\ \varepsilon_{yk} + \Gamma_o\ S_u\ \varepsilon_{uk} + S_x\ \bar{\varepsilon}_k \tag{119}$$

where ε_{yk} and ε_{uk} are the round-off errors introduced by representing Y_k as $S_y \tilde{Y}_k$, and U_k as $S_u \tilde{U}_k$, respectively; i.e., input quantization. To obtain a measure of the magnitude of the errors $\hat{E}_k$, let

$$R_{\hat{E}} = \lim_{k\to\infty} E\left(\hat{E}_k \hat{E}_k^T\right) \quad , \qquad R_{\varepsilon} = E\left(\varepsilon_k \varepsilon_k^T\right) \quad , \tag{120}$$

where E denotes the expectation operator. From (118),

$$R_{\hat{E}} = \phi_o \left(I - F_o C_o\right) R_{\hat{E}} \left(I - F_o C_o\right)^T \phi_o^T + R_{\varepsilon} \quad . \tag{121}$$

The solution of this Lyapunov equation provides the covariance of the error due to round-off after a large number of iterations of the Kalman filter.

$$R_{\bar{\varepsilon}} = \sigma^2 \left[n_{\hat{x}k} + \phi_1 \, n_{xk} \, \phi_1^T + \phi_1 \, F_1 \, n_{\nu k} \, F_1^T \, \phi_1^T\right] \quad , \tag{122}$$

where σ^2 is the variance of the error due to rounding one variable. For a 16 bit fixed-point machine,

$$\sigma^2 = \frac{2^{-32}}{3} \tag{123}$$

The matrices $n_{\hat{x}k}$, n_{xk}, $n_{\nu k}$ are diagonal, with the entry in each row corresponding to the number of times a round-off error is introduced in the corresponding equation in (112) - (114). Usually this is the number of multiply operations performed in each scalar equation.

It should be noted that the effects of scaling, the order in which the equations are implemented (i.e., (112) - (114)), the word size, as well as some special procedures can be computed and analyzed with this approach. Tables 2 - 7 shows the resolution, range and accuracy required for the DIALS implementation.

When appropriate scaling is done, the error introduced by a small number of round-off errors can usually be neglected. From (99), it can be seen that the error in the control commands u_k due to round-off can be approximated by

$H_e \hat{E}_k$ with covariance $H_e R_{\hat{E}} H_e^T$.

Consideration of these effects shows that the position computations, and the innovation computations should be performed in double precision to have sufficient accuracy in the control commands.

B. CONTROL IMPLEMENTATION FORM

The Experimental Avionics System Integration Laboratory (EASILY) at the Langley Research Center (LRC) provides a facility where a control law implementation can be tested in real-time. The basic procedure is to code the control law to be tested in the flight computer which will be used onboard the aircraft. The flight computer is then brought to the EASILY lab and interfaced with a detailed, nonlinear, six-degrees-of-freedom, real-time digital simulation of the aircraft and its subsystems. The facility contains CRT displays which simulate the displays on the TSRV research aircraft so that the simulated flight can be monitored. As the digital real-time simulation of the aircraft dynamics and its subsystems is located in a different building, the flight computer and displays at the EASILY laboratory are connected to the simulation through communication lines.

While the communication lines linking the digital aircraft simulation to the flight computer containing the control law are expected to introduce some delay in the signals, the magnitude of such delays was not originally established. Tests of the end-to-end delays show that these can reach 200 msec, with an average lag in the vicinity of 100 msec. The large magnitude of this delay is partially due to the signal conditioning at both the EASILY lab and at the digital simulation facility. A further difficulty is introduced by the fact that the digital flight control computer and the digital aircraft simulation computer operate asynchronously. This introduces delays of random magnitude, partially explaining the variation in the measured amounts.

Considering the fact that DIALS operates at a low sampling rate of 10 Hz (a sampling interval of 100 msec.), delays of the same magnitude clearly introduce significant difficulties in its performance. It is well-known that delays as low as half the sampling interval of a control law can destabilize the closed-loop system [18]. Thus, the actual implementation of DIALS was modified to accommodate delays of the magnitude of 100 msec.

To minimize the software and design impact, the following approach is used to implement the DIALS equations. Consider the system equations given in (90) and (91), and the form of the control law given in (93). Let $\rho \geq 0$, and consider

$$u_k - \rho\, u_{k-1} = - H_1\left(\bar{e}_k - \rho\, \bar{e}_{k-1}\right) - H_2\left(\bar{d}_k - \rho \bar{d}_{k-1}\right) \quad . \tag{124}$$

From the filter equations, it can be seen that

$$\bar{e}_k = \phi\, \bar{e}_{k-1} + \Gamma_d\, \bar{d}_{k-1} + \Gamma\, u_{k-1} + G_1\, \nu_k \quad , \tag{125}$$

$$\bar{d}_k = \phi_d\, \bar{d}_{k-1} + G_2\, \nu_k \tag{126}$$

Substituting (125) and (126) into (124), regrouping terms neglecting ν_k results in

$$u_k = \left(\rho\, I - H_1\, \Gamma\right) u_{k-1} - H_1\left(\phi - \rho\, I\right)\bar{e}_{k-1} - \left[H_2\left(\phi_d - \rho\, I\right) + H_1\, \Gamma_d\right] d_{k-1} \tag{127}$$

It is important to note that in this form, u_k depends only on previous samples, and can be computed ahead of time; so that if the simulation has a known delay, then u_k can be commanded as soon as it is computed to counteract, or reduce, the actual delay. While during the flight tests, it can be commanded at its intended time. It is important to note that neglecting the innovation terms corresponds precisely to using the predicted state rather than the filtered state; i.e.,

$$u_k = - H_1 \hat{e}_k - H_2 \hat{d}_k \quad . \tag{128}$$

Also note that, except for the first term, (127) is of the same form as before in terms of software, whereas $\hat{e}_k$ is obtained at a later time. Furthermore, (127) introduces a smoothing of the control commands which is preferable.

It is interesting to note that the closed-loop poles with this control form are the same as before. However, new poles have been introduced, as the order of the system has increased by augmenting the state by u_k. The new system contains a real closed-loop pole at $\lambda = \rho$ of order r, the number of controls. This can be seen by noting that the eigenvalue/eigenvector equations

$$\phi\, e + \Gamma\, u = \lambda\, e \quad , \tag{129}$$

$$- H_1\left(\phi - \rho\, I\right)e + \left(\rho\, I - H_1\, \Gamma\right)u = \lambda\, u \quad , \tag{130}$$

hold if, and only if,

$$\phi\, e + \Gamma\, u = \lambda\, e, \quad \text{and} \left\{u = - K\, e \quad \text{or} \quad \lambda = \rho\right\} \quad . \tag{131}$$

Now, if u equals - K e, then

$$\left(\phi - \Gamma\, K\right) e = \lambda\, e \quad , \tag{132}$$

so that λ is an eigenvalue of $\left(\phi - \Gamma\, K\right)$, the closed-loop system with (93). While if $\lambda = \rho$, ρ is an eigenvalue of the new system. The eigenvalues equal to ρ have linearly independent eigenvectors. Appropriate choice of ρ, i.e., $-1 < \rho < 1$, maintains the stability of the closed-loop system.

C. MISCELLANEOUS IMPLEMENTATION ISSUES

While it is almost impossible to mention all the issues that come up in designing and implementing a complex system such as DIALS, a few of these are

mentioned in the following.

1. Stabilizer Trim

DIALS is designed with an independent stabilizer trim control. The stabilizer command has the tendency to seek a stabilizer position where the elevator position is zero. This is desirable to reduce the moment load on the elevator hinges.

On the other hand, the stabilizer trim design on the TSRV is difficult to modify to allow independent operation. Thus, the implementation of DIALS in the flight tests uses the TSRV's original trim to reduce costly mechanical modifications to the aircraft systems.

The approach used to modify the original DIALS design is to form a new elevator command by combining the original elevator and stabilizer commands. Noting that the stabilizer effectiveness in the flight regime considered is approximately twice as high as that of the elevator, the elevator command implemented adds the DIALS stabilizer command, multiplied by a factor of two, to the original elevator command. This elevator command and the TSRV stabilizer trim function operate simultaneously.

The stability of the system with this modification was investigated along heuristic lines, by noting that the elevator command implemented produces essentially the same moments on the aircraft as the original design. The stabilizer trim only acts to rearrange the proportion of these moments produced by the elevator and the stabilizer.

2. Sampling Rate

The design of the control and filter gains in DIALS is based on a sampling rate of 10 Hz (i.e., 100 msec sampling interval) for both the control commands and the sensor signals. On the other hand, the GE 703 digital flight computers on which DIALS is implemented has a major cycle of 49.152 msec. Thus, DIALS

is implemented at a rate of 2 major cycles per iteration, or a sampling interval of about 98.3 msec, rather than the 100 msec used in the design.

To assess the magnitude of the effects introduced by such a mismatch in the sampling rate, consider

$$\phi(T+\varepsilon) = e^{A(T+\varepsilon)} = e^{AT}\, e^{A\varepsilon} \simeq e^{AT}\, (I+A\varepsilon) \ , \tag{133}$$

$$\Gamma(T+\varepsilon) = \int_0^{T+\varepsilon} \phi(\tau)\, d\tau\, B = \Gamma(T) + \phi(T)\, \Gamma(\varepsilon) \simeq \Gamma(T) + \phi(T)\, B\varepsilon \ . \tag{134}$$

It can be seen that the effect of a sampling mismatch can be viewed in terms of controlling a modified plant with gains designed for a somewhat different plant. The variation in the plant parameters is of first order in the sampling interval mismatch ε, with sensitivity directions along $\phi(T)A$ and $\phi(T)B$.

During the development phase of DIALS, in numerous simulations corresponding to various flight conditions, the original gains have been slightly modified to attain a level of insensitivity to parameter variations. Thus, it would be expected that, given the small magnitude of the mismatch, the effects would not be large. Simulations of this condition show that the effects are not particularly noticeable when sensor noise and gusts are present. The flight test results tend to confirm the simulation results.

3. Use of "Easy-on" Smoothing

During the final approach and landing, the aircraft captures the localizer and glideslope (sometimes simultaneously), tracks the localizer and glideslope, crabs and decrabs, and flares to touchdown. Each of these phases introduces a new mode in the control law, as will be described in the following sections. In each mode, the commanded trajectory changes. Similarly, when the aircraft reaches a low altitude, the MLS elevation signal degrades and is essentially unavailable past its antenna located at the glidepath intercept point (GPIP).

Thus, the DIALS filter switches from the elevation signal to the radar altimeter signal.

To enhance the smoothness of the flight and avoid undesirable transient effects, easy-on smoothing is used in switching from one commanded path to another, when sensor signals are switched, or when control gains are changed. The easy-ons used are mostly linear and exponential. The period over which an easy-on operates is obtained by heuristic considerations, simulation results and flight tests, as the theoretical formulation does not include this particular type of smoothing. The effect of the smoothing is to avoid transients excited by sudden changes in velocity and acceleration; the stability of the system, however, is unaffected by such smoothing.

4. Barometric Sink Rate

The longitudinal Kalman filter in DIALS uses a sink rate measurement obtained from barometric altitude augmented by a normal accelerometer. During the implementation phase, it was found that the barometric sink rate signal available on the aircraft is obtained by mechanically differentiating the barometric altitude signal, and does not contain a normal accelerometer. So that this sink rate signal is of very low quality, particularly in turbulence, with errors reaching 30 - 40 ft/sec depending on the wind conditions.

The implementation of DIALS during the flight tests uses a sink rate signal obtained by complementary filtering the MLS altitude signal with body-mounted accelerometers avoiding a redesign of the longitudinal Kalman filters.

5. Engine Pressure Ratio Versus Thrust

While the thrust provided by the engines at a given level of throttle is not directly measured, the engine pressure ratio (EPR) for both engines is measured and available in the flight computers. An estimate of the thrust can be obtained using the measured values of the engine pressure ratios.

To obtain an analytical relationship between EPR and thrust for the range of expected flight conditions, data are obtained using steady state or trim values of EPR and thrust from a detailed simulation of the aircraft and its subsystems for a range of mach numbers varying from .17 to .24. A c.g. location of .25, altitude of 1000 ft, and various glidepath angles, airspeeds, weights, etc., are used in obtaining the data. A linear fit of the form

$$T = a(EPR) + b \quad , \tag{135}$$

$$a = 26.7878, \quad b = -25.9395 \quad , \tag{136}$$

fits the data obtained with a maximum error of 30 lb over the range of mach numbers expected. This relationship is used to obtain an estimate of the thrust is the units of 1000 lb. As the data are obtained from the simulation model, and for steady-state conditions, the actual accuracy of the estimate in a dynamic, gusty environment is not clearly determined.

Finally, the flight software was tested successfully in static tests, by comparing results with those obtained from the simulation of DIALS on the LRC Computer System. Dynamic tests of the flight software were also performed. Dynamic tests require the use of an aircraft simulation as part of the dynamics. Due to synchronization requirements, the aircraft simulation used in the dynamic tests was implemented on a different computer than the one used for control law design. Thus, due to differences in the two aircraft simulations, the dynamic tests were only able to produce a less-than-perfect check of the flight software. Despite lengthy debugging attempts, some software bugs made their way to the flight tests and were discovered during the flights, while others probably were not.

IV. FLIGHT TEST RESULTS

The Digital Integrated Automatic Landing System (DIALS) described in the previous sections was flight tested on the Transport Systems Research Vehicle (TSRV), a Boeing 737-100, to test and demonstrate a modern control direct-digital-design automatic landing system. The flight tests were conducted by the National Aeronautics and Space Administration's Langley Research Center at Wallops Island Center. This section discusses the performance of the automatic control system during each phase of the final approach and landing and describes the corresponding control mode in further detail.

The phases of flight for which the flight tests were conducted follow.

1) Localizer capture
2) Steep glideslope capture
3) Localizer track
4) Glideslope track
5) Decrab
6) Flare

The localizer and glideslope captures can be performed independently or simultaneously depending on the aircraft position relative to the Glide Path Intercept Point (GPIP). Another feature of the automatic landing system is that it can perform steep approaches. This is achieved by selecting the glideslope angle at any time prior to glideslope capture within the limits of 2.5° to 5.5°. Typically, the aircraft is positioned, manually or automatically, below the selected glideslope so as to intercept the localizer at a selected airspeed, as shown in Figure 1. When the localizer or glideslope capture criteria are satisfied, the corresponding capture mode is engaged; so that depending on the initial aircraft position and attitude, the localizer and glideslope can

be captured simultaneously or sequentially. As the aircraft reaches the localizer or glideslope, the corresponding track (or hold) modes are engaged. When a cross-wind component is present, the control system crabs the aircraft into the wind, followed by a decrab maneuver when a decrab altitude is reached. A flare path which depends on the glideslope selected for a given approach is generated on-line, and the aircraft is controlled about this path until touchdown.

The runway at NASA Wallops Flight Center used for the DIALS flight tests is equipped with a high accuracy Microwave Landing System (MLS). The MLS receiver onboard demodulates the signals and feeds the elevation azimuth and DME information into the flight computer.

A. LOCALIZER CAPTURE

In the localizer capture mode, the control law tries to perform a smooth transition from the aircraft's initial position to the runway centerline, so that the aircraft can quickly settle and stabilize on the localizer. Two characteristics are stressed in the design and development of DIALS for this mode: the reduction of overshoots, and rolling away from the localizer during the capture. Consistently low overshoots of the localizer are particularly important in airports with close parallel runways. This property can be used to increase the efficiency of the terminal area as it allows the two parallel runways to be operated independently. A low overshoot reduces the settling time on the localizer, thus allowing close-in captures when necessary.

The second characteristis is to initiate the capture maneuver by rolling the aircraft away from the runway centerline. Pilots usually initiate localizer capture in this fashion, and consider rolling towards the runway centerline "the wrong direction". This property can be obtained by initiating the localizer capture when the natural tendency of the control law is to roll in the

desired direction. To achieve this property, consider the component of u_k in (99) corresponding to the aileron command. The distance, y_k, from the localizer at which the aileron command crosses zero was selected to initiate the localizer capture mode. Assuming level wings and using the inital conditions for the filter states, and neglecting small terms, a localizer capture criterion of the following form can be obtained

$$|\bar{y}_k| < U_o|c_1 \bar{\psi}_k + c_2 \bar{\beta}_k + c_3 \bar{\beta}_{wk}| \quad , \tag{137}$$

$$c_1 = H_{e\,1\,2}/H_{e\,1\,6} \quad , \qquad c_2 = H_{e\,1\,3}/H_{e\,1\,6} \tag{138}$$

$$c_{1\,3} = (H_{w\,1\,5} + H_{\zeta\,1\,3} A_{3\,3} + H_{\zeta\,1\,4} A_{4\,3} + H_{\zeta\,1\,5} A_{5\,3} + H_{\zeta\,1\,6} A_{6\,3})/H_{e\,1\,6} \tag{139}$$

where $\bar{y}_k$ $\bar{\psi}_k$, $\bar{\beta}_k$, and $\bar{\beta}_{wk}$ are estimates of the distance from runway centerline, the heading relative to the runway, the inertial normalized side velocity and the normalized cross-wind velocity, respectively.

The localizer capture mode is initiated automatically when the inequality holds. The constants are chosen so that the initial tendency is to roll away from the localizer with the possible exception of conditions when the aircraft is already rolled as desired, say due to gusting winds. It should be noted that the localizer capture mode is engaged farther away from the runway centerline when the desired speed U_o is higher, as would be expected. To further ensure a smooth transition, an "easy-on" function was used on the aileron command signal.

To avoid large overshoots beyond the runway centerline, appropriate closed-loop damping of the control law was obtained by proper selection of the weighting matrices Q and R, with subsequent testing in the simulation of the localizer capture.

Figures 5 - 10 show the localizer capture phase of the landing during the flight tests. As can be seen from the plots, the localizer overshoot is rather small even in the presence wind conditions with 15 knot cross-wind components. The flights test included localizer intercept angles up to 50°. The average value of the localizer overshoot over all the flights is 24.2 ft, with a standard deviation of 25.7 ft, as shown in Table 8.

It should be noted that the aircraft can be considered to have settled on the localizer within approximately 40 sec in most cases. Also note that the initial tendency of the aircraft is to roll away from the runway, as desired. It should also be noted that the design does not use an integrator on the sideslip angle in order to null it; so that during the capture the sideslip angle is not centered about zero. Although in steady wind conditions the angle is small, in high gust conditions it can reach higher values. It is desirable to modify the design to produce lower sideslip, particularly in high gust conditions, without modifying the other characteristics of the control law.

It should be noted that while all three runs show the presence of cross-winds, the flight shown in Figure 9 corresponds to high turbulence conditions, as can be seen by the cross-wind estimate and the variation in the attitude.

B. GLIDESLOPE CAPTURE

The desirable properties of the glideslope capture mode include low overshoot and the tendency to pitch down at the initiation of the capture. To have a low overshoot of the glideslope for the various steep glideslope angles that may be selected (i.e., 2.5° - 5.5°), it is desirable to initiate the capture when the aircraft is well below the glideslope. This approach is different than the practice of engaging the glideslope hold mode when the glideslope is intercepted (e.g., see [9]), where an overshoot, even if small, cannot be avoided.

Initiation of the capture mode below the glideslope alone does not guarantee a low overshoot. Thus, some experimentation in the selection of the weighting matrices coupled with simulation was used to achieve this property. In particular, for both overshoot characteristics and smoothness of maneuver, the sink rate command was eased on from zero to the glideslope sink rate. This implementation provides a simple method of adjusting the speed with which the capture maneuver is performed without an appreciable overshoot.

While engaging the capture mode below the glideslope is desirable for overshoot characteristics, it also produces an initial tendency for the aircraft to pitch up. To avoid this effect, the capture engage logic was selected so that the initial tendency of the elevator is to produce a negative pitching moment.

To achieve this property, consider the component of u_k, in (99), corresponding to the elevator command. If the glideslope capture mode is engaged at the altitude, h_{GSC}, where the elevator command crosses zero, it can be seen that the initial elevator command will tend to gradually produce a negative pitching moment.

While the thrust also has a considerable contribution to the pitching moment in this aircraft, due to the engine location, the DIALS autothrottle and engine dynamics have much longer time constants than those associated with the elevator. Thus, changes in the throttle command and thrust are of small magnitude over a short period of time, so that the initial pitching tendency is mainly determined by the faster elevator command. Although the initial tendency of the DIALS throttle command is to lower the thrust level, which is the desirable action, the glideslope capture criterion was selected by considering only the elevator action. After some manipulation, and neglecting terms of small magnitude, the following glideslope capture altitude can be obtained.

$$h_{GSC} = -\tan\gamma_o \bar{x}_e - U_o \left[c_{\ell 1} \bar{e}_{\ell 1} + c_{\ell 2} \bar{e}_{\ell 2} + c_{\ell 3} \bar{e}_{\ell 3} + c_{\ell 7} \bar{e}_{\ell 7} + c_{\ell 8} \bar{e}_{\ell 8} + c_{\ell 9} \bar{e}_{\ell 9} + d_{\ell 3} z_{\ell 3} \right] \quad (140)$$

$$c_{\ell i} = \frac{H_{e_\ell 1\, i}}{H_{e_\ell 1\, 6}} \quad , \quad i = 1, 2, 3, 7, 8, 9 \quad , \quad (141)$$

$$d_{\ell 3} = \frac{H_{z_\ell 1\, 3}}{H_{e_\ell 1\, 6}} \quad , \quad (142)$$

where γ_o is the selected glideslope angle, $\bar{x}_e$ is the estimated ground distance to the glide path intercept point (GPIP), $\bar{e}_i$ is the estimated error in the state x_i, and $z_{\ell 3}$ is the commanded inertial angle of attack. Note, that, as in the localizer capture, the glideslope capture altitude is lower when the desired speed is higher. Further note that the criterion is applicable to the capture of an arbitrary glideslope by using the glideslope angle selected by the pilot as γ_o in (140).

Figures 11 - 16 show the glideslope capture phase of the final approach during the flight tests. The glideslope angle desired for the final approach is entered into the flight computer prior to the glideslope capture. Until the glideslope capture criterion is met, the longitudunal dynamics are controlled usually by a different control system designed using classical methods.

When the glideslope capture criterion is met, the system automatically engages the glideslope capture mode. In a given approach the point at which capture is initiated varies largely according to the initial position of the aircraft, the glideslope selected, and the airspeed selected.

On the plots shown in Figures 11, 13, and 15, it is seen that at glideslope capture initiation, the control law produces the desired combined actions of pitching the aircraft down even though it is still below the glideslope, and

lowering the thrust level. Accordingly, the sink rate is brought to the level necessary to track the glideslope selected for the approach under the prevalent wind conditions, at the selected airspeed.

It should be noted that depending on wind conditions, and the performance of the control system in operation prior to the capture, the aircraft pitch rate, sink rate, and thrust rate may be noticeably different than zero, even though a steady level flight is desired. The flight results indicate an insensitivity to such variations, presumably due to the capture criterion. So that the capture is initiated in a coordinated fashion under the various wind conditions encountered.

The approach shown in Figure 13 corresponds to a conventional 3° glideslope, whereas Figures 11 and 15 show steep glideslope captures corresponding to a 4.5° glideslope. The flight results indicate that the control law performance is insensitive to the particular glideslope selected. Except for the pitch attitude and sink rate levels needed for the particular glideslope, the basic behavior of the longitudinal variables during the capture appears to be similar, variations being largely due to wind conditions.

As seen in the plots of vertical path deviation, the glideslope overshoots are quite small for steep as well as conventional glideslopes. The average glideslope overshoot in the flights performed is 4.5 ft, with a standard deviation of 2.3 ft, as shown in Table 9. In fact, it may be noted that the overshoot is no larger than the vertical path deviations on the glideslope which are due to wind gust disturbance.

The time required to settle on the glideslope selected is seen to be about 20 sec from a performance standpoint, quick settling on the glideslope is desirable as it enhances close-in captures. On the other hand, from a

passenger comfort standpoint, a slower, more gradual capture may be preferable.

Finally, it may be noted that the glideslope capture maneuver appears to produce no undesired transient activity in the airspeed, as measured by the calibrated airspeed (CAS). So that, even through the aircraft is pitching down during capture, the reduction of the thrust during the same period largely counteracts the effects of the pitch on airspeed while enhancing the pitch-down action. The latter effect is due to the fact that the engines are located below the aircraft center-of-gravity, thus, reducing thrust also reduces the pitching moment.

C. LOCALIZER AND GLIDESLOPE TRACK

As the aircraft gets closer to the localizer or glideslope, the localizer or the glideslope track (or hold) modes are engaged, the order depending on the particular approach path. In comparison to the capture modes, the main objectives considered in the design of the track modes were to achieve quick settling on the localizer and glideslope, insensitivity to wind disturbances (gusts, shear and steady winds), and accurate tracking of the localizer and glideslope.

Since it is not desirable to start the flare maneuver before the aircraft is fully stabilized on the glideslope, a low settling time for the track modes is important to enable "close-in captures". The capability to accurately capture and track a shallow or steep glideslope provides a flexibility which can be used to avoid vortices when following large aircraft, reduce the noise perceived by airport communities, and generally increase terminal area operations efficiency.

The localizer track mode is engaged when the aircraft is 30 ft from the runway centerline or 25 sec after the localizer capture has been engaged. Since the main objective of the track mode is to minimize excursions away from the runway centerline, the gains feeding back the cross-track error estimate to the aileron and rudder are increased gradually for a smooth mode transition. Since a type 1 system is desirable in this mode, an integrator for the cross-track error is also initiated to avoid steady-state offsets from the runway centerline. Initially, the integrator gains were set equal to a tenth of the gains for the cross-track error, i.e., the product of the sampling interval and the cross-track error/gain. The gains were then adjusted using simulation results to improve the performance under the various conditions expected to occur.

The glideslope track mode is engaged when the aircraft intercepts the glideslope, or 25 sec after the glideslope capture mode has been engaged. The latter criterion is used to ensure that the track mode is engaged even if the aircraft does not overshoot and cross the glideslope. To reduce any excursions from the selected glideslope, the gains feeding back the deviation from the glideslope and the error in the normalized vertical velocity are increased gradually using an easy-on. To avoid steady-state offsets from the glideslope, an integrator on the glideslope deviation is introduced when the track mode is initiated.

During both the capture and track modes, the DIALS filters estimate the components of the wind velocities. These estimates are fed to the controller to compute the surface command signals. Thus, to the extent that the wind velocities are estimated, the control law performs a gust alleviation function; i.e., even if no position or inertial velocity errors are

present, the wind velocity estimates will produce surface commands which tend to counteract the effects of winds, thus reducing excursions away from the glideslope. The wind velocity estimates are also used to maintain a constant airspeed. This is obtained by commanding an inertial speed deviation equal to the negative of the wind estimate in the along-track direction. The commanded airspeed thus remains constant at the desired nominal value.

$$z_{\ell 2k} = - \varepsilon_1' \, C_{w\ell} \, \bar{W}_{\ell k} \tag{143}$$

$$\zeta_{\ell 2k} = - \varepsilon_1' \, C_{w\ell} \, A_{w\ell} \, \bar{W}_{\ell k} \tag{144}$$

The performance of the system in the localizer and glideslope track modes are shown in Figures 5 - 16. As mentioned in the previous sections, the aircraft settling time on both the localizer and glideslope is short. Due to the lack of overshoots, by the time the track modes engage, the aircraft is largely settled on both the localizer and glideslope.

The main function of tracking the localizer and glideslope is performed satisfactorily, with small deviations about the desired path. In the high gust case, the localizer offsets during the track mode are seen to be below 30 ft while the aircraft adjusts to gusts and changing wind conditions. The variations in the roll and yaw angles also appear to be appropriate for the high gust conditions encountered.

The glideslope deviations in the high gust condition tend to be of the order of 8 ft except for a rather high deviation of about 16 ft presumably due to a high vertical gust. In general, the sink rate and pitch behavior seems appropriate. However, the thrust is seen to have an oscillatory motion, which may be due to unmodeled throttle or engine dynamics.

Figure 16(a) shows the throttle rate command of the control law and the measured throttle position. Comparing the zero crossings of the throttle rate with maxima and minima of the measured throttle position shows that the throttle lags its command by 1 - 2 sec. As this large lag, presumably in the throttle servo, is not included in the design model the control law does not account for its existence in the control loop. As the nonlinear simulation used in the development of the control law does not contain such a long time constant in the throttle servo, the effect was not noticed in the simulations, and only became clear in the flight tests under high gust conditions where the throttle rate commands are high and may reach their rate limit.

D. A WIND SHEAR ENCOUNTER

An excellent example of the performance of the control law under wind shear conditions was encountered on the flight shown in Figure 7. As seen from the yaw angle behavior, the aircraft, has a crab angle while tracking the localizer due to an estimated cross-wind velocity of about 12 knots. At about 100 sec, the crab angle is seen to be reduced to almost zero. At first glance, this appears as a normal decrab maneuver. However, the decrab altitude has not been reached.

The reason for the behavior can be seen in the estimated cross-wind velocity, which indicates that the cross-wind of approximately 12 knots has very quickly died down, and may even have reversed direction. Thus, the behavior of the yaw angle was a response to a sudden change in the steady wind. Similar adjustments are seen in the roll angle and localizer deviation.

Although a wind change of about 15 knots in 15 sec (or approximately 150 ft of altitude on a 3° glideslope) which corresponds to a wind shear of about 9 knots per 100 ft is not as severe as some reported cases, the ease with which DIALS handles this particular encounter demonstrates a desirable performance. The magnitude of the maximum localizer deviation is seen to be less than 30 ft. The flight continued to make a normal automatic landing.

E. CRAB AND DECRAB

In the presents of cross-winds, the desired behavior is to crab into the wind, i.e., to head into the wind with level wings and no slidslip while remaining on the localizer. If this condition is not specifically accommodated, an optimal quadratic regulator will usually both yaw and roll into the wind, thus having a nonzero steady-state sideslip angle which is not desirable. In addition, the bank angle can be uncomfortable. To obtain the crab condition in DIALS, a roll integrator is fed back when the aircraft roll reaches 2°, provided that the localizer track mode has been engaged. This ensures a zero steady-state roll angle forcing the yaw angle to automatically adjust itself to the angle necessary for crab. To obtain crab with a quick and smooth transient response, the commanded (aerodynamic) sideslip angle is set to zero, i.e.,

$$z_3 = - \bar{\beta}_{ws} \tag{145}$$

where z_3 is the normalized lateral velocity (inertial sideslip) and $\bar{\beta}_{ws}$ is the estimate of the steady wind velocity. As a small sideslip is desirable in all the phases of flight, except for decrab, the commanded sideslip angle is set to zero at localizer capture initiation and remains active until decrab.

During decrab the aircraft heading is aligned with the runway centerline, while the roll angle is used to maintain the aircraft on the localizer. The decrab mode is initiated at an estimated altitude of 250 ft. It should be noted that this decrab altitude is somewhat arbitrarily selected, and can be reduced to initiate the maneuver at a lower altitude. To obtain the decrab maneuver, first the commands which produce the crab condition are phased out; the roll integrator is phased out and the inertial sideslip command z_3 is set to zero gradually. Since this corresponds to a nonzero commanded aerodynamic sideslip angle, the wind velocity estimates fed into the controller produce a decrab tendency. To enhance this tendency and ensure decrab as a steady-state condition, an integrator of the heading relative to the runway is introduced to aid the aileron and rudder actions necessary for decrab. Initially the integrator gains were set equal to a tenth of the heading error gains. These were later adjusted using simulation results to improve the performance throughout the flight regime.

Figures 5 - 10 show the aircraft lateral dynamics during crab and decrab. After the localizer capture, the roll angle settles at a average value of zero as desired until the decrab altitude. Similarly, the sideslip angle remains small. On the other hand, the heading relative to the runway settles at a nonzero value in order to maintain the localizer deviation at zero. It may be noted that the yaw angle settles at the crab angle quickly and smoothly. This is essentially due to the use of cross-wind velocity estimates in the control law. To the extent that the estimated cross-wind is correct, the yaw angle settles smoothly at its desired value, and the localizer overshoot is small. As the control law does not use a measurement of the sideslip angle, this information is provided by the wind velocity estimate.

When the decrab altitude is reached, the decrab mode is engaged. During the flight shown in Figure 5, the cross-wind estimate shows a steadily decreasing cross-wind velocity, along with a steadily decreasing crab angle. So that when the decrab mode is engaged, the aircraft is nearly aligned with the runway.

On the other hand, the flight shown in Figure 9, the cross-wind has a steady component of about 20 knots throughout the final approach, gusting to over 20 knots on occasion. The decrab mode reduces the yaw angle to align the aircraft heading with the runway. The decrab law contains a roll limit of 4.5°; i.e., the system decrabs as much as possible up to a 4.5° bank angle, as rolling further entails greater risk of the engine touching the runway if a heavy gust were to occur at touchdown. Thus, any remaining misalignment would be taken by the landing gear, or the landing would be aborted by the pilot in higher cross-winds. As can be seen, the performance of both crab and decrab appears to be satisfactory in these flights.

F. FLARE

During the flare maneuver, the main objectives are to reduce the aircraft's sink rate to an appropriately lower level and to touch down with a sufficient margin on the pitch attitude, aligned with the runway, near the selected touch-down point. As DIALS is required to flare from steeper glideslopes than usual for a B-737, the aircraft has a higher sink rate than usual on the higher glideslopes. The approach taken was to generate a flare trajectory on line as a function of the glideslope angle, the desired touch-down flight path angle and the touch-down point; so that when the glideslope is steeper, the flare (initiation) altitude is higher. It should be noted that, for a given approach, the flare path is fixed in space, and is

fed to the automatic control system as the desired or commanded trajectory.

The family of flare paths was developed starting from the desired vertical acceleration profile. The following form was selected for this purpose

$$h''(x_e) = \begin{cases} \dfrac{1+\cos\, 2\Pi(x_e+\Delta X_f) \quad /P}{2(H_f - X_f \tan \gamma_o)} & , \quad 2|x_e+\Delta X_f| < P \\ 0 & , \quad \text{otherwise*} \end{cases} \tag{146}$$

$$P = 2\,\frac{H_f - X_f \tan \gamma_o}{\tan \gamma_{td} - \tan \gamma_o} \quad , \tag{147}$$

$$\Delta X_f = (P - 2\,X_f)\ /2 \quad , \tag{148}$$

where x_e is the x-coordinate of the aircraft's position vector, X_f the touchdown point, H_f the altitude at X_f (zero for touchdown), γ_o and γ_{td} the selected flight path angles on the glideslope and at touchdown, respectively. The desirable characteristics of this profile included the smoothness of transition (e.g., h", hence $\ddot{h}$, has a continuous first derivative at flare initiation), the simplicity of the parametric form (i.e., flare profiles from various glideslopes are obtained according to the value of γ_o), and the ease with which h" can be integrated analytically to obtain an expression for h' and h to determine an altitude profile for flare.

It is of interest to note that the flare profile described above was selected after some experimentation with an altitude versus x_e profile of

---

*The prime " ' " denotes differentiation with respect to the distance variable x_e.

exponential form. These formulations resulted in undesirable transient behavior at flare initiation, presumably due to the discontinuity in the commanded vertical acceleration when starting flare. The cosine type acceleration profile provides a smooth transition in this variable, while incorporating all the parameters of interest in the flare path such as glideslope angle, touchdown point, etc. For a constant ground speed, $\dot{x}_e$, the vertical acceleration profile is seen to be

$$\dot{h}(x_e) = \dot{x}_e h'(x_e) \quad , \tag{149}$$

$$\ddot{h}(x_e) = \dot{x}_e^2 h''(x_e) \tag{150}$$

The vertical profile $h(x_e)$, $\dot{h}(x_e)$, $\ddot{h}(x_e)$ is used in the desired path or command vectors, z_ℓ and ζ_ℓ in order to follow the flare path for the selected glideslope. However, the altitude profile alone does not guarantee all of the desirable and critical properties necessary for an acceptable touchdown. The pitch attitude at touchdown is of utmost importance. A negative pitch angle at touchdown would result in the nose gear touching down before the landing gear and being subjected to high levels of loading. Thus, a positive pitch angle safety margin is usually desirable. It is also usual to have a decreasing airspeed profile during flare to aid the pitch profile during flare, as well as ease the touchdown speed, sink rate, and rollout. To obtain these characteristics the command variables z_ℓ and ζ_ℓ were set as follows.

$$z_{\ell\ 1\ k+1} = z_{\ell\ 1\ k} + .1\ z_{\ell\ 4\ k} \tag{151}$$

$$z_{\ell\ 2\ k+1} = -\ \varepsilon_1^T\ C_{w\ell}\ W_{\ell\ k+1} + DELVF_k \tag{152}$$

$$DELVF_{k+1} = DELVF_k - .1\ DELVFR/U_o \quad , \qquad \text{if } DELVF_k \leq -25/U_o \tag{153}$$

$$z_{\ell\ 3\ k+1} = -\frac{(\bar{L}_{3\ 1} + \tan\gamma_{d\ k+1}\ \bar{L}_{1\ 1})(1+z_{\ell\ 2\ k+1}) + (\bar{L}_{3\ 2} + \tan\gamma_{d\ k+1}\bar{L}_{1\ 2})\bar{\beta}_{k+1}}{\bar{L}_{1\ 3} + \tan\gamma_{d\ k+1}\ \bar{L}_{1\ 3}} \tag{154}$$

$$z_{\ell\ 4\ k+1} = \frac{U_o\ h''_{k+1}\ \dot{\bar{x}}^2_{e\ k+1}}{\cos(\alpha_o - \bar{\theta}_{k+1})} \tag{155}$$

$$z_{\ell\ 6\ k+1} = Z'_{ed\ k+1}\ \tan\gamma_o\ \hat{x}_{\ell\ 5\ k+1} \tag{156}$$

$$\zeta_{\ell\ 1\ k} = 0 \tag{157}$$

$$\zeta_{\ell\ 2\ k} = -\ \varepsilon_1^T\ C_{w\ell}\ A_{w\ell}\ W_{\ell k} - DELVFR \cdot GEZ5/U_o \tag{158}$$

$$\zeta_{\ell\ 3\ k} = 0 \tag{159}$$

$$\zeta_{\ell\ 4\ k} = G_{\zeta 4}\ U_o^2\ \dot{\bar{x}}^3_{e_k}\ h'''_k/\cos(\alpha_o - \bar{\theta}_k) \tag{160}$$

$$\zeta_{\ell\ 6\ k} = \dot{z}_{\ell\ 6\ k} + z_{\ell\ 1\ k} - \sec\gamma_o\ z_{\ell\ 3\ k} \tag{161}$$

$$\dot{z}_{\ell\ 6\ k} = (\tan\gamma_o - \tan\gamma_{d\ k})\ \dot{\bar{x}}_{e\ k} \tag{162}$$

where $\gamma_{d\ k}$ is the desired flight path angle at time t_k, GEZ5 is an easy-on, $Z'_{ed\ k}$ is the desired altitude in the Earth coordinate axes, $\bar{L}_{ij}$ is the estimate of $L_{ES}(i,j)$, and ε_1 is the first column of the identity matrix. DELVFR and $G_{\zeta 4}$ are constants which can be set according to the amount of

decrease in airspeed and the pitch profile desired, respectively. These values were also modified using the profiles obtained in simulation runs.

The performance of the automatic landing system during the flare maneuver is shown in Figures 11 - 16. It should be noted that the plots of the vertical path deviation in these figures show the difference between the aircraft altitude estimate and the flare path generated on-line corresponding to the selected glideslope. The on-line flare path was generated with the equations shown above.

During the DIALS flights, ten "hands-off" automatic landings were performed. Of these, three approaches were made with a selected glideslope of 3°, while steep approaches on 4.5° glideslopes were selected for seven flights.

The plots of the sink rate during flare show that the control law reduces the sink rate from its level on the glideslope to a lower level for touchdown. This is largely achieved by pitching up to increase the lift, as well as to obtain a positive pitch attitude at touchdown. The vertical path deviation remains small throughout flare; however, the deviations at touchdown largely determine the actual touchdown point.

Of the ten automatic landings made, the flight where the wind shear was encountered resulted in the highest touchdown sink rate of 3.5 ft/sec, which is quite acceptable even if considered hard. The other two landings resulted in touchdown sink rates of 2 ft/sec, and 3 ft/sec. The average touchdown sink rate of all the automatic landings was 2.4 ft/sec, with a standard deviation of 0.74 ft/sec.

It should be noted that the commanded touchdown sink rate at 125 knots is 2.2 ft/sec. Thus, the touchdown sink rate statistics with its low standard

deviation shows the desired performance. The average touchdown point was 1026 ft, with a standard deviation of 244 ft. The commanded touchdown point was 1152 ft. Tables 10 and 11 show the touchdown statistics for the automatic landings performed.

The control performance during flare shows similar characteristics for 3° and 4.5° glideslopes. The flare altitude for a 3° glideslope was 102 ft, with an altitude of 134 ft for a 4.5° glideslope. While the flare altitudes used are higher than usual, a higher than usual flare altitude is reasonable for steeper glideslopes. Nevertheless, the particular values used do not have a special significance, and can be easily modified by an appropriate modification of flare path parameter values.

G. FILTER PERFORMANCE

In the context of control law design, the filter plays the role of a dynamic compensator; i.e., a dynamic system whose outputs are available for use in controlling the plant. In the sampled data LQG problem posed in section II C, as well as other LQG formulations, the optimal dynamic compensator is the least-mean square estimator of all the states. Thus, the filter smooths noisy measurements and produces estimates of the variables which are not directly measured. The smoothed signal necessarily lags the measured signal. The use of the dynamic plant model in the filter provides important lead information which is used to reduce the lag. However, if the accuracy of the model used is not sufficient, significant lags can be produced which tend to destabilize the overall closed-loop system, and may lead to the divergence of the filter itself.

As discussed earlier, DIALS uses fixed-gain (steady-state) Kalman filters for both the longitudinal and lateral dynamics. As the flight conditions considered vary from one approach to the next, the plant dynamics model used in the design is certain to have mismatches in some flight condition. Thus, it is important to accommodate errors in the filter design. model appropriately. This entails the use of plant noise to account for model uncertainties, and has the effect of increasing the filter gains at the expense of some extra noise in the estimates.

A feature of DIALS is the direct use of wind velocity estimates in the control law. In particular, the estimation of cross-wind velocity is necessary for use in the crab and decrab maneuvers, but more significantly, in reducing the localizer overshoot. While the inertial cross-track velocity can be estimated using the MLS position and body-mounted accelerometers, a measurement of the lateral airspeed, such as a sideslip sensor, was not allowed in the design, although a sideslip sensor is available on the TSRV. So that the main sensor available for wind estimation is the airspeed sensor, where the cross-wind is of second order. Thus, to estimate the cross-wind speed with some accuracy, and more significantly, to estimate sudden changes in the cross-wind without long lags, it is necessary to use more information. The aircraft dynamic model provides such information even though the model may have some parameter uncertainty.

From the flight performance of the overall automatic control system discussed in the previous sections, it is clear that, the filters are providing the necessary dynamic compensation without introducing large lags in the feedback loop, despite the presence of plant model errors. Comparison of the longitudinal wind estimate with the airspeed signal in Figures 11,

13, and 15 indicates a small lag which may be improved. However, it is also clear that the filter, appropriately, does not attribute every variation in the airspeed to a change in wind speed, and does not show the initial tendency to do so and correct itself later.

As the actual lateral wind velocity is not measured, the accuracy of the cross-wind estimate cannot be directly ascertained. However, the "sure-footed" manner of the crab decrab maneuvers while remaining on the localizer indicate that the error in the estimate must be small. More importantly, the response to the wind shear condition shown in Figure 7 indicates that the lags in the estimate are small, although perceptible. Comparison with the sideslip angle is also interesting.

Plots of the innovations for Flight No. 2 which contains the wind shear condition discussed are shown in Figure 17. It is interesting to note that the noise in lateral position and altitude get smaller as the aircraft approaches the runway, and therefore the MLS antennas. As these variables are obtained from the angular measurements of azimuth and elevation, the noise variance is directly proportional to the range of the aircraft. Note that the altitude innovations show a transient behavior which stabilizes about zero. Also note that the roll and pitch innovations show a small bias.

In general, the innovations show a behavior indicative of white noise which is the expected behavior. However, considering the known modeling uncertainties, some coloring of the innovations should be expected.

V. CONCLUSIONS AND RECOMMENDATIONS

The flight testing of the Digital Integrated Automatic Landing System (DIALS) is among the currently rare occasions where a complex modern control digital design has been demonstrated in flight. To the author's knowledge, it is the first automatic landing system designed by optimal direct-digital-design techniques which has been successfully flight tested. As indicated in the report, the design of a modern control system for a complex, flight critical task is not straight-forward, despite a large body of literature on some aspects of the techniques involved. In the following, some areas of theoretical research which address problems encountered in designing practical automatic control systems are also recommended.

DIALS has six modes corresponding to the phases of the final approach and landing: (1) localizer capture, (2) steep glidelsope capture, (3) localizer track, (4) glideslope track, (5) crab/decrab, and (6) flare. The control law uses MLS position information, body-mounted acceleromaters, and sensors usually available on commercial jets, but does not require inertial platforms. Using the MLS, DIALS has the capability of performing steep approaches to landing by selecting the desired glideslope angle.

During the DIALS flight tests, ten "hands-off" automatic landings were performed on the TSRV aircraft. These automatic landings were performed under diverse wind conditions, including a wind shear case. The final approach flights included the modes of localizer capture, steep glideslope capture, localizer and glideslope track, crab/decrab, and flare to touchdown. On three of the approaches, a conventional 3° glideslope was selected. On

the remaining seven automatic landings, steep approaches with a 4.5° glideslope were made.

All the modes of the control law were exercised during the flight tests. The flight test results indicate improved performance in the following areas under all wind conditions encountered: (1) reduced localizer overshoots, (2) reduced glideslope overshoots, (3) reduced settling time for both localizer and glideslope, (4) flexibility of performing steep final approaches, (5) accurate tracking of the localizer and glideslope, (6) smooth crab and decrab maneuvers, (7) smooth touchdowns from steep glideslopes, and (8) excellent handling of a wind shear condition encountered. It should be noted that the accuracy of the localizer and glideslope tracking relative to the runway is enhanced by the high accuracy of the MLS signals. It should also be noted that the sampling rate of the control system is 10 Hz, which is lower than that usually required in analog designs which are implemented digitally. In general, the DIALS flight tests demonstrate that modern control methods can successfully be used to design automatic control laws for complex tasks.

Areas where the performance of the control law can be improved include: (1) the inclusion of the lags present in the throttle loop into the design model to improve autothrottle performance and (2) the reduction to the sideslip angle during localizer capture. The importance of the design model is clearly illustrated by the autothrottle performance. Of course, classical design techniques also require adequate modeling of the plant, as evidenced by similar autothrottle behavior observed in flight tests of a classical control system on the same aircraft. As a simulation, no matter how detailed, is only an approximation of the actual plant, the importance of flight testing is also illustrated.

DIALS is a full-state feedback law as it is based on a sampled-data LQG formulation. For numerous reasons, including flexibility of control structure and ease of implementation, it is desirable to design control laws where the variables used in the feedback loop can be selected by the designer. Thus, the development and application of output feedback and dynamic compensation provide useful avenues of further research.

The insensitivity of a control law to particular parameter variations, as well as possible variations in all the parameters has always played an important role in control system design. In the development of DIALS, insensitivity to flight condition parameters such as glideslope angle, airspeed, weight, c.g. location, steady wind conditions, sensor jitter, sampling rate variations, etc., was obtained by extensive simulations in a heuristic manner. However, this is a lengthy and difficult approach. Research on design methods where insensitivity, or robustness, are a part of the cost function can provide solutions which shorten the design time and effort considerably.

Finally, practical control laws are designed for systems which most often contain nonlinearities. Few systems are free of nonlinearities such as hysteresis or backlash, nonlinear gains, etc. Such well-known nonlinearities often produce undesired instabilities in control designs which do not accommodate them. It would be desirable to develop modern control methods and control structures which accommodate such often encountered system nonlinearities.

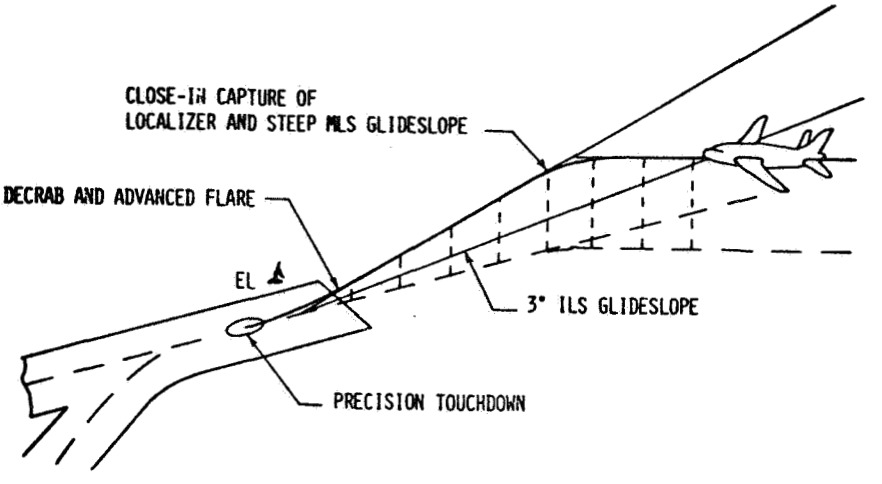

FIGURE 1. DIALS FLIGHT PATH GEOMETRY

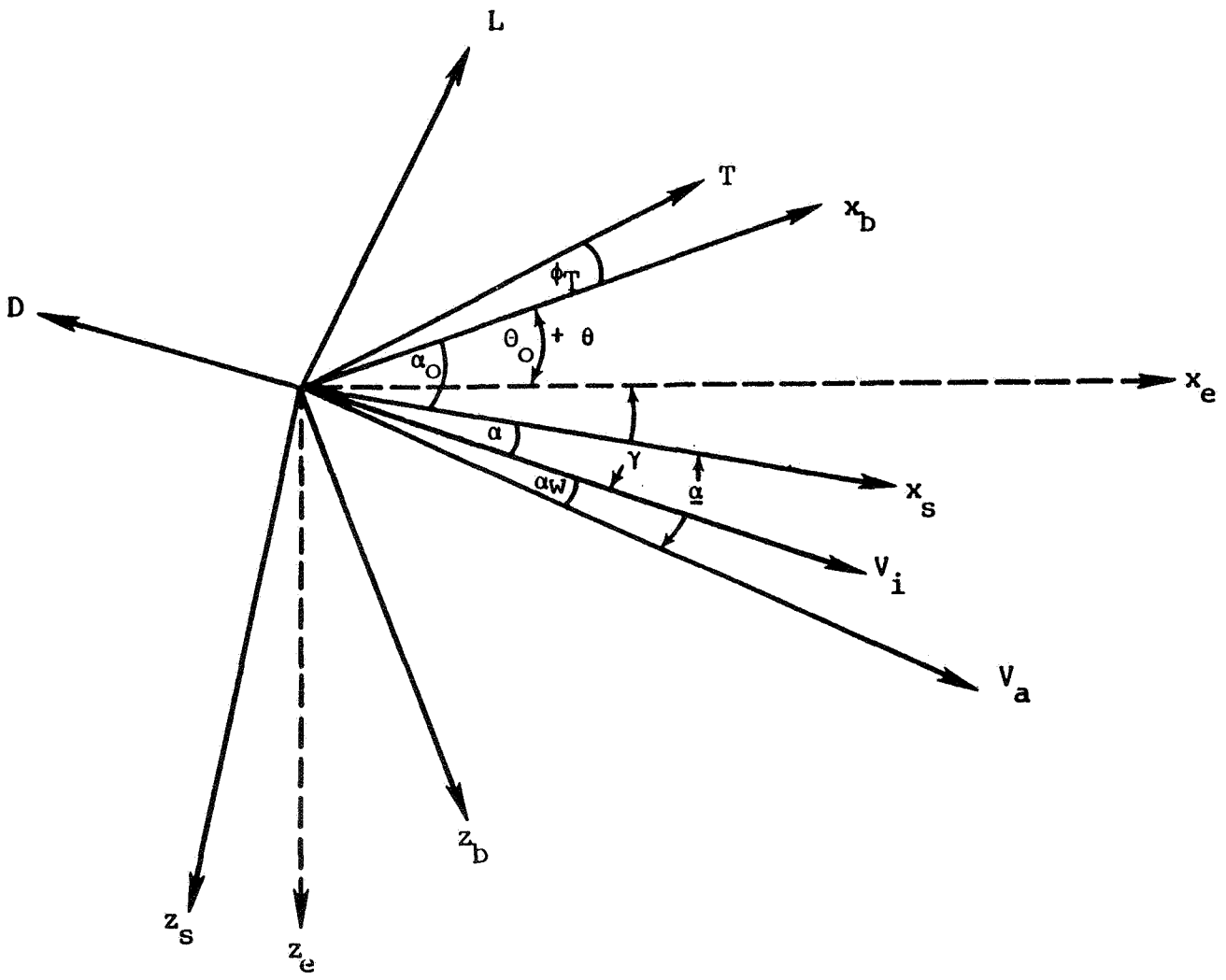

FIGURE 2. DEFINITION OF COORDINATE AXES, ANGLES AND FORCES.
(θ_o, θ, ϕ_T ARE MEASURED POSITIVE ccw, α_o, $\underline{\alpha}$, cw)

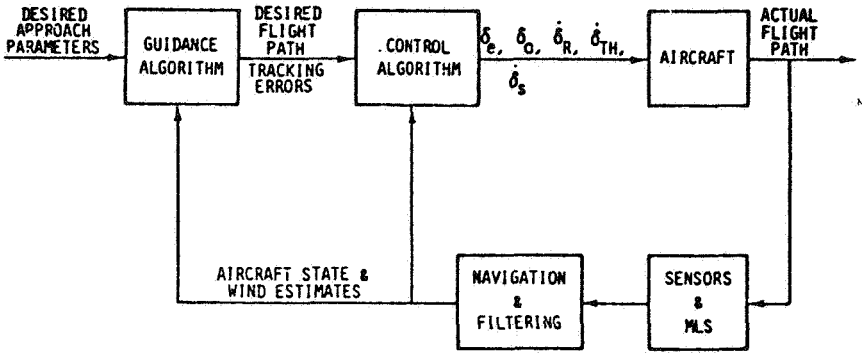

FIGURE 3. DIALS FUNCTIONAL BLOCK DIAGRAM

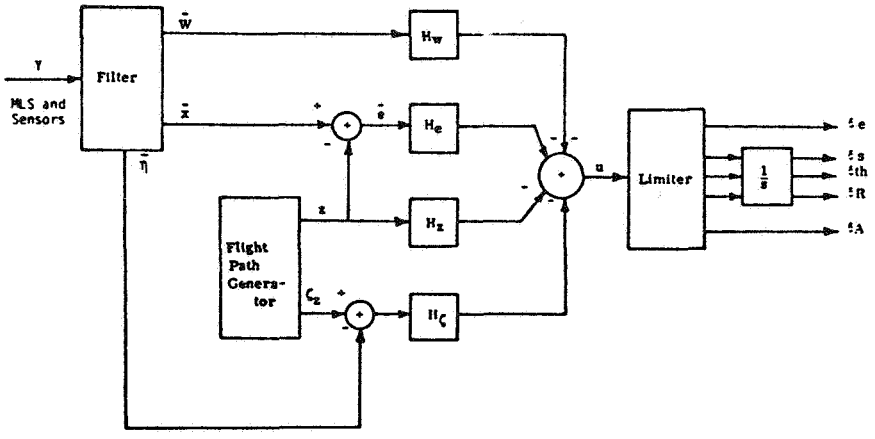

FIGURE 4. BLOCK DIAGRAM OF FEEDBACK LOOP

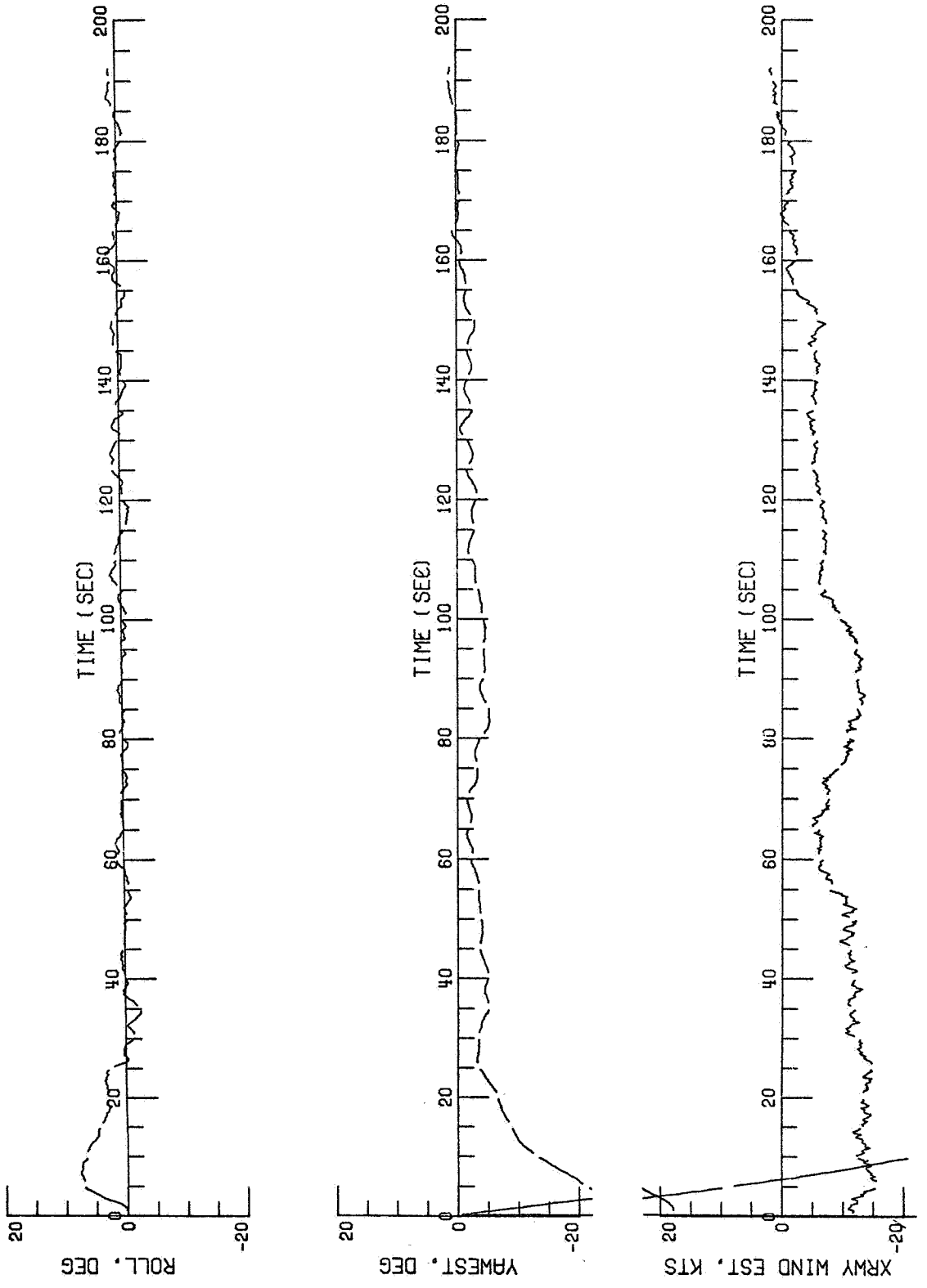

FIGURE 5(a). LATERAL FLIGHT PATH VARIABLES (FLIGHT NO. 1)

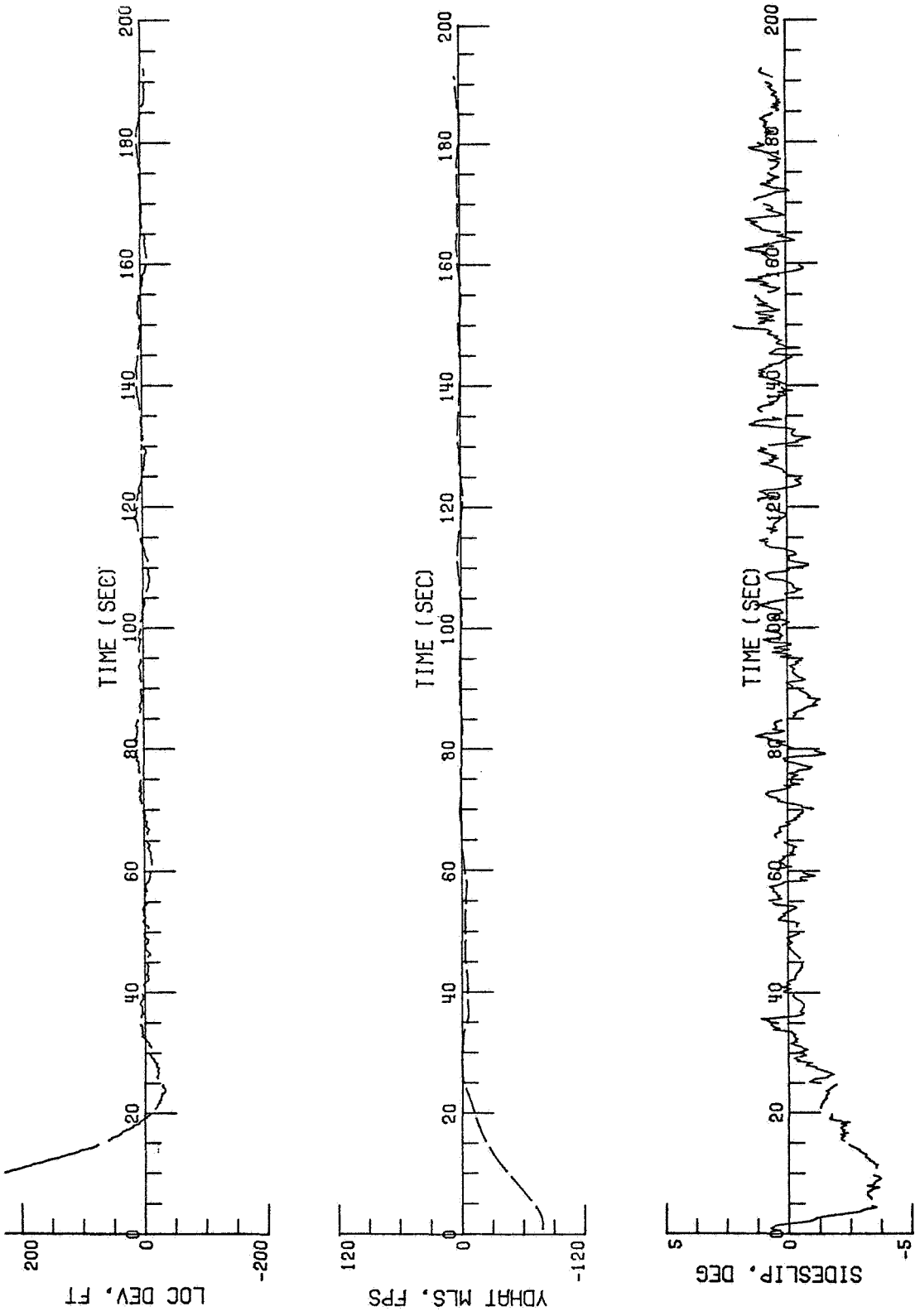

FIGURE 5(b). LATERAL FLIGHT PATH VARIABLES (FLIGHT NO. 1)

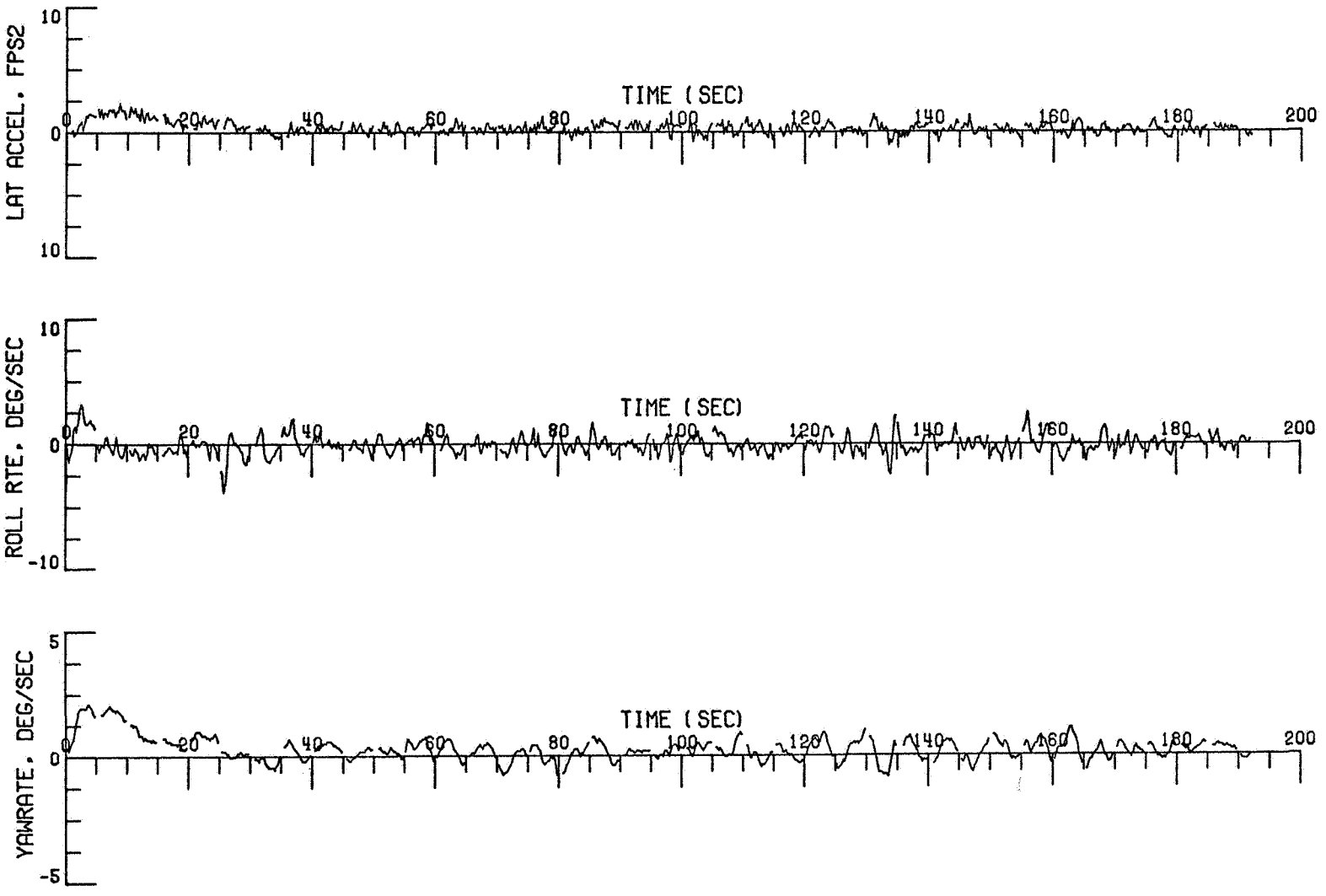

FIGURE 5(c). LATERAL FLIGHT PATH VARIABLES (FLIGHT NO. 1)

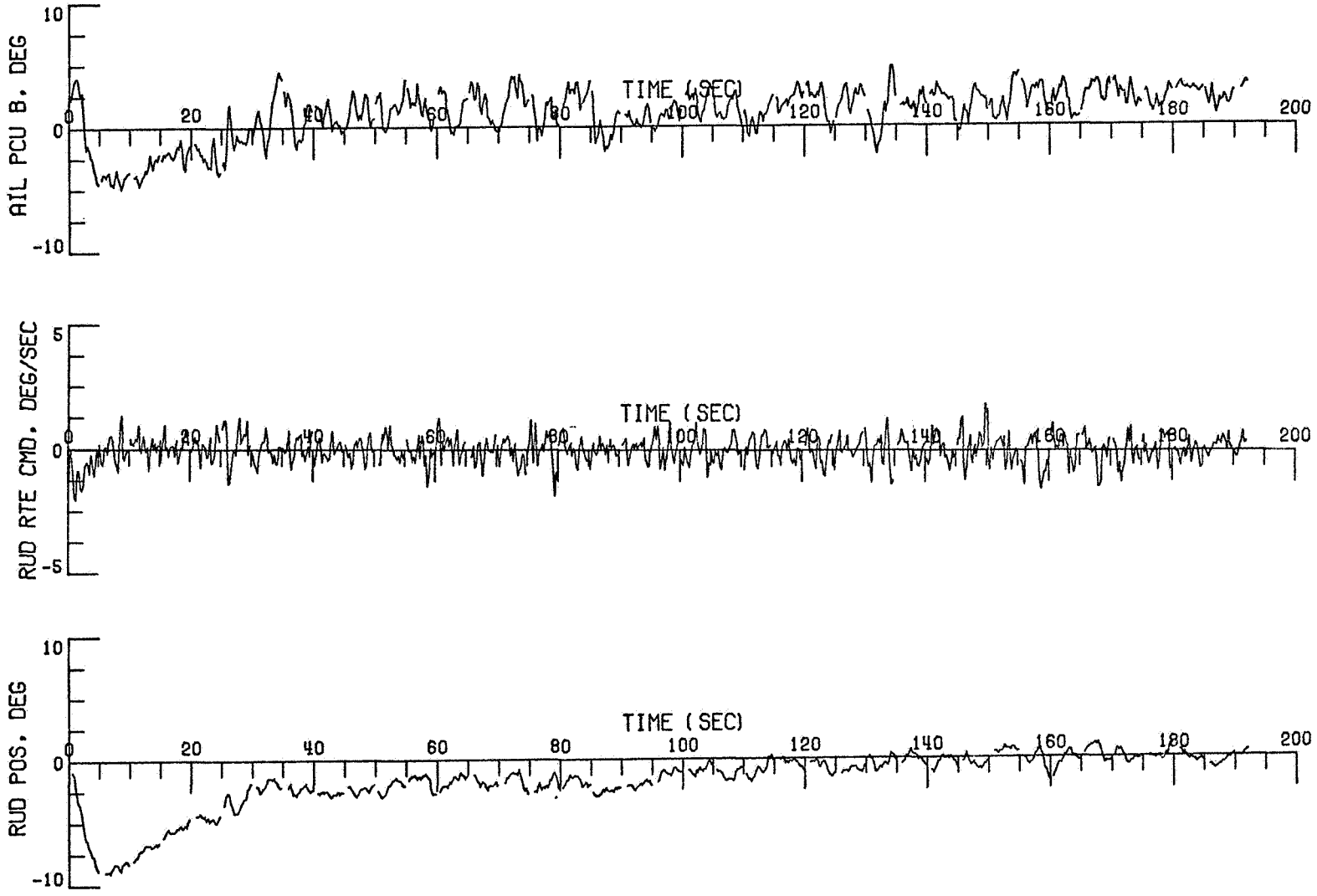

FIGURE 6. LATERAL CONTROL VARIABLES (FLIGHT NO. 1)

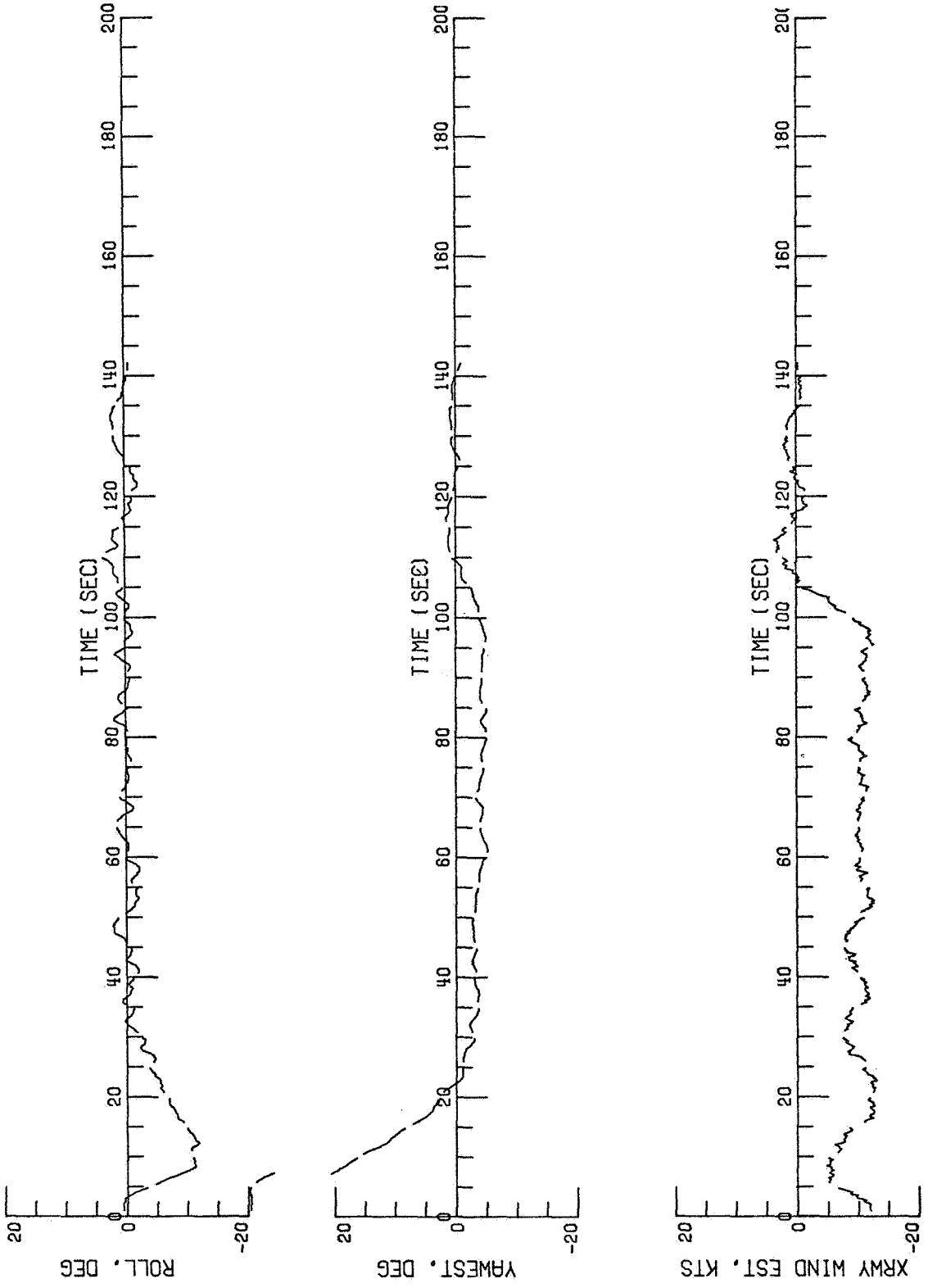

FIGURE 7(a). LATERAL FLIGHT PATH VARIABLES (FLIGHT NO. 2)

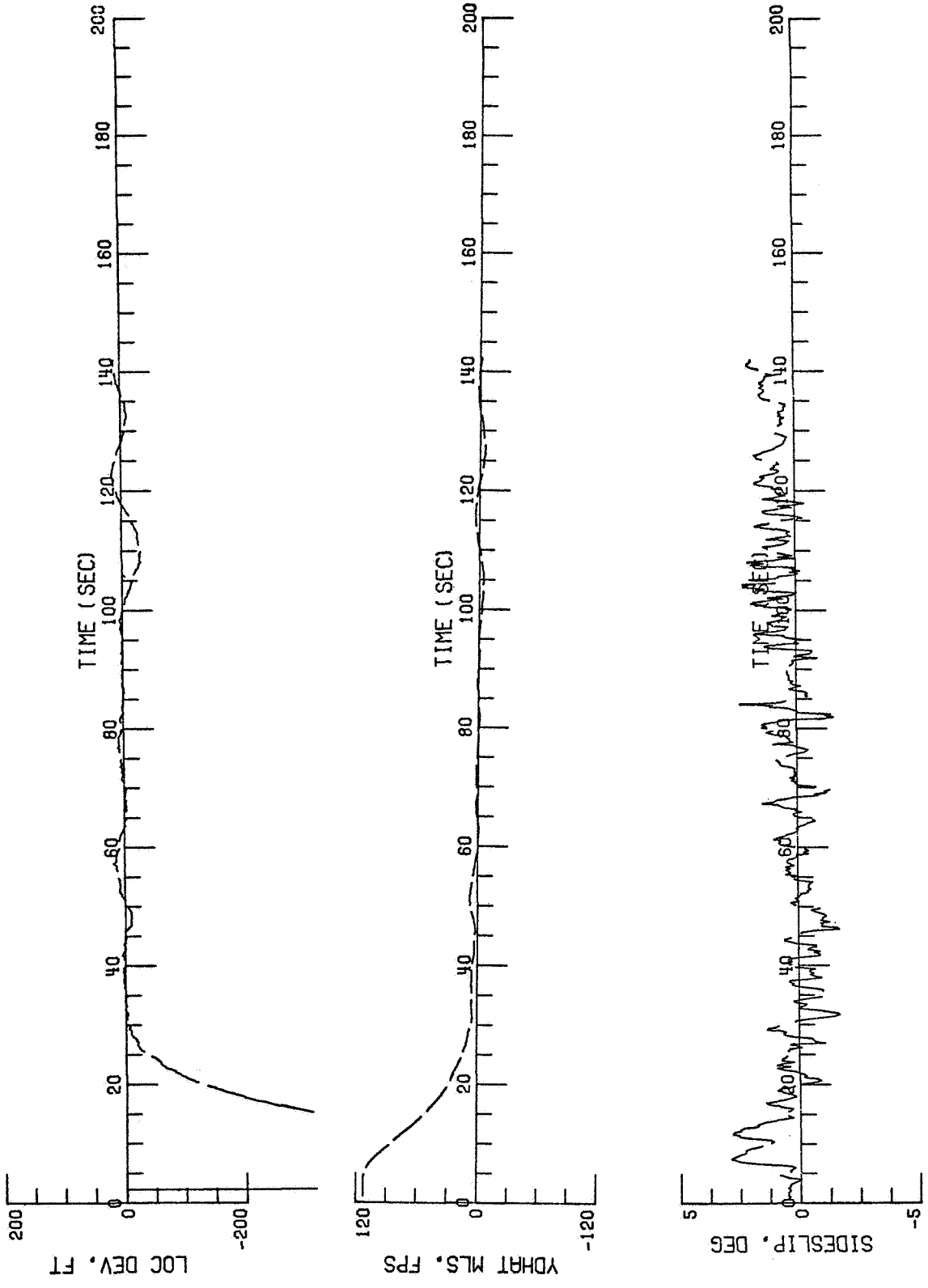

FIGURE 7(b). LATERAL FLIGHT PATH VARIABLES (FLIGHT NO. 2)

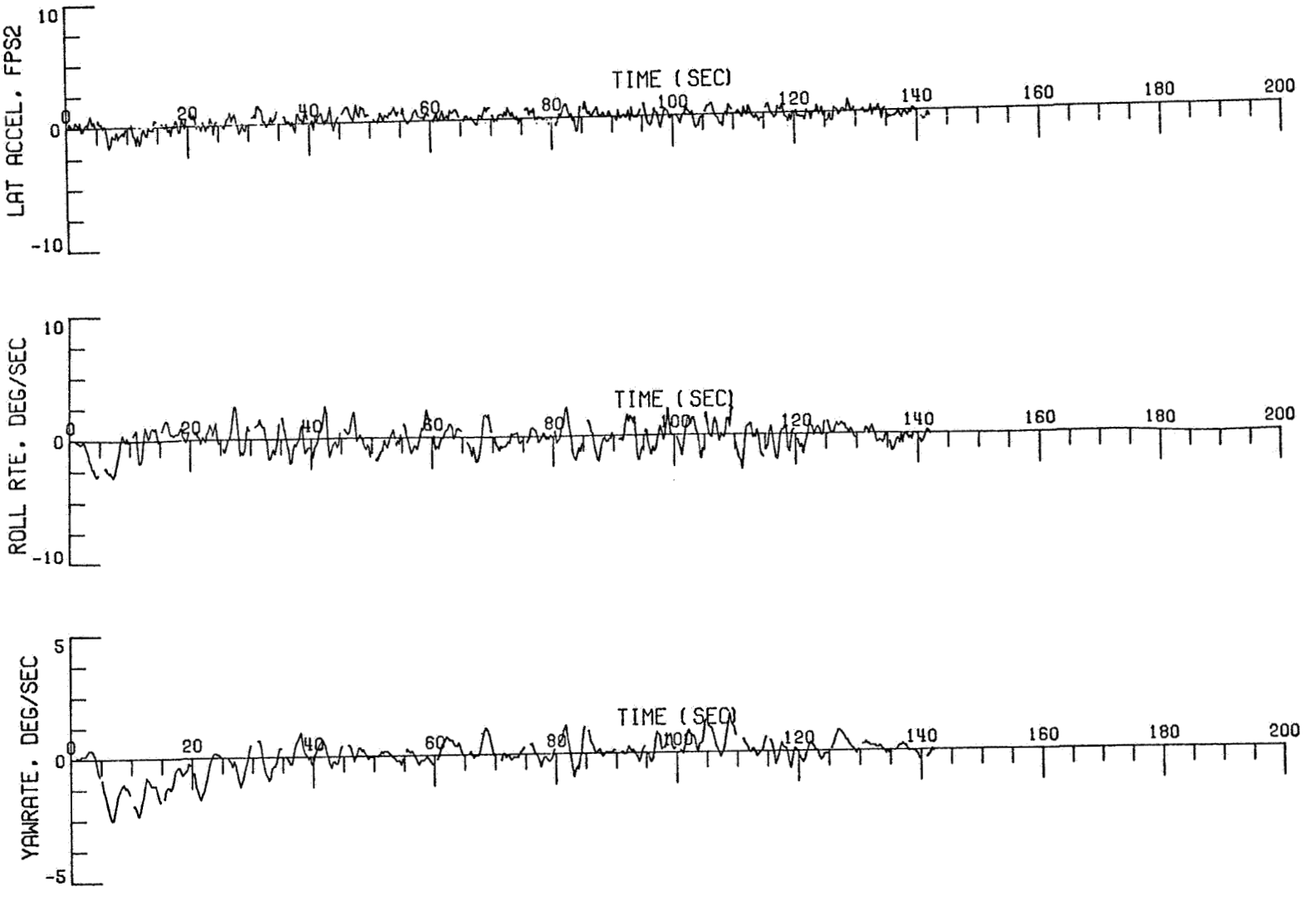

FIGURE 7(c). LATERAL FLIGHT PATH VARIABLES (FLIGHT NO. 2)

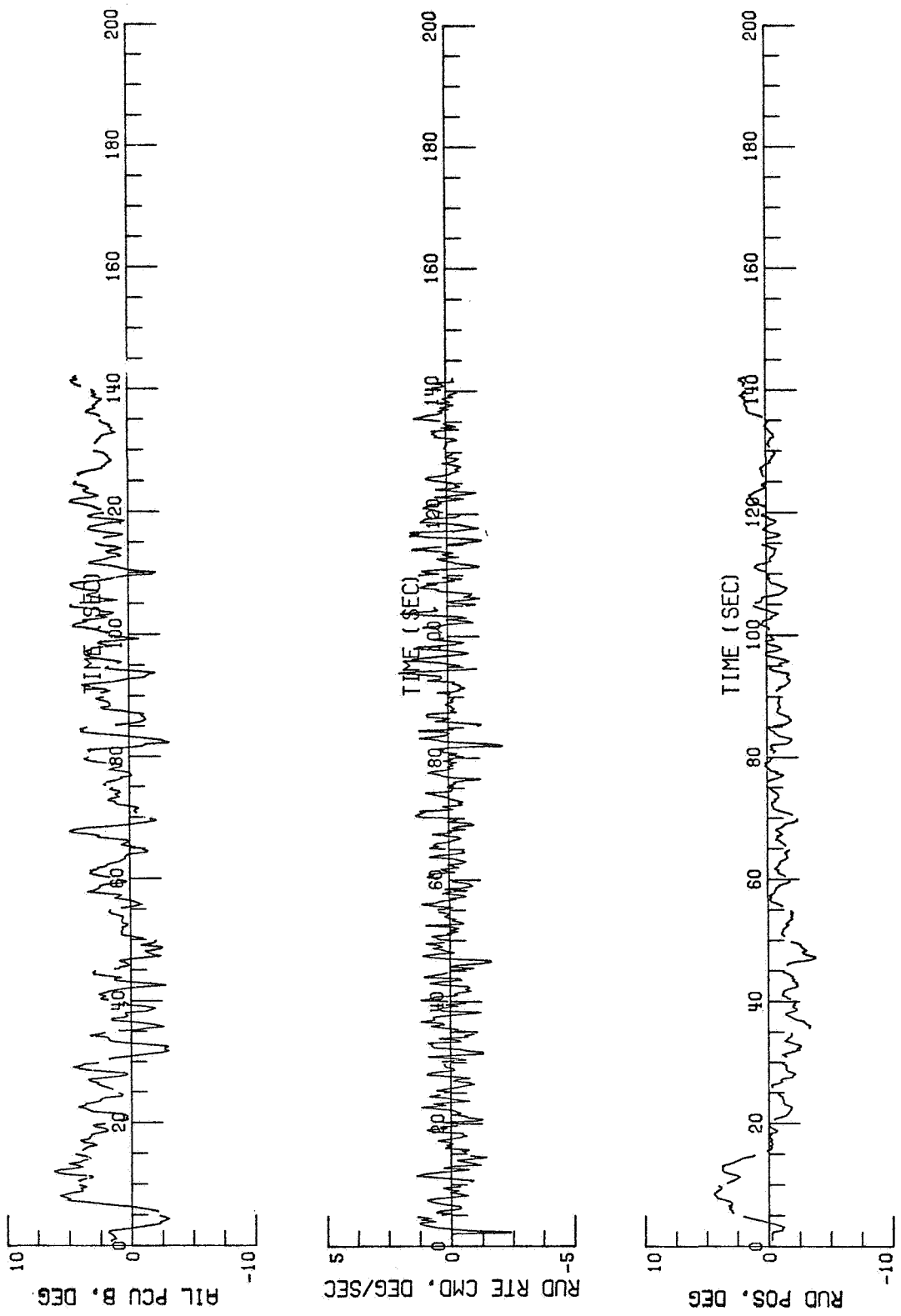

FIGURE 8. LATERAL CONTROL VARIABLES (FLIGHT NO. 2)

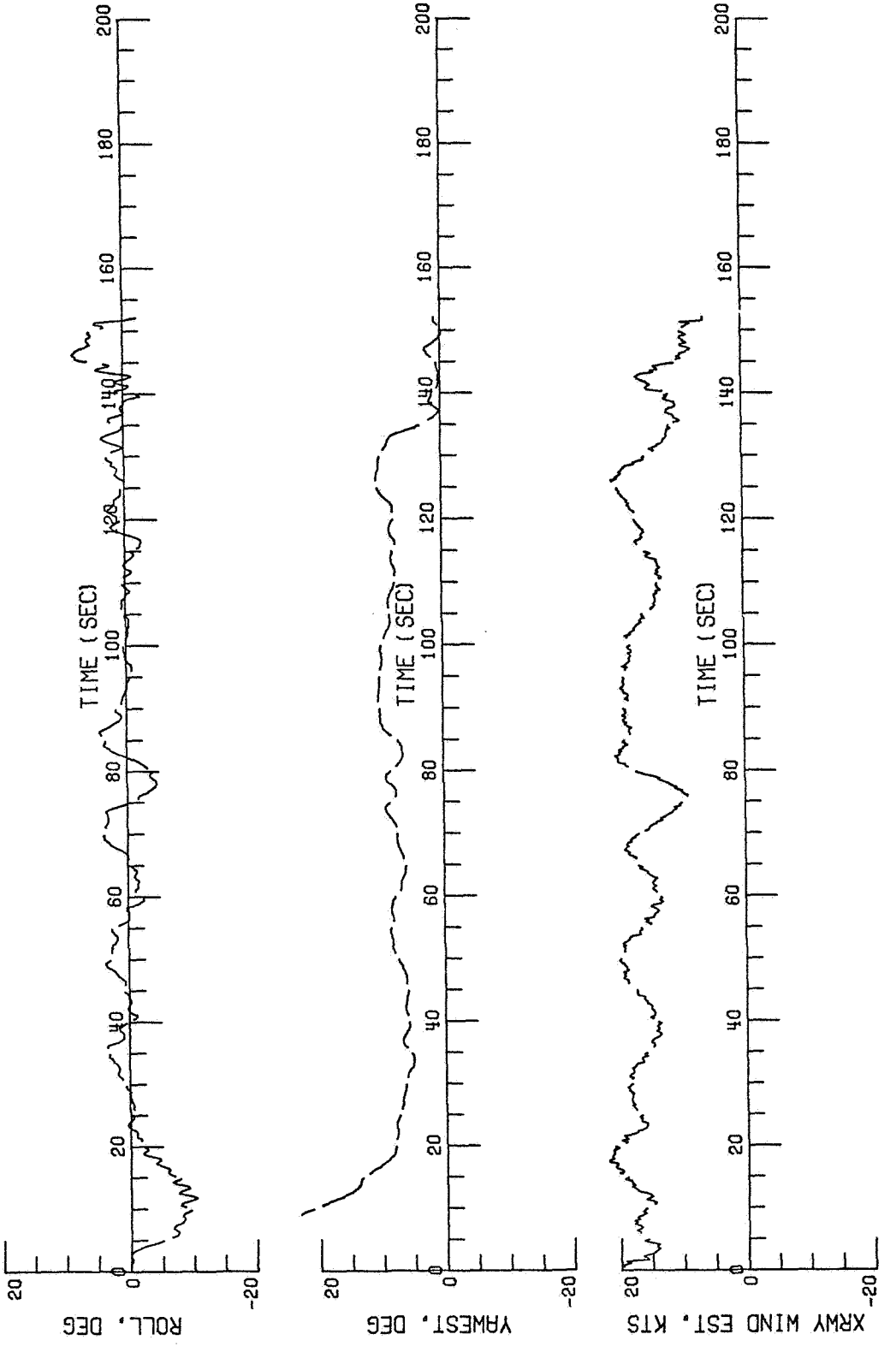

FIGURE 9(a). LATERAL FLIGHT PATH VARIABLES (FLIGHT NO. 3)

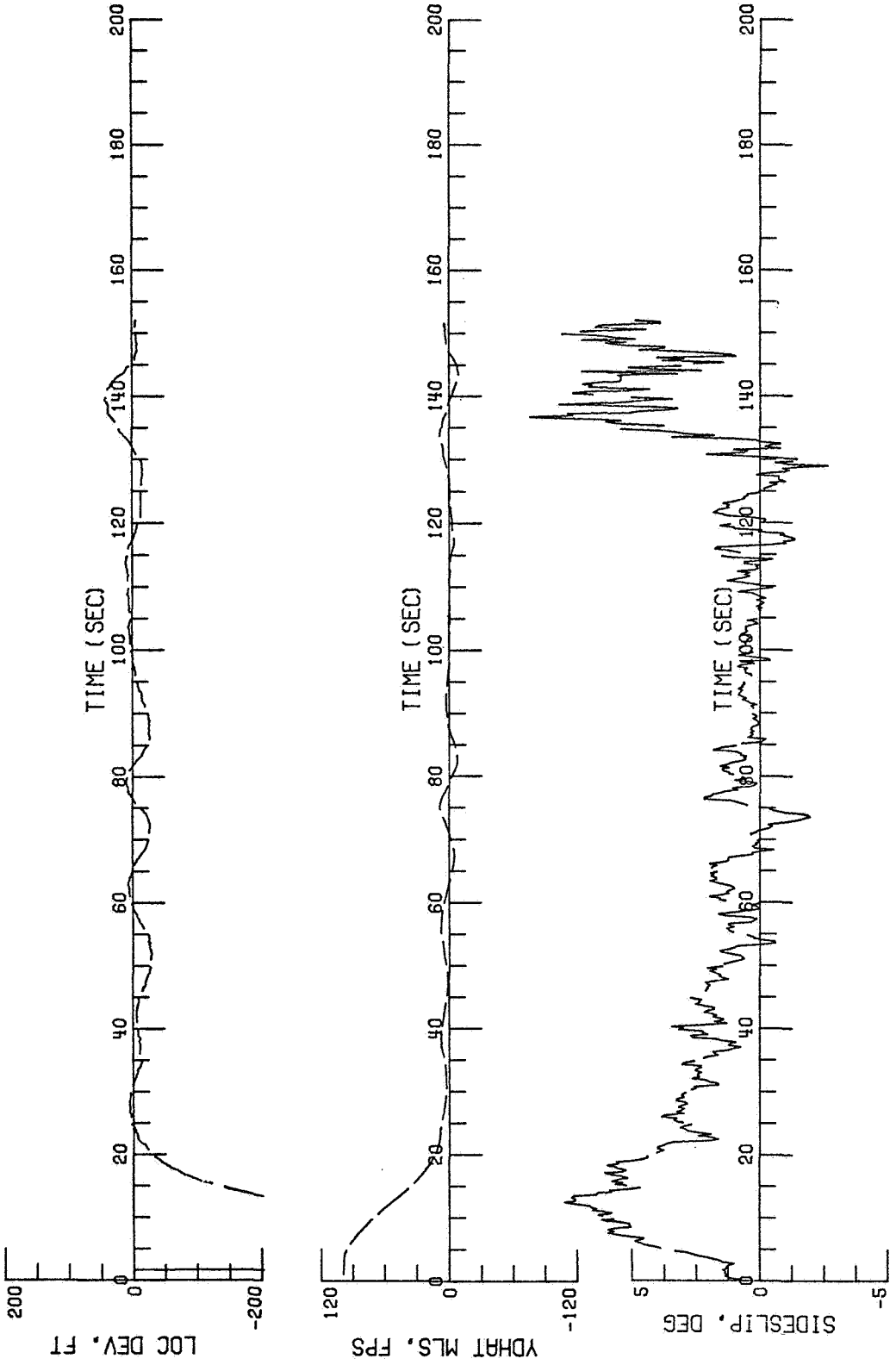

FIGURE 9(b). LATERAL FLIGHT PATH VARIABLES (FLIGHT NO. 3)

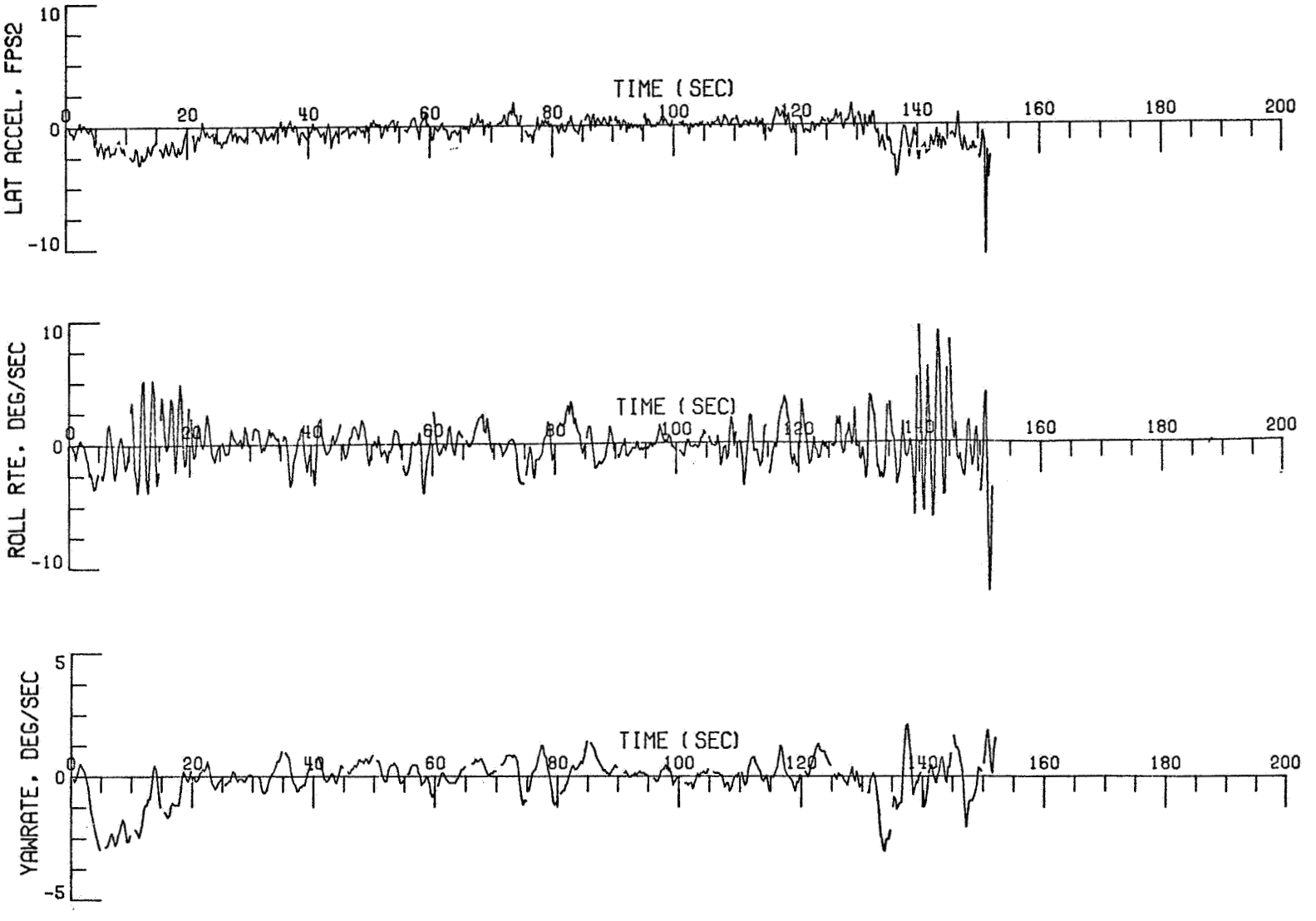

FIGURE 9(c). LATERAL FLIGHT PATH VARIABLES (FLIGHT NO. 3)

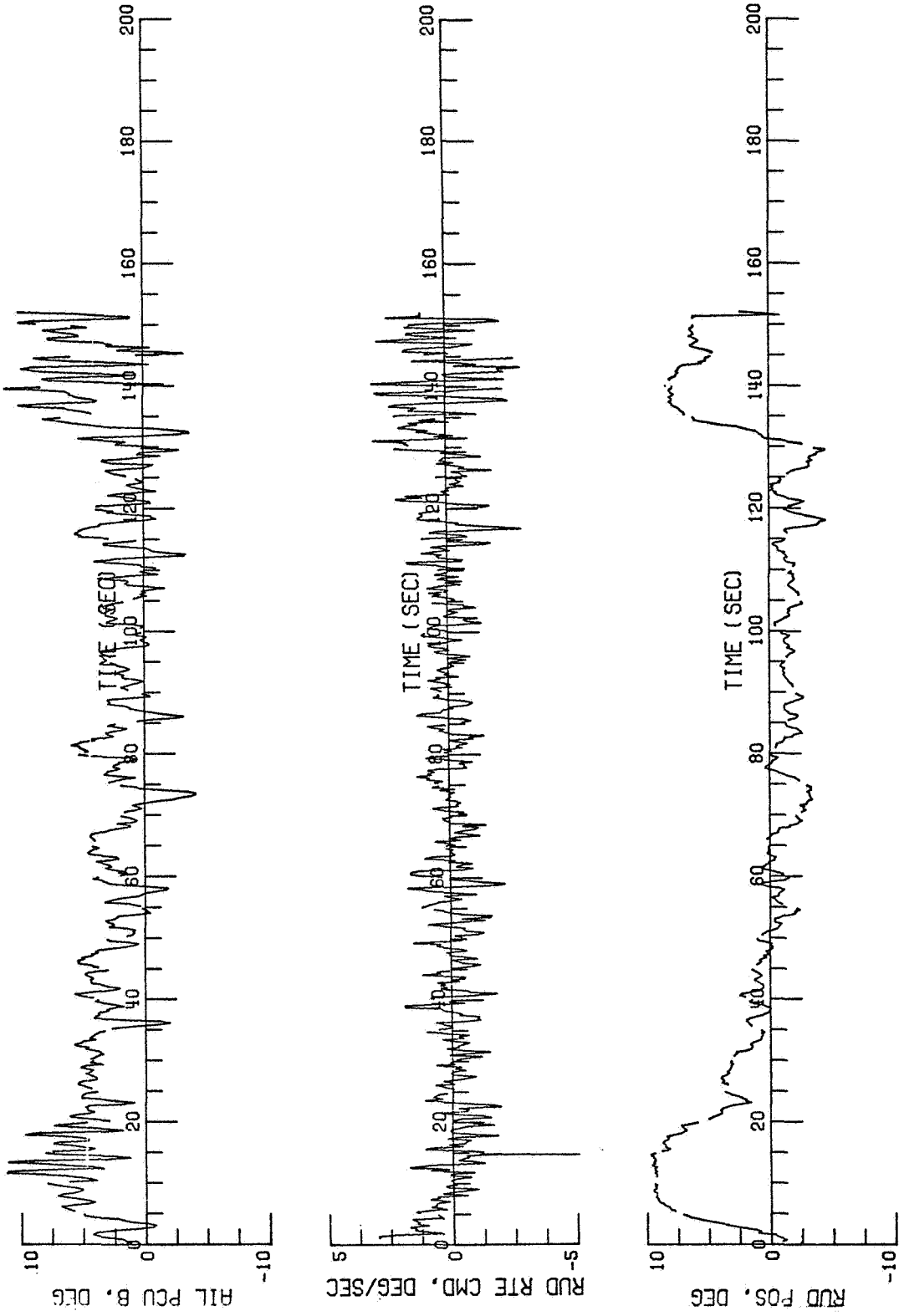

FIGURE 10. LATERAL CONTROL VARIABLES (FLIGHT NO. 3)

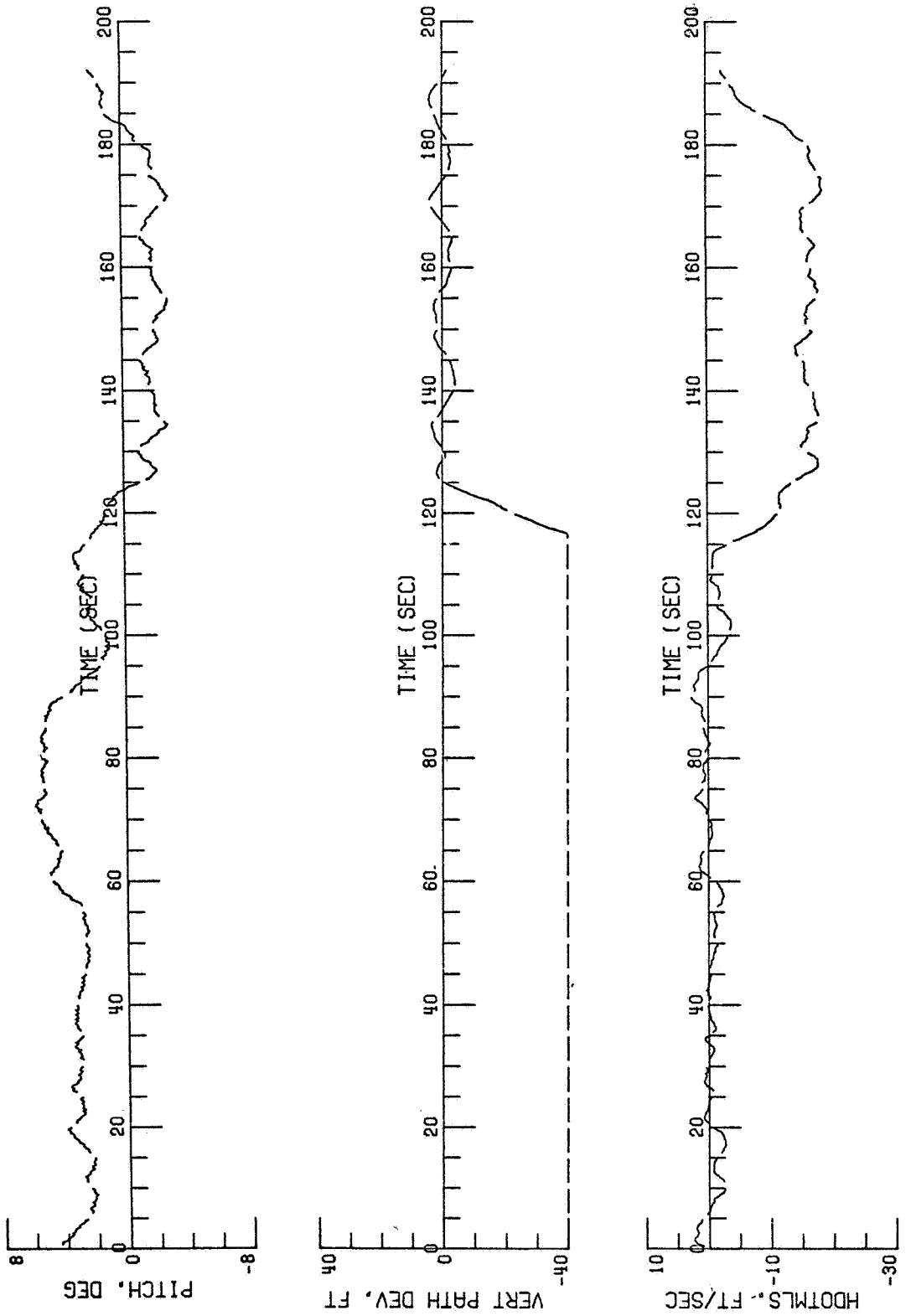

FIGURE 11(a). LONGITUDINAL FLIGHT PATH VARIABLES (FLIGHT NO. 1)

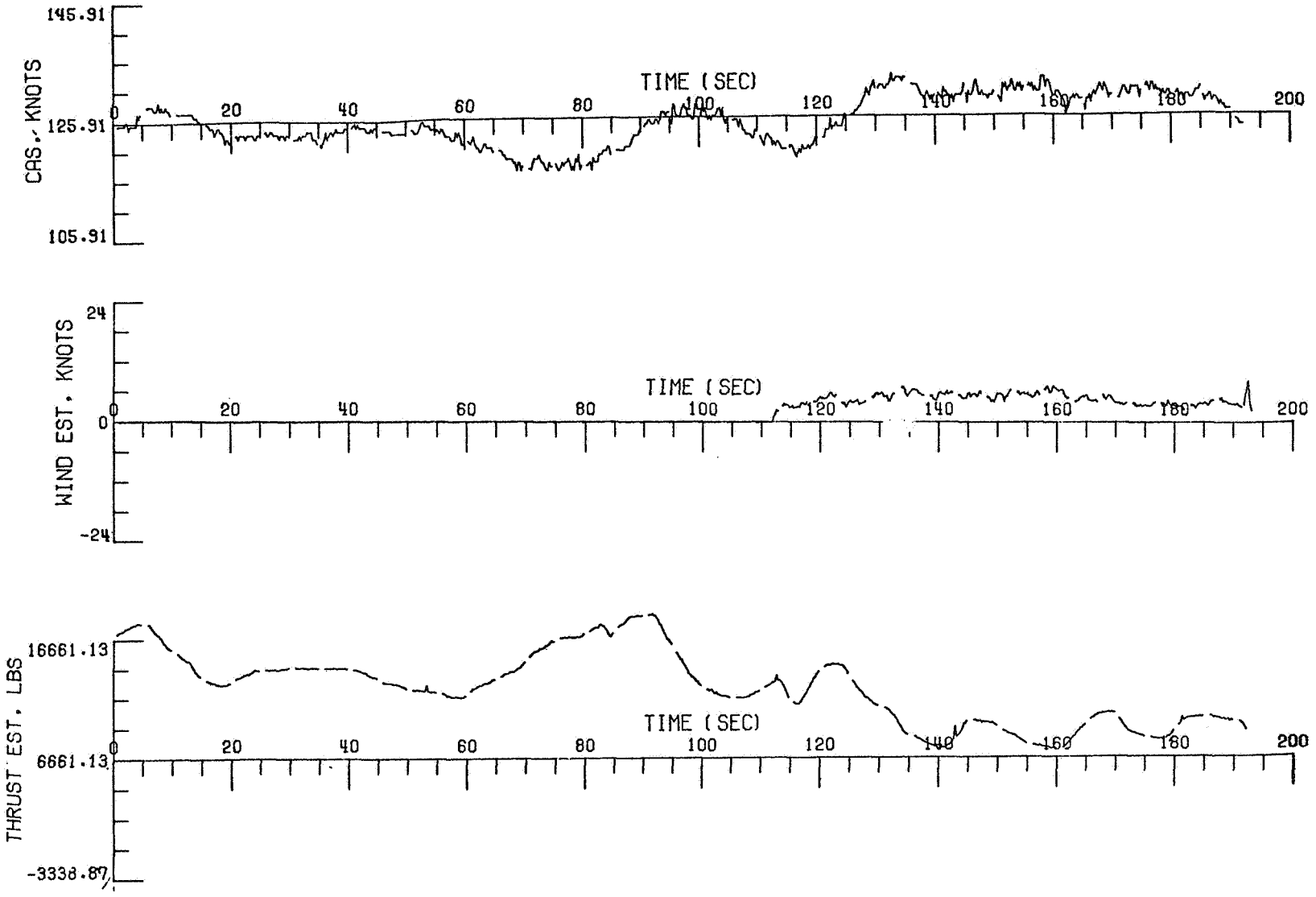

FIGURE 11(b). LONGITUDINAL FLIGHT PATH VARIABLES (FLIGHT NO. 1)

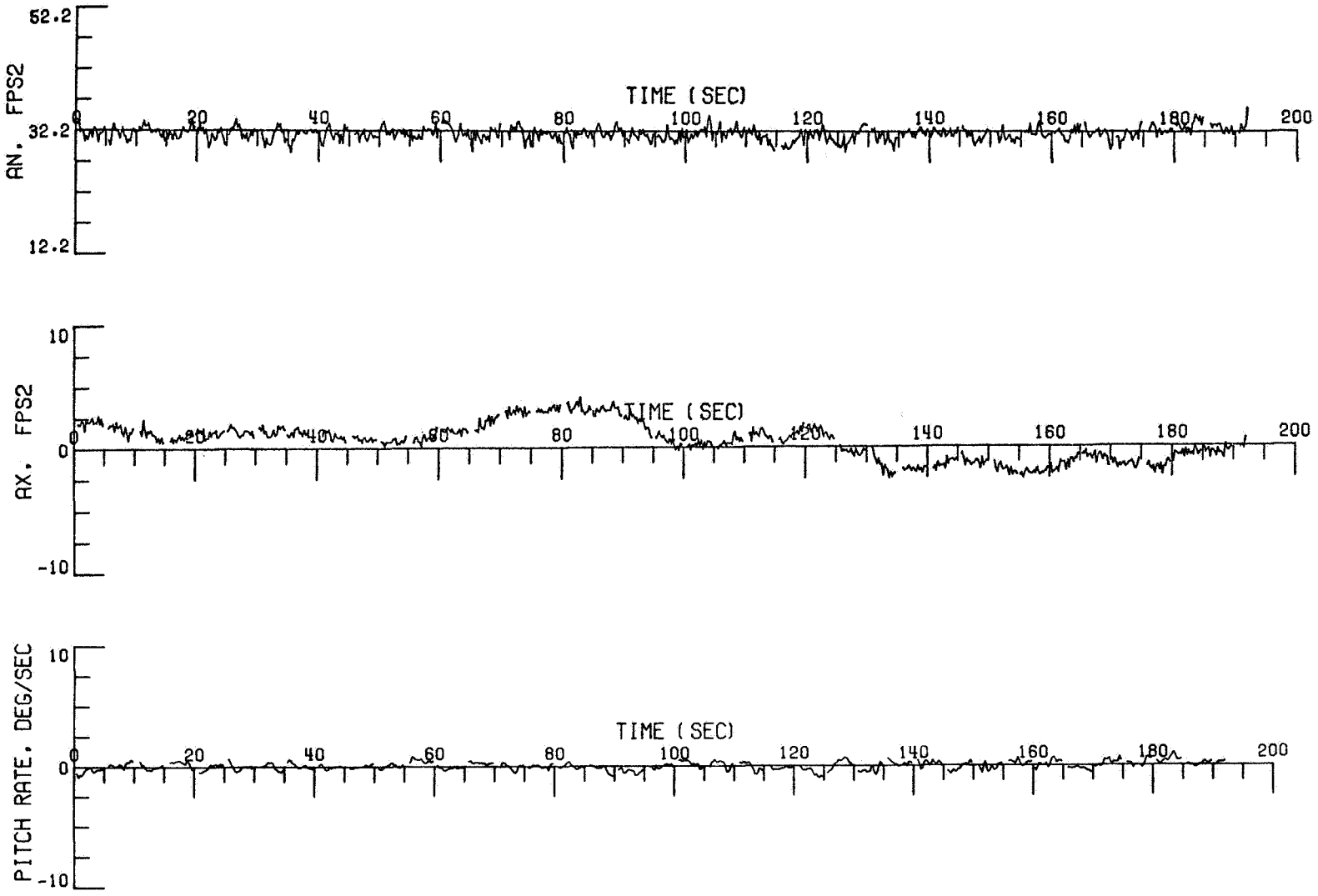

FIGURE 11(c). LONGITUDINAL FLIGHT PATH VARIABLES (FLIGHT NO. 1)

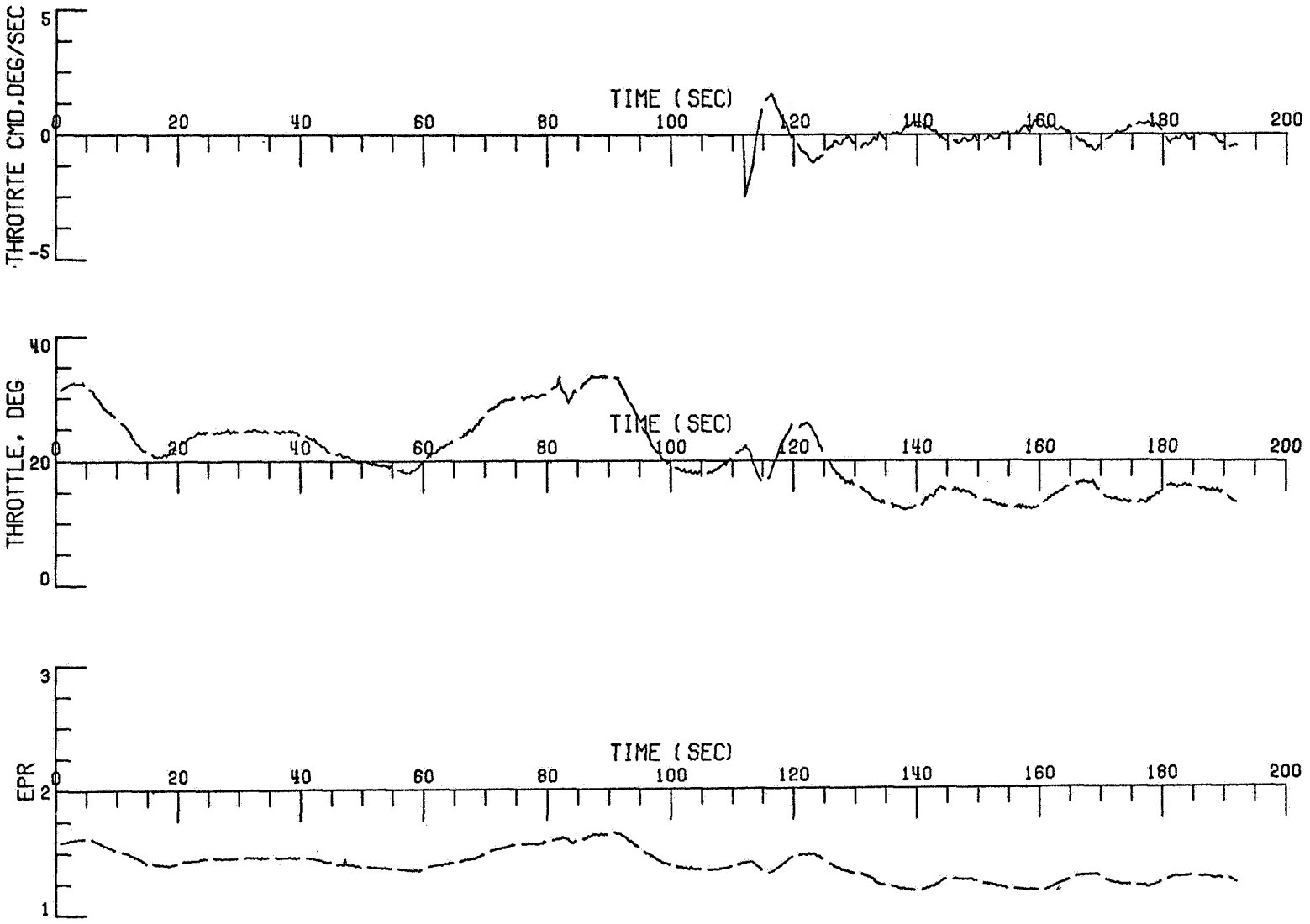

FIGURE 12(a). LONGITUDINAL CONTROL VARIABLES (FLIGHT NO. 1)

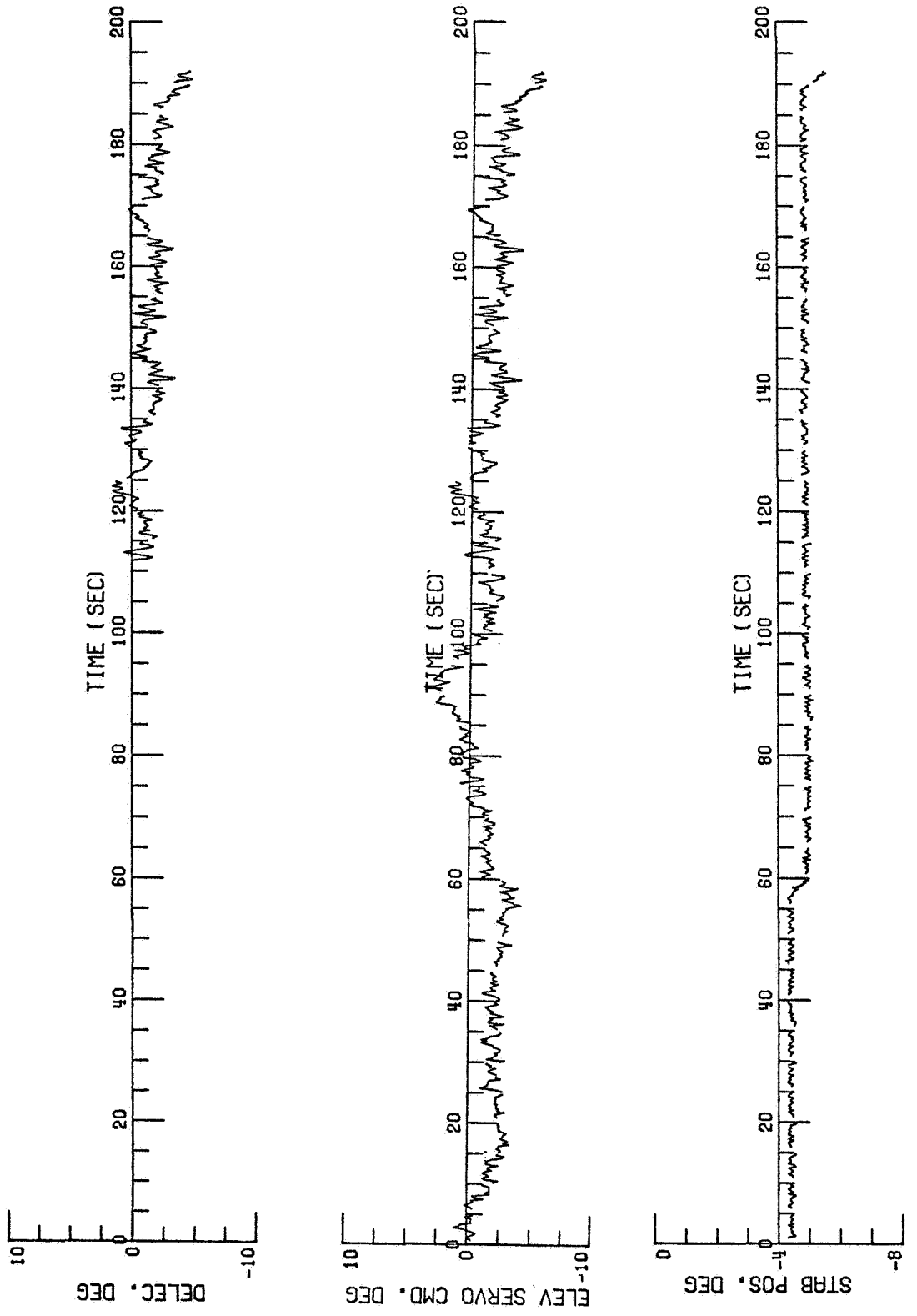

FIGURE 12(b). LONGITUDINAL CONTROL VARIABLES (FLIGHT NO. 1)

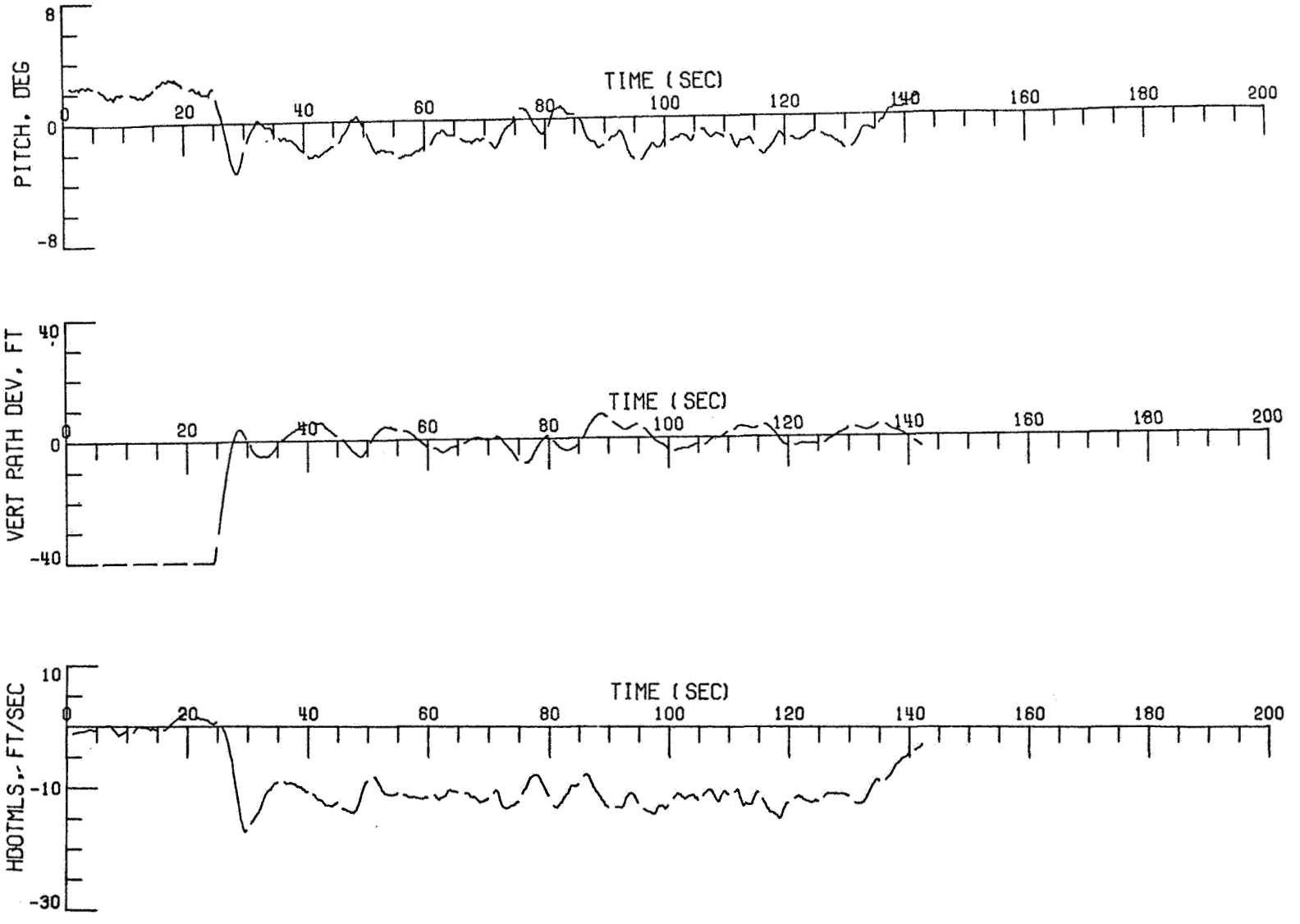

FIGURE 13(a). LONGITUDINAL FLIGHT PATH VARIABLES (FLIGHT NO. 2)

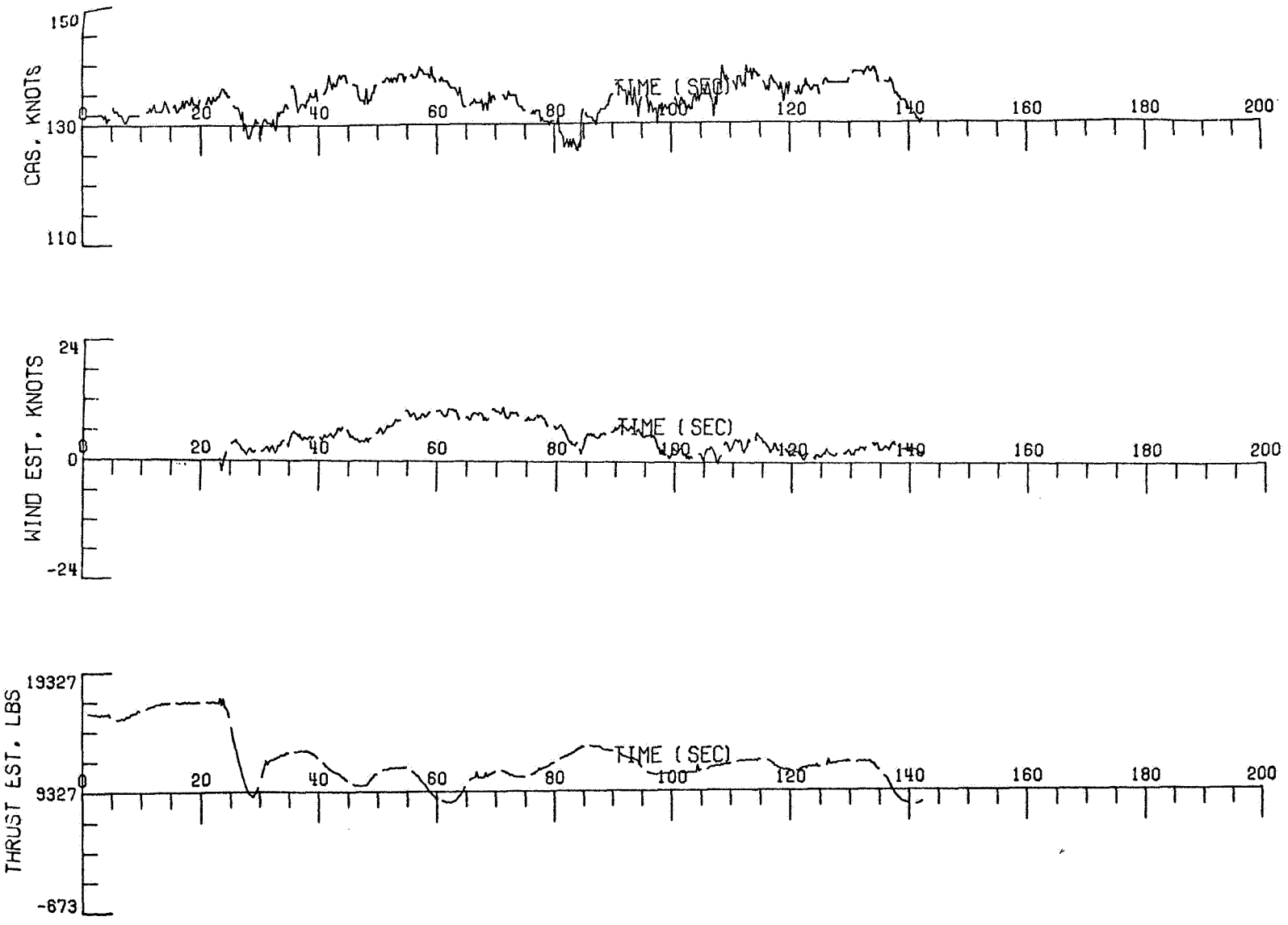

FIGURE 13(b). LONGITUDINAL FLIGHT PATH VARIABLES (FLIGHT NO. 2)

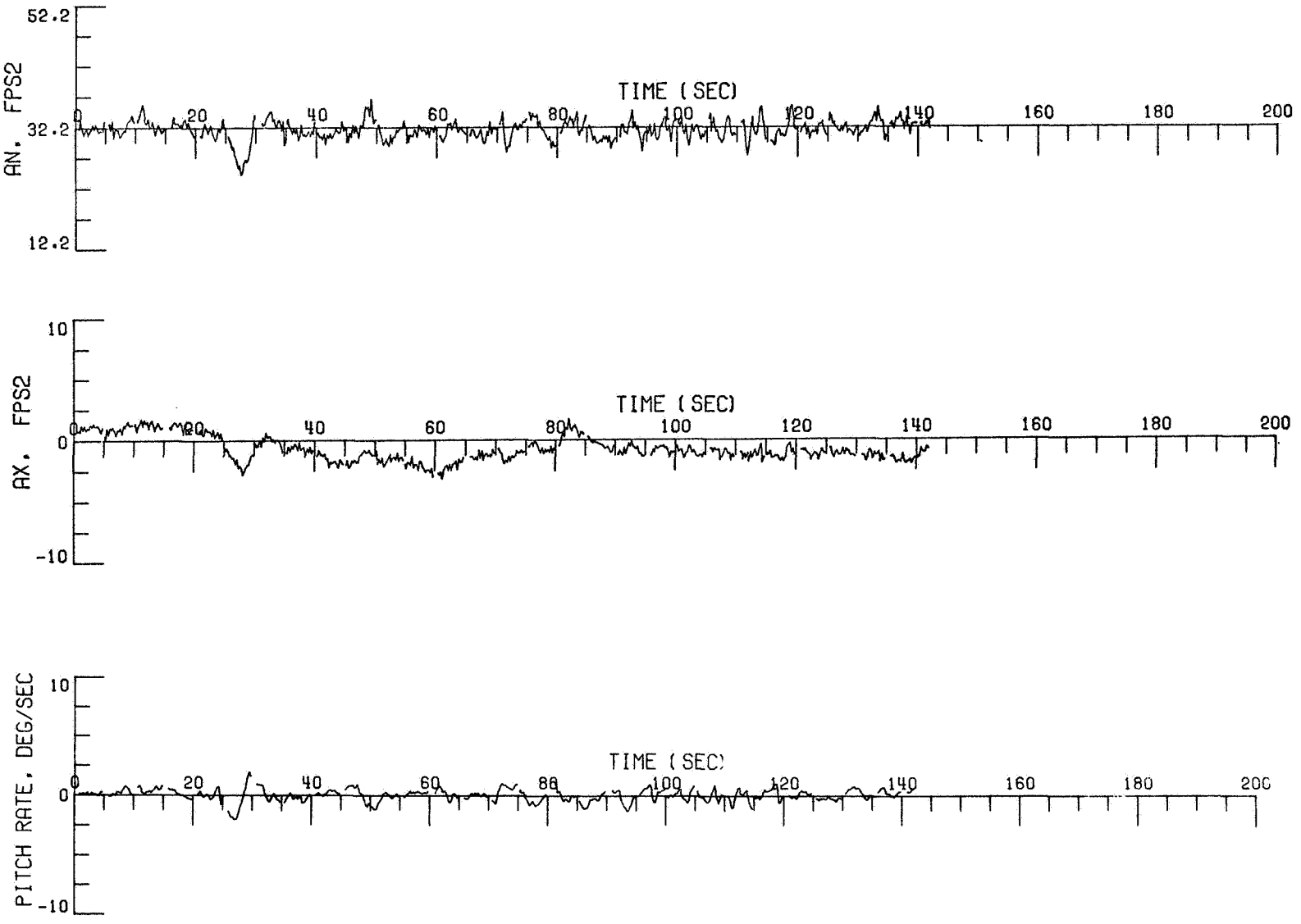

FIGURE 13(c). LONGITUDINAL FLIGHT PATH VARIABLES (FLIGHT NO. 2)

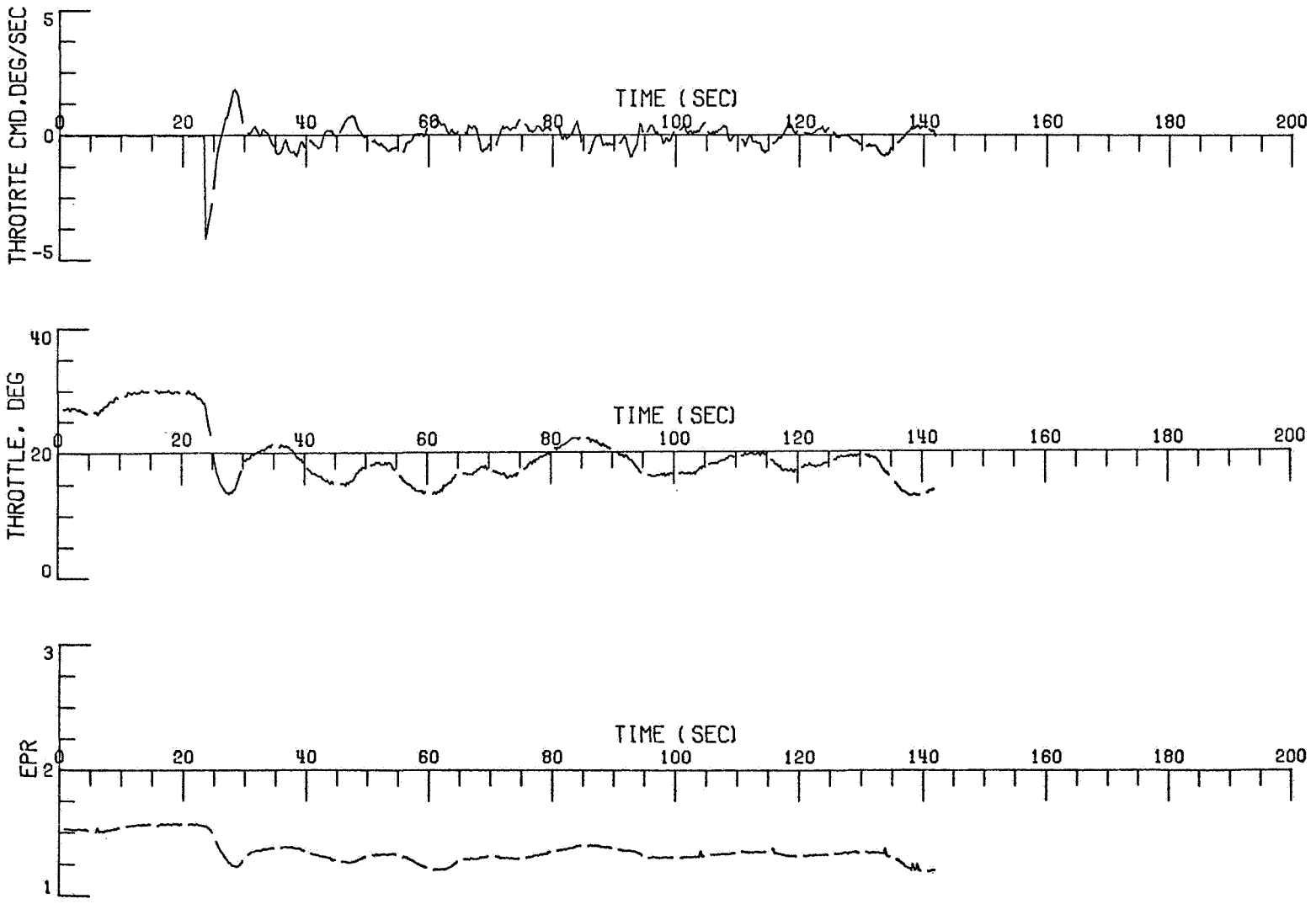

FIGURE 14(a). LONGITUDINAL CONTROL VARIABLES (FLIGHT NO. 2)

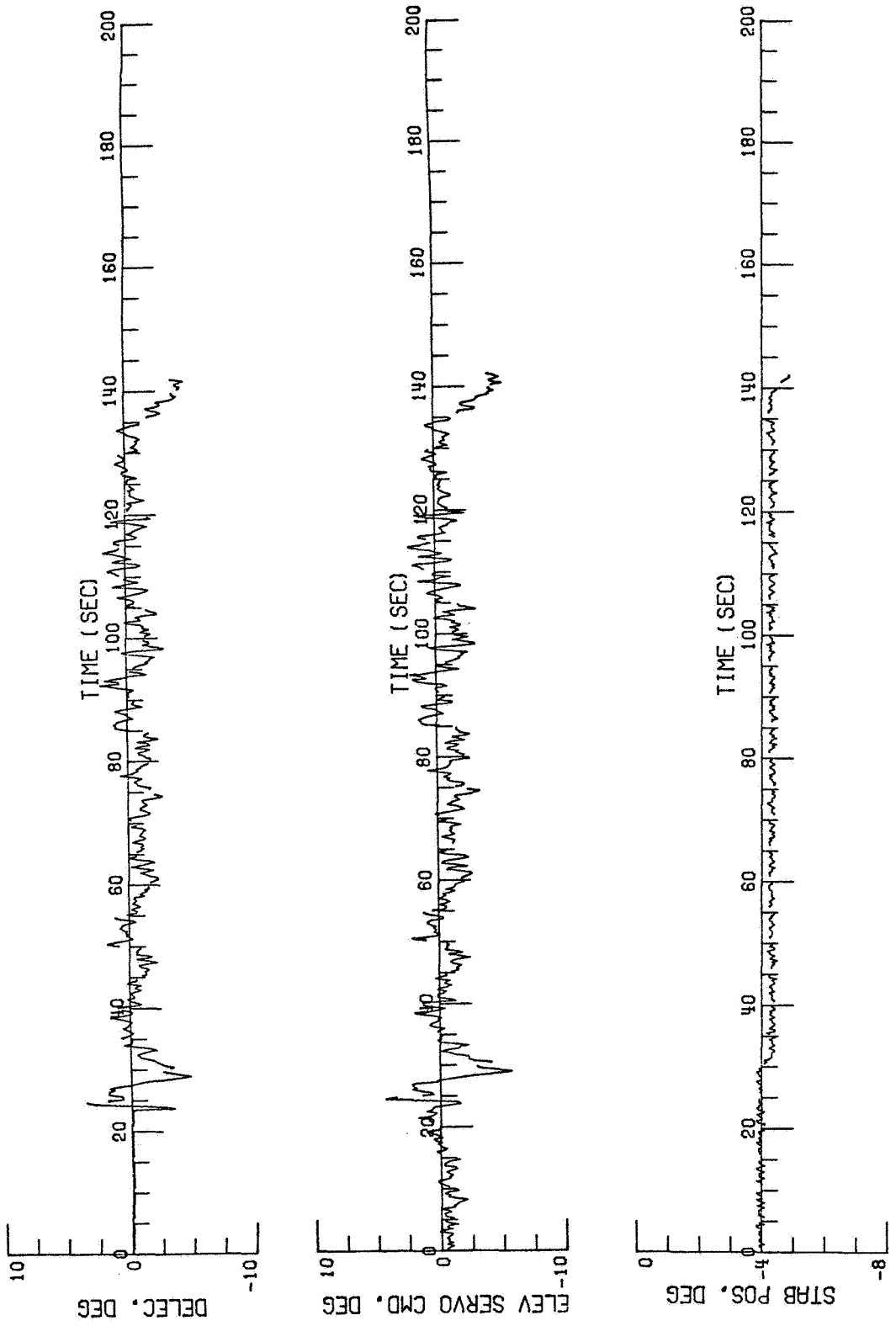

FIGURE 14(b). LONGITUDINAL CONTROL VARIABLES (FLIGHT NO. 2)

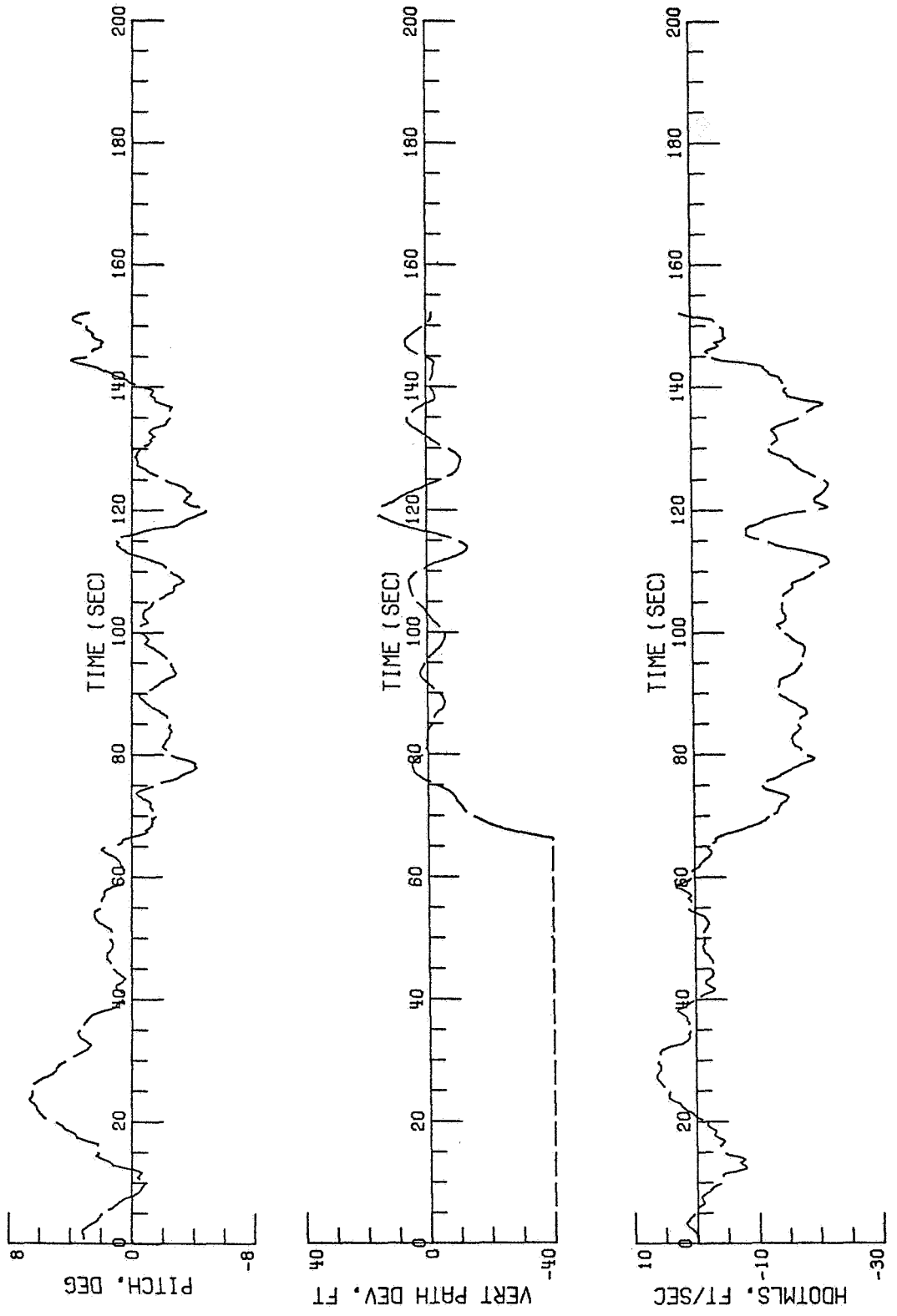

FIGURE 15(a). LONGITUDINAL FLIGHT PATH VARIABLES (FLIGHT NO. 3)

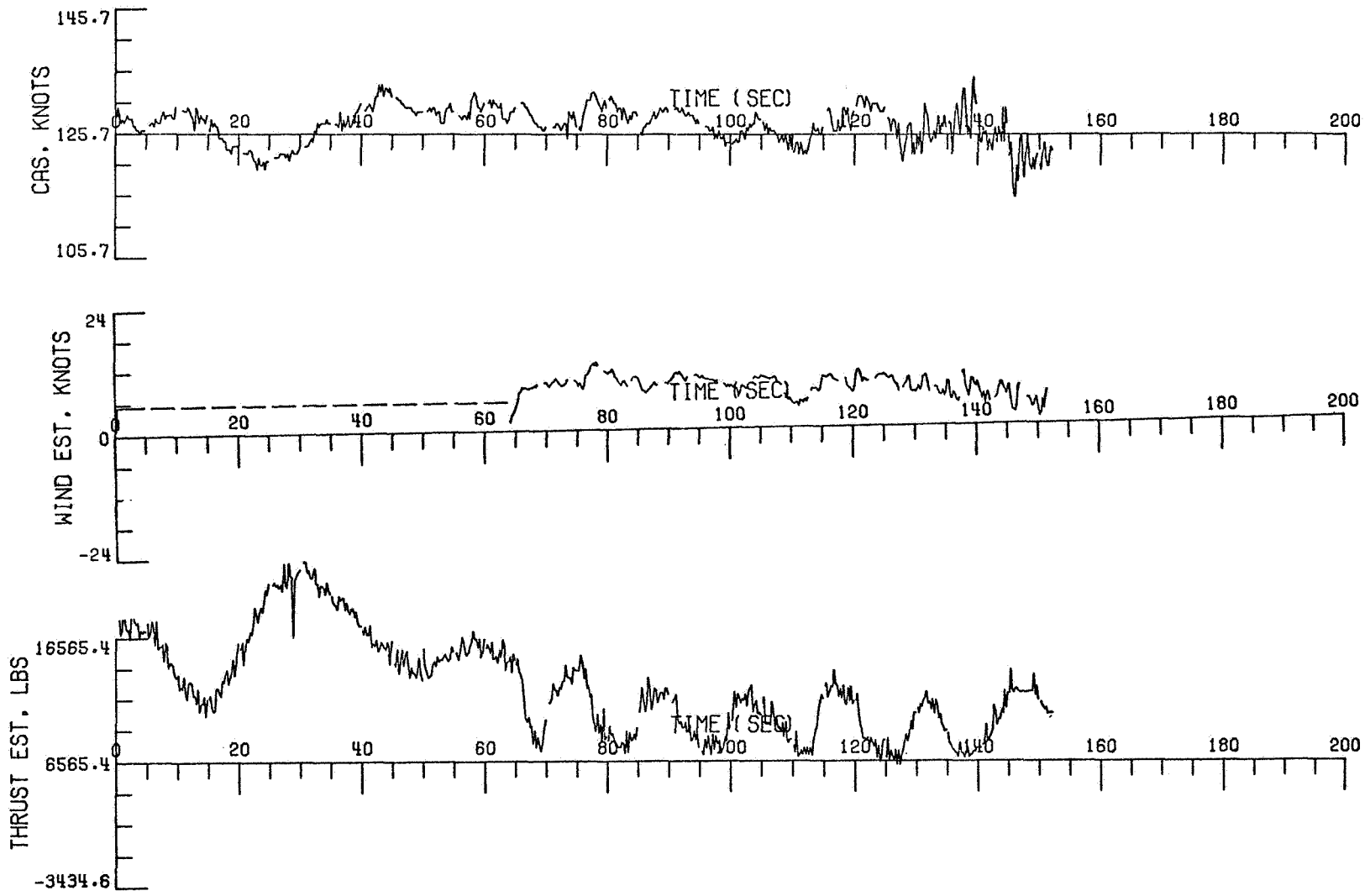

FIGURE 15(b). LONGITUDINAL FLIGHT PATH VARIABLES (FLIGHT NO. 3)

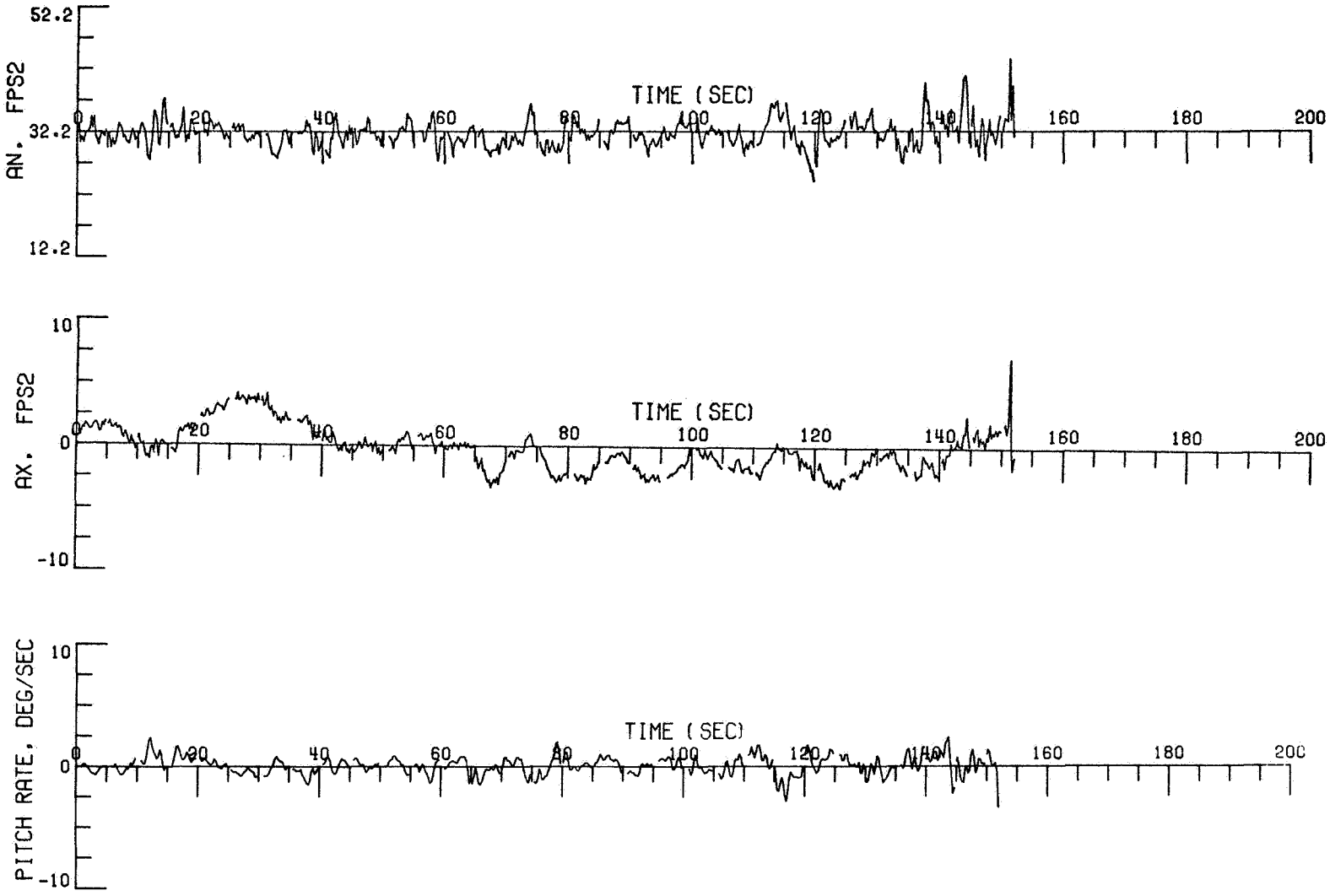

FIGURE 15(c). LONGITUDINAL FLIGHT PATH VARIABLES (FLIGHT NO. 3)

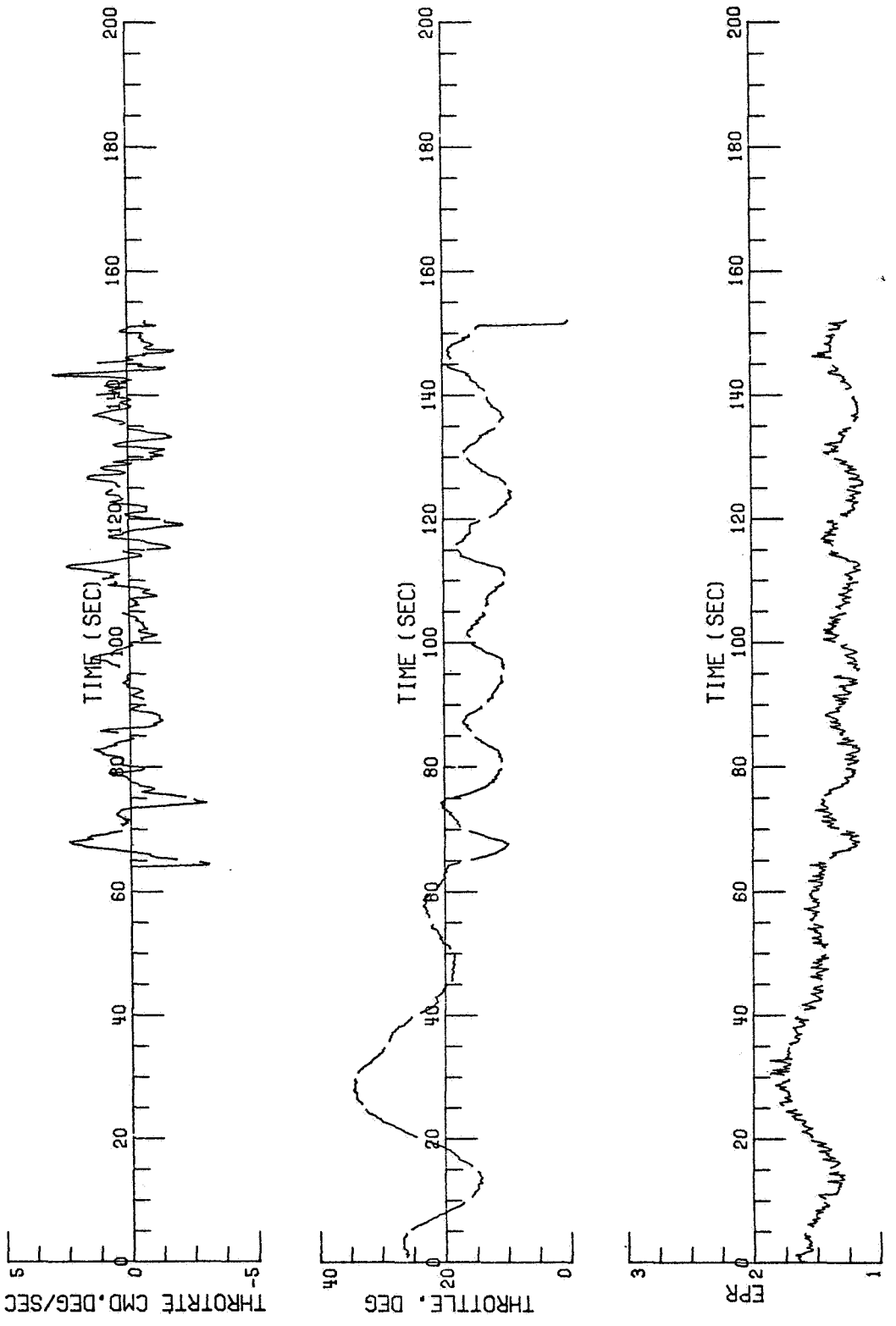

FIGURE 16(a). LONGITUDINAL CONTROL VARIABLES (FLIGHT NO. 3)

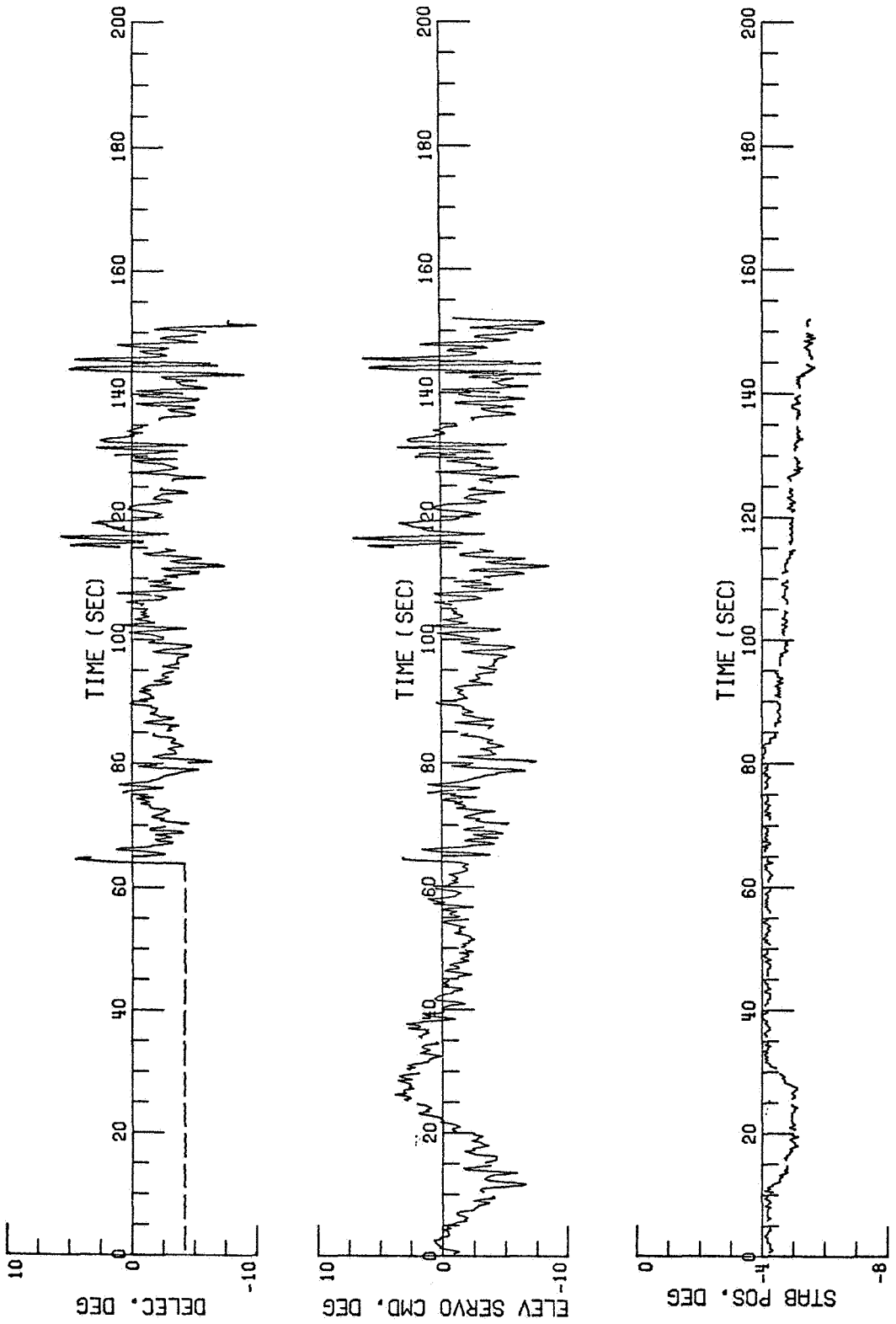

FIGURE 16(b). LONGITUDINAL CONTROL VARIABLES (FLIGHT NO. 3)

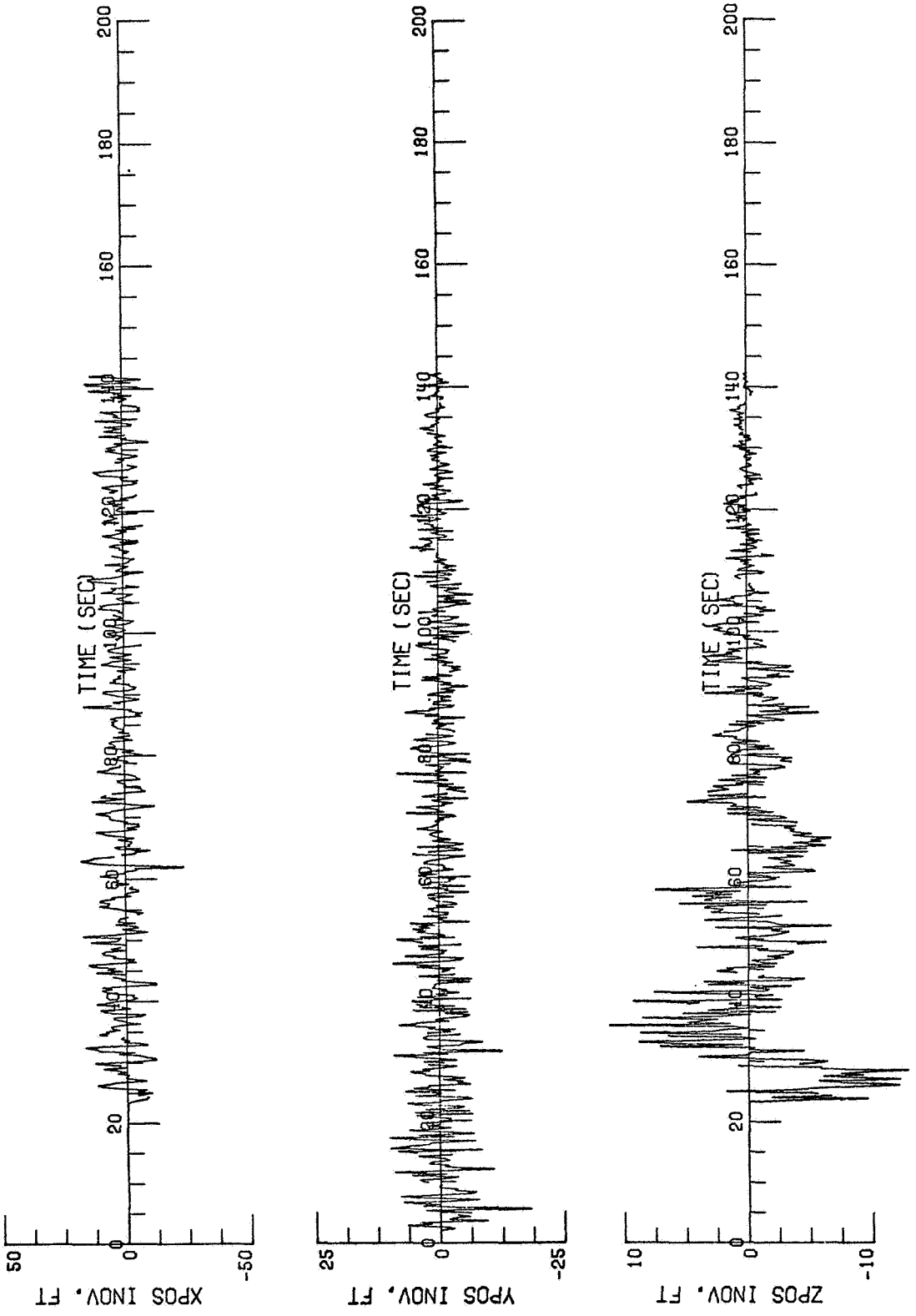

FIGURE 17(a). POSITION INNOVATIONS (FLIGHT NO. 2)

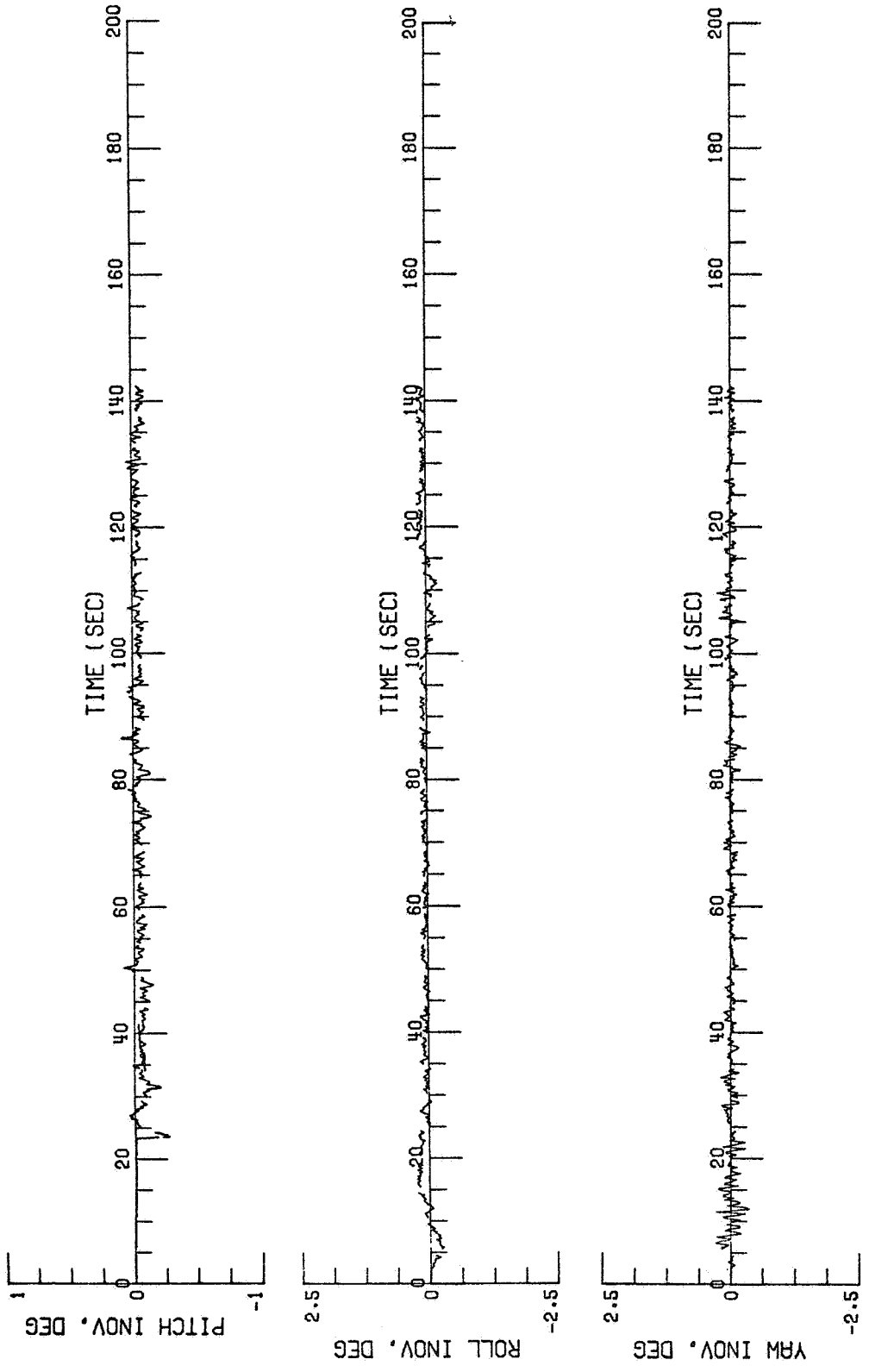

FIGURE 17(b). ATTITUDE INNOVATIONS (FLIGHT NO. 2)

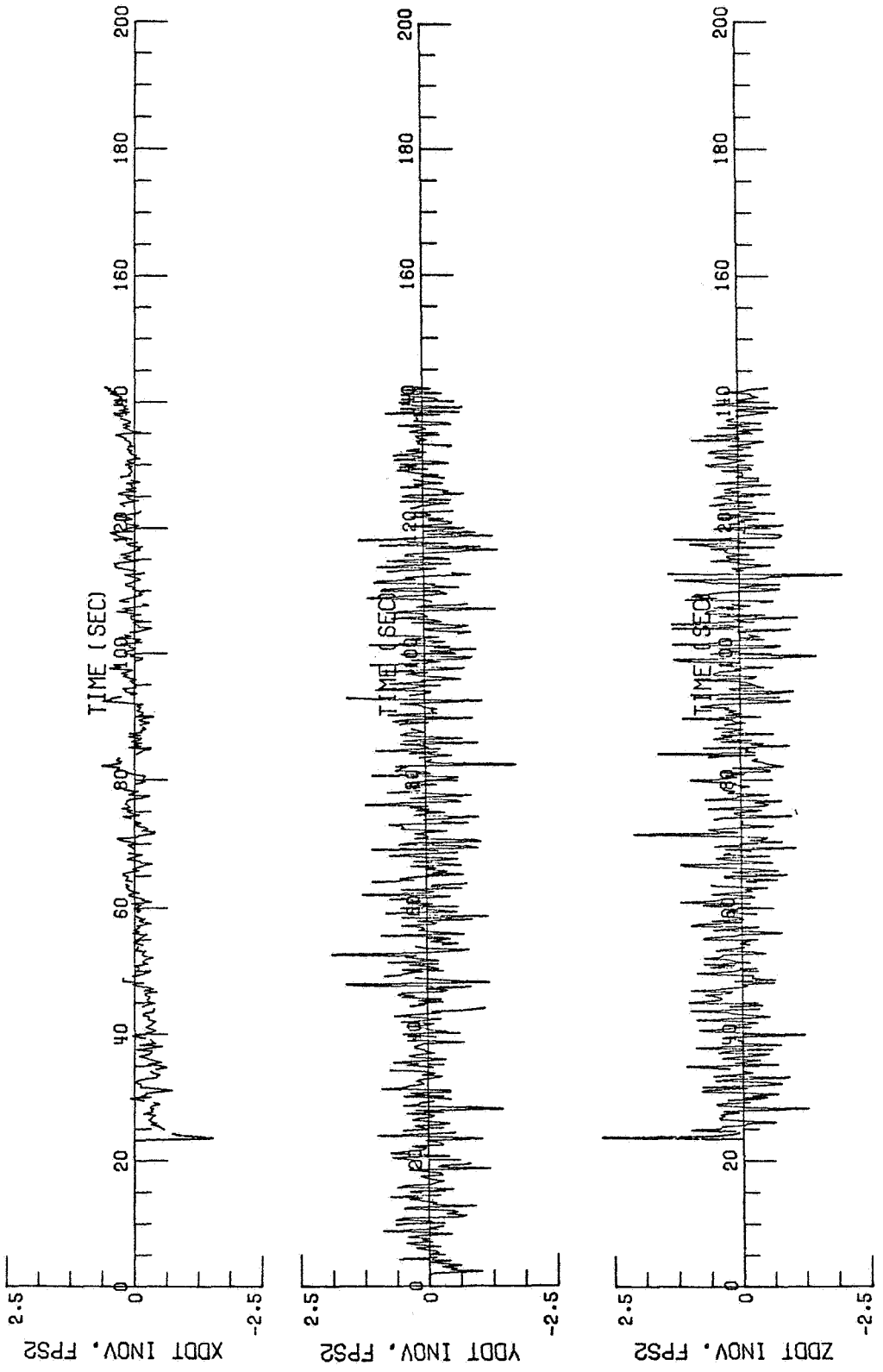

FIGURE 17(c). ACCELEROMETER INNOVATIONS (FLIGHT NO. 2)

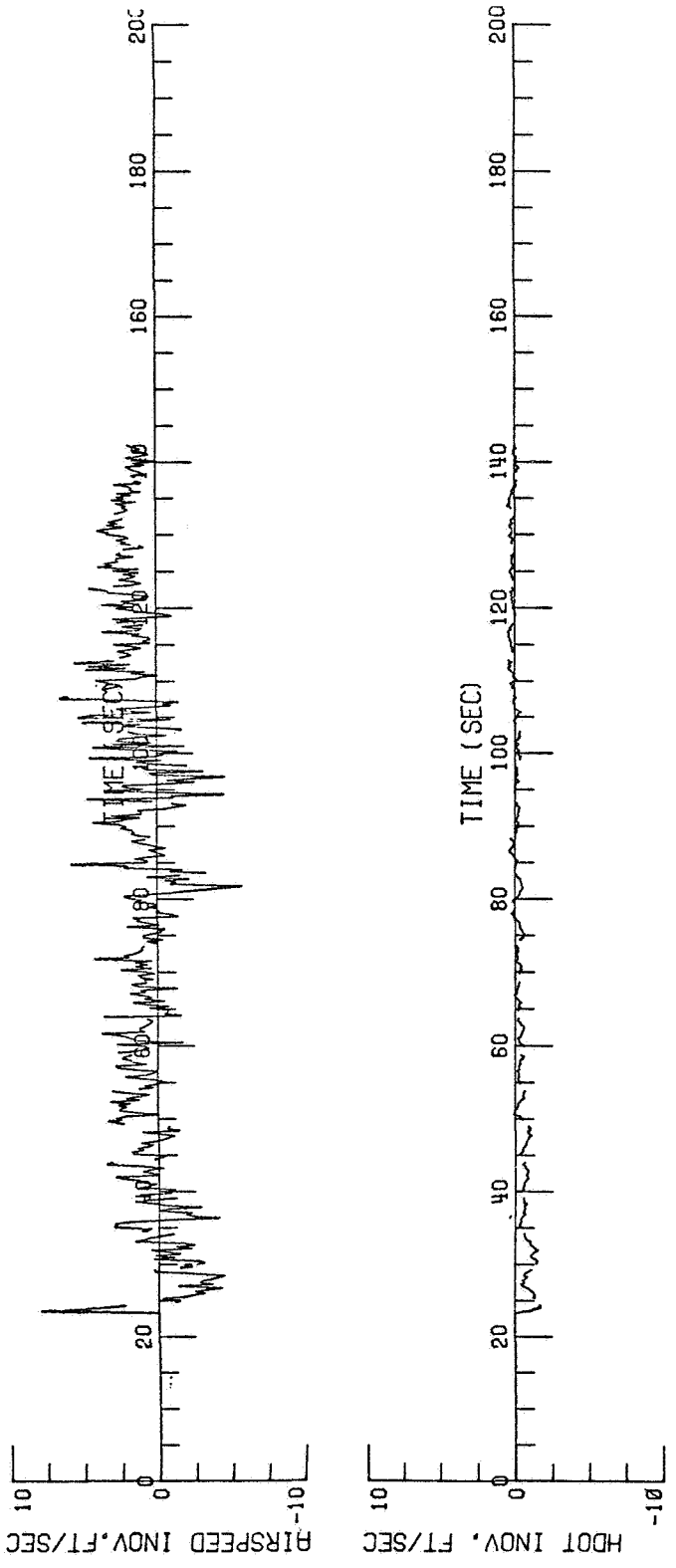

FIGURE 17(d). AIRSPEED AND SINK RATE INNOVATIONS (FLIGHT NO. 2)

TABLE 1. SENSOR ERROR MODEL PARAMETERS

Sensor	Noise standard deviation	Bias	Comments
Attitude gyro	.229°	.229°	
Rate gyro	.02°/sec	0	
Body-mounted accelerometers	1% of g	1% of g	.229° misalignment and .25% scaling errors also modeled
MLS - aximuth	.01°	.0125°	jitter added
MLS - elevation	.01°	.0125°	jitter added
MLS - DME	2.29m	2.29m	
Radar altimeter	.305m	.305m	
Barometric altimeter	.305m	1.52m	
Barometric sink rate	.305m/sec	.61m/sec	
Airspeed indicator	2%	0	Noise is multiplicative

$g = 9.81\ m/sec^2$

TABLE 2. RANGE/RESOLUTION/UNITS FOR PRIMARY INPUTS

Variable	Min.	Max.	Units	Resolution
θ	-0.5	0.5	rad	3.4×10^{-4}
q	-0.5	+0.5	rad/sec	8.7×10^{-5}
X	0	90,000	ft	Resolution used in FCC MLS coordinate transformations
Y	-5000.	5000	ft	
Z	-20.0	10,000	ft	
h_B	0	10,000	ft	0.5
$\dot{h}_B$	-64	64	ft/sec	0.03
CAS	120.0	300	ft/sec	0.2
f_x	-16.0	16	ft/sec^2	0.01
f_y	-16.0	16	ft/sec^2	0.01
f_z	-52.2	-12.2	ft/sec^2	0.01
ϕ	-1.0	-1.0	radian	4.26×10^{-4}
ψ_T	0	2π	radian	4.26×10^{-4}
p	-0.5	+0.5	rad/sec	8.7×10^{-5}
r	-0.5	+0.5	rad/sec	8.7×10^{-5}

TABLE 3. RANGE/UNITS FOR MEASUREMENT VECTORS

Variable	Min.	Max.	Units
y_{L1}	-0.5	0.5	rad
y_{L2}	-0.5	0.5	rad/sec
y_{L3}	-550.0	100.0	sec
y_{L4}	-55.0	1.0	sec
y_{L5}	-55.0	1.0	sec
y_{L6}	-.5	0.5	non-dim.
y_{L7}	-.125	.125	sec^{-1}
y_{L8}	-.5	.5	non-dim.
y_{L9}	-.125	.125	sec^{-1}
y_1	-1.0	1.0	rad
y_2	$-\pi$	π	rad
y_3	-0.5	0.5	rad/sec
y_4	-0.5	0.5	rad/sec
y_5	-32.	32.	sec
y_6	-.125	.125	sec^{-1}

TABLE 4. RANGE/UNITS AND ACCURACY FOR ESTIMATED AND PREDICTED STATE VECTORS

Variable	Min.	Max.	Units	Computational Accuracy
x_{L1}, $\hat{x}_{L1}$	-0.25	0.25	rad	8.7×10^{-5} rad (.005 deg)
x_{L2}, $\hat{x}_{L2}$	-0.5	0.5	non-dim.	2.3×10^{-4} (.05 ft/sec)
x_{L3}, $\hat{x}_{L3}$	-.25	0.25	rad	5.2×10^{-4} rad (.03 deg)
x_{L4}, $\hat{x}_{L4}$	-0.5	0.5	rad/sec	6.1×10^{-5} rad/sec (.0035 deg/sec)
x_{L5}, $\hat{x}_{L5}$	-550.0	100.0	sec	1.6×10^{-4} sec (.035 ft)
x_{L6}, $\hat{x}_{L6}$	-55.0	1.0	sec	2.7×10^{-4} sec (.06 ft)
x_{L7}, $\hat{x}_{L7}$	-10.0	28.0	1000 lbs.	5×10^{-3}/1000 lbs. (5 lbs)
x_{L8}, $\hat{x}_{L8}$	-30.0	50.0	degrees	8.4×10^{-3} deg (5 lbs)
x_{L9}, $\hat{x}_{L9}$	-0.25	0.25	rad	1.2×10^{-4} rad (.007 deg)
x_1, $\hat{x}_1$	-1.0	1.0	rad	8.7×10^{-4} rad (.05 deg)
x_2, $\hat{x}_2$	$-\pi$	π	rad	8.7×10^{-4} rad (.05 deg)
x_3, $\hat{x}_3$	$-\pi/4$	$\pi/4$	rad	5×10^{-4} rad (.029 deg)
x_4, $\hat{x}_4$	-0.5	0.5	rad/sec	N. A.
x_5, $\hat{x}_5$	-0.5	0.5	rad/sec	N. A.
x_6, $\hat{x}_6$	-32.0	32.0	sec	6.2×10^{-4} sec (.16 ft)
x_7, $\hat{x}_7$	-.5	.5	rad	N. A.

TABLE 5. RANGE/UNITS AND ACCURACY FOR WIND STATES AND BIASES

Variable	Min.	Max.	Units	Computational Accuracy
w_{L1}, $\hat{w}_{L1}$	-.25	.25	non-dim.	2.4×10^{-4} (.06 ft/sec)
w_{L2}, $\hat{w}_{L2}$	-.25	.25	rad/sec	8.8×10^{-5} rad/sec (.022 ft/sec^2)
w_{L3}, $\hat{w}_{L3}$	-.25	.25	rad/sec	2.6×10^{-4} rad/sec (.015 deg/sec)
w_{L4}, $\hat{w}_{L4}$	-.5	.5	non-dim.	4×10^{-4} (.10 ft/sec)
w_{L5}, $\hat{w}_{L5}$	-.5	.5	non-dim.	4×10^{-4} (.10 ft/sec)
w_{L6}, $\hat{w}_{L6}$	-.25	.26	rad	2×10^{-4} rad (.05 ft/sec)
w_{L7}, $\hat{w}_{L7}$	-.25	.25	sec^{-1}	1.2×10^{-4} sec^{-1} (.03 ft/sec^2)
$\hat{b}_{L1}$	-.03125	.03125	rad	1.2×10^{-4} rad (.007 deg)
$\hat{b}_{L5}$	-2.0	2.0	sec	2×10^{-4} sec (.05 ft)
$\hat{b}_{L6}$	-.03125	.03125	non-dim.	1.2×10^{-4} (.029 ft/sec)
$\hat{b}_{L7}$	-.015625	.015625	sec^{-1}	3.2×10^{-5} sec^{-1} (.008 ft/sec^2)
$\hat{b}_{L9}$	-.015625	.015625	sec^{-1}	2.8×10^{-5} sec^{-1} (.007 ft/sec^2)
w_1, $\hat{w}_1$	-.5	.5	non-dim.	$8. \times 10^{-4}$ (.2 ft/sec)
w_2, $\hat{w}_2$	-.25	.25	sec^{-1}	$8. \times 10^{-5}$ sec^{-1} (.02 ft/sec^2)
w_3, $\hat{w}_3$	-.25	.25	rad/sec	1.7×10^{-4} rad/sec (.01 deg/sec)
w_4, $\hat{w}_4$	-.25	.25	rad/sec	1.7×10^{-4} rad/sec (.01 deg/sec)
w_5, $\hat{w}_5$	-.5	.5	non-dim.	8×10^{-4} (.2 ft/sec)
w_6, $\hat{w}_6$	-.25	.25	non-dim.	$8. \times 10^{-5}$ (.02 ft/sec)
b_ϕ	-.03125	.03125	rad	3.6×10^{-4} (.02 deg)
b_ψ	-.03125	.03125	rad	3.5×10^{-4} (.02 deg)
b_{fy}	-.015625	.015625	sec^{-1}	2.4×10^{-5} (.006 ft/sec^2)

TABLE 6. RANGE/UNITS FOR RESIDUALS OR INNOVATIONS

Variable	Min.	Max.	Units
ν_{L1}	-.125	.125	rad
ν_{L3}	-5.0	5.0	sec
ν_{L4}	-.25	.25	sec
ν_{L5}	-.25	.25	sec
ν_{L6}	-.0625	.0625	non-dim.
ν_{L7}	-.03125	.03125	sec^{-1}
ν_{L8}	-.125	.125	non-dim.
ν_{L9}	-.03125	.03125	sec^{-1}
ν_1	-.125	.125	rad
ν_2	-.125	.25	rad
ν_5	-4.0	4.0	sec
ν_6	-.03125	.03125	sec^{-1}

TABLE 7. RANGE/UNITS AND ACCURACY FOR COMMAND VARIABLES

Variable	Min.	Max.	Units	Computational Accuracy
z_{L1}	-.25	.25	rad	8.7×10^{-5} rad (.00r deg)
z_{L2}	-.5	.5	non-dim.	2.3×10^{-4} (.05 ft/sec)
z_{L3}	-.25	.25	rad	5.2×10^{-4} rad (.03 deg)
z_{L4}	-.5	.5	rad/sec	6.1×10^{-5} rad/sec (.0035 deg/sec)
z_{L6}	-1.0	1.0	sec	1.6×10^{-4} sec (.035 ft)
ζ_{L2}	-.25	.25	non-dim.	2.3×10^{-4} (.05 ft/sec)
ζ_{L4}	-.125	.125	rad/sec	6.1×10^{-5} rad/sec (.0035 deg/sec)
ζ_{L6}	-.25	.25	sec	1.6×10^{-4} sec (.035 ft)
z_1	-1.0	1.0	rad	8.7×10^{-5} rad (.005 deg)
z_2	$-\pi$	π	rad	8.7×10^{-5} rad (.005 deg)
z_3	$-\pi/4$	$\pi/4$	rad	5×10^{-4} rad (.029 deg)
z_4	-.5	.5	rad/sec	6.1×10^{-5} rad/sec (.0035 deg/sec)
z_5	-.5	.5	rad/sec	6.1×10^{-5} rad/sec (.0035 deg/sec)
z_6	-32.0	32.0	sec	6.2×10^{-4} sec (.16 ft)
ζ_{u1}	-.125	.125	rad	6.1×10^{-5} rad (.0035 deg)
ζ_{u2}	-.125	.125	rad	6.1×10^{-5} rad (.0035 deg)
ζ_{u3}	-.5	.5	rad	6.1×10^{-5} rad (.0035 deg)
ζ_{u4}	-1.0	1.0	rad/sec	6.1×10^{-5} rad/sec (.0035 deg/sec)
ζ_{u5}	-.5	.5	rad/sec	6.1×10^{-5} rad/sec (.0035 deg/sec)
ζ_{u6}	-.5	.5	sec	2.7×10^{-4} sec (.06 ft)

TABLE 8. LOCALIZER OVERSHOOT STATISTICS

Localizer Overshoot (ft)	
Average	Standard Deviation
24.2	25.7

TABLE 9. GLIDESLOPE OVERSHOOT STATISTICS

Glideslope Overshoot (ft)	
Average	Standard Deviation
4.6	2.3

TABLE 10. AUTOMATIC TOUCHDOWN STANDARD DEVIATIONS

Sink Rate (ft/sec)		Touchdown Point (ft)	
Average	Standard Deviation	Average	Standard Deviation
2.4	0.74	1026	244

TABLE 11. AUTOMATIC TOUCHDOWN STATISTICS

Glideslope angle (deg)	Touchdown sink rate (ft/sec)	Touchdown point (ft)
4.5	2.5	N.A.
3.0	1.5	1100
3.0	2.5	680
4.5	2.5	680
4.5	2.5	1500
3.0	3.5	800
4.5	2.0	1120
4.5	1.0	1400
4.5	3.0	864
4.5	3.0	984

Commanded Sink Rate at 125 knots: 2.21 ft/sec.

Commanded Touchdown Point: 1152.5 ft.

REFERENCES

1. Anon.: "A New Guidance System for Approach and Landing". Vol. 2, Radio Technical Commission for Aeronautics, 1717 H Street N. W., Washington, DC. Document DO-148, Dec. 18, 1970.

2. Reeder, J. P., Taylor, R. T., and Walsh, T. M.: "New Designs and Operating Techniques for Improved Terminal Area Compatability". SAE, Air Transportation Meeting, Dalas, TX, Apr. 30, 1974.

3. Halyo, N.: "Terminal Area Automatic Navigation, Guidance and Control Research Using the Microwave Landing System (MLS). Part 5 -- Design and Development of a Digital Integrated Automatic Landing System (DIALS) for Steep Final Approach Using Modern Control Techniques". NASA CR-3681, Apr. 1983.

4. Halyo, N.: "Development of a Digital Guidance and Control Law for Steep Approach Automatic Landings Using Modern Control Techniques". NASA CR-3074, Feb. 1979.

5. Halyo, N.: "Development of a Digital Automatic Control Law for Steep Glideslope Capture and Flare". NASA CR-2834, June 1977.

6. Halyo, N.: "Development of an Optimal Automatic Control Law and Filter Algorithm for Steep Glideslope Capture and Glideslope Tracking". NASA CR-2720, Aug. 1976.

7. Halyo, N.: and Foulkes, R. E.: "On the Quadratic Sampled-Data Regulator with Unstable Random Disturbances". IEEE SMC Cos. Proc. 1974 International Conf. on Syst., Man and Cybern., pp. 99-103, Oct. 1974.

8. Halyo, N. and Caglayan, A, K.: "A Separation Theorem for the Stochastic Sampled-Data LQG Problem". International J of Control, Vol. 23, No. 2, pp. 237-244, Feb. 1976.

9. Roskam, J.: Flight Dynamics of Rigid and Elastic Airplanes. Parts I & II, Roskam Aviation and Engineering Corp., 519 Boulder, Lawrence, KS, 1972.

10. Etkin, B.: Dynamics of Atmospheric Flight. John Wiley & Sons, Inc., New York, NY, 1972.

11. Halyo, N., and McAlpine, G. A.: "On the Spectral Factorization of Non-Stationary Vector Random Processes". IEEE Trans on Automatic Control, Vol. AC-19, No. 6, pp. 674-679, Dec. 1974.

12. Kirk, D. E.: Optimal Control Theory: An Introduction. Prentice Hall, Inc., Englewood Cliffs, NJ, 1970.

13. Kushner, H. J.: Introduction to Stochastic Control. New York: Holt, Rinehart, and Winston, 1971.

14. Broussard, J. R.; and O'Brien, M. J.: "Feedforward Control to Track the Output of a Forced Model". IEEE Trans. on Automatic Control, Vol. AC-25, No. 4., pp. 851-854, Aug. 1980.

15. Halyo, N.; and Broussard, J. R.: "A Convergent Algorithm for the Stochastic Infinite-Time Discrete Optimal Output Feedback Problem", Proc. 1981 Joint Auto. Control Conference, Charlottesville, VA, June 1981.

16. Bennett, W. R.: "Spectra of Quantizied Signals". Bell System Technical Journal, Vol. 27, pp. 446-472, July 1948.

17. Halyo, N.: "Quantization Error Analysis in Digital Filters". MS Thesis, University of Virginia, Charlottesville, VA, June 1970.

18. Montgomery, R. C.: "Analytic Design of Digital Flight Controllers to Realize Aircraft Flying Quality Specifications". AIAA J. Aircraft, Vol. 9, No. 7, pp. 456-460, July 1972.

1. Report No.	2. Government Accession No.	3. Recipient's Catalog No.
NASA CR-3859		

4. Title and Subtitle	5. Report Date
FLIGHT TESTS OF THE DIGITAL INTEGRATED AUTOMATIC LANDING SYSTEM (DIALS)	December 1984
	6. Performing Organization Code
7. Author(s)	8. Performing Organization Report No.
Nesim Halyo	TR 683106
	10. Work Unit No.
9. Performing Organization Name and Address Information & Control Systems, Incorporated 28 Research Drive Hampton, VA 23666	11. Contract or Grant No. NAS1-16158
	13. Type of Report and Period Covered Contractor Report
12. Sponsoring Agency Name and Address National Aeronautics and Space Administration Washington, DC 20546	14. Sponsoring Agency Code 505-45-33-04

15. Supplementary Notes
Langley Technical Monitor: Richard M. Hueschen
Final Report

16. Abstract

This report describes the design, development, implementation and flight tests of the Digital Integrated Automatic Landing System (DIALS). The system was implemented and flight tested on the Transport Systems Research Vehicle (TSRV), a Boeing 737-100. The design uses modern optimal control methods. In particular, a stochastic sampled-data LQG formulation was employed. The direct-digital-design obtained uses a 10 Hz rate for the sampling of sensors and the control commands. The basic structure of the control law consists of a steady-state Kalman filter followed by a control gain matrix. The sensor information used includes Microwave Landing System (MLS) position, attitude, attitude rates, altitude, calibrated airspeed, and body accelerations. The phases of the final approach considered are localizer and steep glideslope capture (which may be performed simultaneously or independently), localizer and glideslope track, crab/decrab, and flare to touchdown. The system can capture, track, and flare from conventional, as well as steep, glideslopes ranging from 2.5° to 5.5°. All of the modes of the control law including the Kalman filters were implemented on the TSRV flight computers which use fixed-point arithmetic with 16 bit words. The implementation considerations are described in Section III. Section IV presents an analysis of the flight test results. Each phase of the flight corresponding to the different modes of the control law are analyzed in detail for three of the ten "hands-off" automatic landings performed. To the author's knowledge, DIALS is the first modern control design demonstrated by flight tests on a jet-class aircraft.

17. Key Words (Suggested by Author(s))		18. Distribution Statement
Automatic landing system	Localizer	Unclassified—Unlimited
Flight tests	Glideslope	
Modern control	Decrab	
Optimal control	Flare	
Direct-digital-design	Microwave Landing System (MLS)	
Stochastic sampled-data control		
Final approach		
Steep approach		Subject Category 08

19. Security Classif. (of this report)	20. Security Classif. (of this page)	21. No. of Pages	22. Price*
Unclassified	Unclassified	127	A07

For sale by the National Technical Information Service, Springfield, Virginia 22161

NASA-Langley, 1984

National Aeronautics and
Space Administration

Washington, D.C.
20546

Official Business
Penalty for Private Use, $300

THIRD-CLASS BULK RATE

Postage and Fees Paid
National Aeronautics and
Space Administration
NASA-451

NASA

POSTMASTER: If Undeliverable (Section 158 Postal Manual) Do Not Return